MODELING AND CONTROL OF FLEXIBLE STRUCTURES

by

Jeffrey Kent Bennighof

Dissertation submitted to the Faculty of the
Virginia Polytechnic Institute and State University
in partial fulfillment of the requirements for the degree of

DOCTOR OF PHILOSOPHY

in

Engineering Mechanics

APPROVED:

L. Meirovitch, Chairman

J. A. Burns

S. L. Hendricks

D. T. Mook

M. P. Singh

August, 1986

Blacksburg, Virginia

MODELING AND CONTROL OF FLEXIBLE STRUCTURES

by

Jeffrey Kent Bennighof

(ABSTRACT)

This dissertation is concerned with some topics in the modeling and control of large flexible structures. In the finite element convergence toward the natural modes and frequencies of a structure, it is found that two mechanisms limiting the accuracy of higher modes are, first, a decrease in the number of active degrees of freedom for higher mode approximations due to orthogonality constraints, and, second, the fact that lower computed, rather than actual, eigenfunctions appear in the orthogonality constraints, so that inaccuracy in lower modes inhibits convergence to higher modes. Refining the elements using the hierarchial p-version proves to be far superior to refining the mesh, as demonstrated by numerical examples.

In the third chapter, a method is presented for solving the algebraic eigenvalue problem for a structure, which combines attractive features of the subspace iteration method and the component-mode synthesis methods. Reduced substructure models are generated automatically and coupled exactly to form a reduced structure model, whose eigensolution is used to refine the substructure models. Convergence is much faster than in the subspace iteration method, as demonstrated by numerical examples.

In the fourth chapter, the effectiveness of modal control (IMSC) and direct feedback control, in which the actuator force depends only on

the local velocity and displacement, are investigated for suppressing traveling waves on a string and on a beam, both with slight material damping. Direct feedback proves superior for the string, as more modes must be controlled than can be handled by modal control with a limited number of actuators, but inferior for the beam, as effort is wasted suppressing motion in higher modes where damping is pervasive, while modal control focuses effort on those lower modes which need to be controlled.

The optimal vibration control for a distributed system subjected to persistent excitation is not available, so a two-part control is proposed in chapter five for suppressing the motion of a distributed system with a moving support. The first part cancels the moving support's excitation to an optimal extent, and the second is a direct velocity feedback control. A numerical example demonstrates the effectiveness of this control method.

ACKNOWLEDGEMENTS

The author would like to thank those who have contributed their support, guidance, and encouragement while this dissertation was being completed. First, thanks are due his advisor, Professor Leonard Meirovitch, for providing a solid background and opportunities for beneficial experience which will surely prove invaluable for years to come. Also the time and effort of the members of his graduate committee, Professors John A. Burns, Scott L. Hendricks, Dean T. Mook, and Mahendra P. Singh are deeply appreciated.

The efforts of my wife, , in keeping our home running smoothly, as well as her faithful encouragement, were especially helpful to me during this time and are gratefully acknowledged. The loving support of my parents, , and of my parents-in-law, , has been very encouraging. I would also like to thank the members of my house group in Blacksburg Christian Fellowship for their encouragement and prayers for my self-dicipline, and the Lord for answering those prayers.

Finally, I would like to thank Mrs. Susanne Davis for her care and efficiency in typing and correcting the manuscript.

TABLE OF CONTENTS

Page

ABSTRACT.....ii

ACKNOWLEDGEMENTS.....iv

TABLE OF CONTENTS.....v

LIST OF FIGURES.....vii

LIST OF TABLES.....viii

CHAPTER

1 INTRODUCTION.....1

1.1 Preliminary Remarks.....1
1.2 Modeling of Flexible Structures.....1
1.3 Control of Flexible Structures.....4

2 EIGENVALUE CONVERGENCE IN THE FINITE ELEMENT METHOD.....7

2.1 Introduction.....7
2.2 Eigenvalue Convergence in the Finite Element Method.....8
2.3 The h-Version and the p-Version of the Finite Element Method.....17
2.4 Numerical Examples.....20
2.5 Conclusions.....25

3 SUBSTRUCTURING WITH SELF-REFINING SUPER-ELEMENTS.....36

3.1 Introduction.....36
3.2 Ensuring Exact Interface Compatibility.....40
3.3 Eigenanalysis Procedure for the Structure.....46
3.4 Determining Substructure Response to Interface Motion..48
3.5 Computational Procedure.....50
3.6 Numerical Examples.....53
3.7 Conclusions.....54

4 CONTROL OF TRAVELING WAVES IN FLEXIBLE STRUCTURES.....62

4.1 Introduction.....62
4.2 Modal Control.....64
4.3 Direct Feedback Control.....68
4.4 Control of Traveling Waves.....71
4.5 Conclusions.....83

CHAPTER Page

5 ACTIVE VIBRATION CONTROL OF A DISTRIBUTED SYSTEM WITH MOVING SUPPORTS....94

5.1 Introduction....94
5.2 Problem Formulation....99
5.3 Optimal Control....100
5.4 A New Approach to Spatial Discretization....107
5.5 Numerical Example....111
5.6 Conclusions....115

REFERENCES....125

VITA....128

LIST OF FIGURES

FIGURE		Page
2.1	Stepped cantilever beam in flexural vibration	29
2.2	Logarithmic plots of eigenvalue convergence paths for the beam in Fig. 2.1 using the h-version	30
2.3	Logarithmic plots of eigenvalue convergence paths for the beam in Fig. 2.1 using the p-version	31
2.4	Logarithmic plots of eigenvalue convergence paths for a rectangular membrane using the h-version with linear elements	32
2.5	Logarithmic plots of eigenvalue convergence paths for a rectangular membrane using the h-version with quadratic elements	33
2.6	Logarithmic plots of eigenalue convergence paths for a rectangular membrane using the h-version with cubic elements	34
2.7	Logarithmic plots of eigenvalue convergence paths for a rectangular membrane using the p-version with up to quintic elements	35
3.1	Assembled and disassembled views of the structure used in the first numerical example	60
3.2	Helicopter tail boom used in the second numerical example	61
4.1	Uncontrolled damped wave motion in a string	85
4.2	Globally optimal (distributed) control of wave motion in a string	86
4.3	Modal control of a wave in a string, using discrete actuators	87
4.4	Modal contributions to the actuator forces and the resulting sum, the actual actuator forces, for the string in Fig. 4.3 at t = 0	88
4.5	Direct feedback control of a wave in a string	89
4.6	Uncontrolled damped wave motion in a beam	90

FIGURE Page

4.7 Globally optimal (distributed) control of wave motion in a beam.....91

4.8 Modal control of a wave in a beam, using discrete actuators.....92

4.9 Direct feedback control of a wave in a beam.....93

5.1 Thin plate simply supported on a rigid frame undergoing a displacement u(t).....118

5.2 The optimal value of α as a function of the frequency of the frame motion ω, with r as a parameter.....119

5.3 The average value of the integrand of the performance index as a function of α, with ω as a parameter.....120

5.4 Displacement of the plate model at the fifth and sixth actuator locations.....121

5.5 The integrand of the performance index as a function of time for the plate model for three values of α. 122

5.6 Displacement of the actual plate at the fifth and sixth actuator locations.....123

5.7 The integrand of the performance index as a function of time for the actual plate for three values of α. 124

LIST OF TABLES

TABLE		Page
2.1	Eigenvalue Error Due to Orthogonality Constraints.....	28
3.1	Computed Nonzero Eigenvalues for the Structure in Figure 3.1.....	58
3.2	Computed Eigenvalues for a Helicopter Tail Boom.....	59

Chapter 1

INTRODUCTION

1.1 PRELIMINARY REMARKS

In recent years, proposed designs for structures to be deployed in space have given considerable impetus to research in the modeling and control of such structures. Because these structures must be extremely lightweight in order to be boosted into orbit economically, and because in some cases they will need to be hundreds or thousands of meters in dimension to carry out their proposed mission tasks, they will be extremely flexible, and susceptible to large-amplitude vibration. For this reason, a number of approaches to the problem of controlling the vibration of large space structures (LSS) have been developed in recent years. Regardless of the control method to be used, the first step in designing a control system is that of obtaining a model which can accurately describe the behavior of the structure.

1.2 MODELING OF FLEXIBLE STRUCTURES

Because of the complexity of LSS, the finite element method will ordinarily be used to model them, due to its versatility and the ease with which it can be used. Ordinarily, very good estimates of a few of a structure's lower modes and natural frequencies can be obtained very easily using the finite element method, but the accuracy deteriorates rapidly for higher modes. Large space structures will be characterized by having many modes which participate significantly in their dynamic response, and since the performance of their control systems will be limited by the quality of the structure model, considerable interest

lies in determining the most effective approach to refining finite element models of structures in order to improve the accuracy of higher modes.

Convergence in the finite element method has been the subject of a number of recent papers,[1-4] which have addressed the question of whether it is more efficient to refine the elements or the mesh or both. However, these papers have only addressed convergence rates in applications in which a single solution is sought, such as elasticity problems, in any depth. Chapter two addresses the question for structural dynamics applications, in which many solutions corresponding to the many modes and natural frequencies of a structure are sought. In particular, the emphasis is on identifying factors which limit convergence to actual eigenvalues and eigenfunctions in the finite element method and selecting an optimal refinement strategy which minimizes the effect of these factors. It is found that the accuracy of higher modes is dependent on the accuracy with which lower modes are approximated, so that the strategy which affords the most rapid convergence to lower modes is most desirable for the sake of both higher and lower modes. Here, the strategy of refining the element rather than the mesh proves most attractive. This is illustrated by numerical examples of both one- and two-dimensional structures.

Once the structure has been discretized by the finite element method so that mass and stiffness matrices are obtained, the task of solving the generalized eigenvalue problem for approximations of modes and natural frequencies remains. This is not a trivial task, as the number of degrees of freedom in a finite element model may be in the

tens or even hundreds of thousands. The efficient computation of a partial eigensolution (corresponding to the lower modes) has also been the subject of a great deal of research in recent years. This has led to the development and refinement of several eigensolution methods, including the subspace iteration method[5-7] and the component-mode synthesis methods.[8-16] In the subspace iteration method, a set of trial vectors converges to the eigenvectors corresponding to a structure's lower modes in a procedure similar to the power method. In the component-mode synthesis methods, the structure is divided into substructures and a set of trial vectors, or "component modes," is generated for each substructure. The substructures are assembled together by satisfying a set of interface compatibility equations, resulting in a reduced eigenvalue problem that must be solved for estimates of the structure's lower modes.

Because the subspace iteration method treats the structure as a whole, very large eigenproblems can require an excessive amount of core so that they are difficult to handle by this method. The reduced eigenproblem resulting from the component-mode synthesis methods is a clear advantage in this regard; however, the accuracy of the modes obtained is dependent on the initial choice of component modes and upon the method used to enforce interface compatibility between substructures. In chapter three a new method is developed in which the attractive features of the subspace iteration method and the component-mode synthesis method are combined, as an initial set of trial vectors for each substructure is iteratively improved based on the solution of a greatly reduced structure eigenproblem. In this method interface compatibility is

automatically satisfied exactly and convergence is extremely rapid due to the fact that iteration is carried out on the substructure level.

1.3 CONTROL OF FLEXIBLE STRUCTURES

In the control of flexible structures, a control method which has been developed in recent years is the independent modal-space control (IMSC) method,[17,18] in which a structure is controlled by controlling its modes. In practice, control is limited to the lower modes of a structure. Because IMSC is concerned with controlling modes, which are global functions defined over the entire domain of a structure, the question arises whether IMSC is appropriate to use in the control of structures which can exhibit disturbances in the form of traveling waves, a localized phenomenon. In chapter four, the performance of IMSC on traveling waves in second- and fourth-order structures is investigated. Also, another form of control, known as direct feedback control (DFC), is developed and compared with IMSC. DFC has some important advantages over IMSC, in that implementation is greatly simplified, as the force exerted by a given actuator depends only on the velocity and displacement of the structure at the actuator location. In addition, DFC is inherently stable when only velocity feedback is used,[19] as it only draws energy out of the structure. DFC is not selective about the modes that it operates on, as it responds to motion contributed by any of the modes of the structure. Also it is not plagued by observation spillover, which is often encountered in estimating modal velocities and displacements for modal control. The gains for direct feedback control can be obtained by an optimal control

approach, based on a reduced model of the structure. This model is constructed by a new spatial discretization technique developed and used for the sole purpose of determining suitable gains. Direct feedback control is obtained by retaining only the diagonal entries in the optimal gain matrices, often with only a negligible decrease in performance.

These two control approaches are evaluated in the suppression of traveling waves, which are a type of disturbance containing a significant amount of energy in higher modes. As it happens, the question of global vs. local approaches may not be as pertinent as the question of how many modes are targeted for control, particularly when the effects of structural damping are considered. In structures with closely spaced natural frequencies, more modes are likely to participate in the response, with less damping due to the structure itself in these modes. Hence, modal control can require an excessive number of sensors and actuators in order to control the modes that participate significantly, so DFC proves to be the superior approach. When the natural frequencies are spaced farther apart, fewer modes are excited by a given disturbance, and energy in higher modes is dissipated very quickly by structural damping, so that the approach of targeting the lower modes for control is more attractive.

In the fifth chapter, the problem of suppressing the vibration of a structure whose support is undergoing significant motion is addressed. This problem has applications in space, where it may be desirable to minimize the motion of certain critical parts of a spacecraft while other areas can be allowed to move more in response to local activity,

as well as on earth, where minimizing the motion of an enclosure for machinery may be desirable for the purpose of noise reduction, for example. Past work in this area has included the design of tuned passive vibration isolators, with no significant work in the active vibration suppression of distributed systems subjected to support motion. Solving the optimal control problem in which the cost to be minimized is a function of both the motion of a distributed structure and the control effort is not possible in closed form when there is a persistent excitation, in general. For this reason, a two-part control is developed, where one part cancels the excitation due to the support motion to some extent and the other part is a regulator control which further reduces the remaining motion of the structure. The extent to which the excitation is cancelled is determined by minimizing a given performance index. Because the structure in this particular case is two-dimensional, being a thin plate, modal estimation would be difficult to carry out, so that modal control does not appear promising. For this reason, the regulator control is designed based on the same type of reduced-order model of the structure described above. The resulting control promises to be very simple to implement, as the actuator forces are simply the sum of a direct velocity feedback component and a component that is proportional to the displacement and acceleration of the support. A numerical example illustrates the method, and shows the type of performance that may be expected.

Chapter 2

EIGENVALUE CONVERGENCE IN THE FINITE ELEMENT METHOD

2.1 INTRODUCTION

Problems concerning the nature of convergence in the finite element method have received considerable attention in recent years. The work of Babuska et al.[1,2] provided a sound theoretical basis for what has been commonly observed in practice, namely, that refining the element (the p-version of the finite element method) is generally more attractive than refining the mesh (the h-version), as far as the number of degrees of freedom required for a given level of accuracy is concerned. Their results are valid for such applications as static force-deflection problems, in which a single solution is sought. However, in the vibration of distributed-parameter systems, generally a large number of eigenvalues and eigenfunctions, corresponding to natural modes of vibration, must be determined rather than a single solution.

In vibrations problems, the interest lies in the convergence to a number of eigenvalues computed concurrently by means of the finite element method, and how this convergence compares for different refinement strategies. Ordinarily, one can obtain acceptable accuracy only for some limited number of lower eigenvalues obtained by the finite element method. Clearly, the superior refinement strategy is the one that yields the greatest accuracy for the largest number of eigenvalues with the smallest number of degrees of freedom.

This chapter examines eigenvalue convergence in the finite element method and identifies the factors responsible for decreasing the

accuracy in higher eigenvalues. The developments here help explain why the p-version yields better accuracy on higher eigenvalues with a much smaller number of degrees of freedom than the h-version.

2.2 EIGENVALUE CONVERGENCE IN THE FINITE ELEMENT METHOD

The solution of the differential eigenvalue problem for a self-adjoint, linear, undamped distributed structure consists of an infinite set of eigenvalues and eigenfunctions. It can be shown that the eigenvalues of a structure are the stationary values of Rayleigh's quotient, defined as

$$R(u) = \frac{[u,u]}{(\sqrt{m}u, \sqrt{m}u)} \tag{2.1}$$

where u is a trial function, [u,u] is the energy inner product (equal to twice the potential energy associated with u) and $(\sqrt{m}u, \sqrt{m}u)$ is a mass-weighted inner product, related to the kinetic energy.[20] This variational characterization is the basis for the Rayleigh-Ritz method, of which the finite element method can be considered a subset, at least for structures.

In the Rayleigh-Ritz method, the motion of the structure is assumed in the form of a finite series of admissible functions multiplied by undetermined coefficients. Estimates of eigenvalues are obtained by seeking stationary values of Rayleigh's quotient, a process amounting to the solution of an algebraic eigenvalue problem.[20] The question of convergence of eigenvalue estimates becomes one of how stationary values of Rayleigh's quotient in the finite-dimensional space are related to the exact eigenvalues, where the latter are stationary values of Rayleigh's quotient in an infinite-dimensional space. Convergence to

the lowest eigenvalue, which is the miminum value of Rayleigh's quotient, can be expected to resemble convergence to the minimum potential energy in force-deflection problems, so that the results of Refs. 1 and 2 should be applicable. However, higher eigenvalues tend to be less accurate, and we propose to identify factors affecting their convergence. Clearly, the choice of admissible functions is important, but we focus our attention first on inaccuracy in higher eigenvalues not directly related to the choice of admissible functions.

The Rayleigh-Ritz representation of the displacement has the form

$$u(P) = \sum_{i=1}^{n} a_i \psi_i(P) = \underset{\sim}{a}^T \underset{\sim}{\psi}(P) \tag{2.2}$$

in which $\underset{\sim}{\psi}(P)$ is a vector of admissible functions and $\underset{\sim}{a}$ is a vector of undetermined coefficients. Inserting Eq. (2.2) into Eq. (2.1) and following the usual steps, Rayleigh's quotient becomes[20]

$$R(\underset{\sim}{a}) = \frac{\underset{\sim}{a}^T K \underset{\sim}{a}}{\underset{\sim}{a}^T M \underset{\sim}{a}} \tag{2.3}$$

in which K and M are the stiffness and mass matrices, with entries $k_{ij} = [\psi_i, \psi_j]$ and $m_{ij} = (\sqrt{m}\psi_i, \sqrt{m}\psi_j)$. In general, we approximate the actual eigenvalue λ_i by carrying out the minimization

$$\Lambda_i^n = \min_{\underset{\sim}{a}} (\underset{\sim}{a}^T K \underset{\sim}{a}) \quad , \quad \underset{\sim}{a}^T M \underset{\sim}{a} = 1 \quad , \quad \underset{\sim}{a}^T M \underset{\sim}{a}_j = 0 \quad , \quad j = 1,2,\ldots,i-1 \tag{2.4}$$

which is identical to the minimization yielding λ_i except that, for actual eigenvalues, Rayleigh's quotient is minimized over an infinite number of degrees of freedom on each eigenvalue,[20] whereas here the minimization is over a finite number of degrees of freedom. We note that the normalization process $\underset{\sim}{a}^T M \underset{\sim}{a} = 1$ acts like a constraint on $\underset{\sim}{a}$.

Moreover, $\underset{\sim}{a}^T M \underset{\sim}{a}_j = 0$ $(j = 1,2,\ldots,i-1)$ represent another i-1 constraints. Because $\underset{\sim}{a}$ has n components and is subject to i constraints, it follows that only n-i components can vary arbitrarily, so that there are only n-i quantities available for the minimization process. We refer to the number of components of $\underset{\sim}{a}$ that can vary arbitrarily as the number of active degrees of freedom. Hence, there are only n-i active degrees of freedom for computing Λ_i^n. The fact that the number of active degrees of freedom decreases as i increases is one major reason for decreasing accuracy in the higher computed eigenvalues.

Clearly, we can never expect good accuracy from the highest computed eigenvalue in any given discretization, because there are no active degrees of freedom left to carry out the minimization. Indeed, there is only one vector satisfying the associated constraints. Noting that we could have considered the process of finding stationary values of Rayleigh's quotient to be equivalent to a series of successive maximizations of Rayleigh's quotient, in which Λ_n^n is computed first, we conclude that the entire upper half of the computed eigenvalues is more directly related to a maximization than to a minimization process, which explains why acceptable accuracy is seldom achieved in the upper half of the computed eigenvalues.

For a given eigenvalue, the minimization described by Eq. (2.4) differs from the minimization yielding the actual eigenvalues in a second important way, in that the lower eigenvalues were obtained with a finite number of active degrees of freedom. The eigenfunction belonging to the given eigenvalue is constrained to be orthogonal in a mass-weighted inner product to lower computed eigenfunctions, rather than to

actual eigenfunctions. If the number of active degrees of freedom were the only factor determining computed eigenvalue accuracy, then we would expect much better accuracy in the thirtieth eigenvalue for a forty-degree-of-freedom approximation than in the third eigenvalue for an eight-degree-of-freedom approximation, as there are twice as many active degrees of freedom in the first case than in the second. But, instead of this, we find that we typically need <u>many</u> more active degrees of freedom for a given level of accuracy in a higher eigenvalue than in a lower eigenvalue. This supports our hypothesis that the use of orthogonality constraints involving inaccurate computed eigenfunctions is partially responsible for poorer accuracy in the higher eigenvalues.

In the minimization carried out for Λ_2^n, the question becomes one of whether the fact that the eigenfunction used in the orthogonality constraint is inaccurate can affect adversely the accuracy of Λ_2^n. In particular, if the second actual eigenfunction participates in the first computed eigenfunction, it seems likely that the orthogonality constraint will require the second computed eigenfunction to be partially orthogonal to the second actual eigenfunction. To verify whether this is true, we assume that a computed lowest eigenfunction $w_1^n(P)$ has been obtained by the Rayleigh-Ritz method, and we seek to determine the lowest value of Λ_2^n that can be obtained with an "ideal" set of admissible functions, subject to constraints imposed by using the Rayleigh-Ritz method.

Because the set of eigenfunctions for a structure is complete, the first and second computed eigenfunctions $w_1^n(P)$ and $w_2^n(P)$ can be represented in terms of them, as follows:

$$w_1^n(P) = \sum_{i=1}^{\infty} a_i \phi_i(P) \quad , \quad w_2^n(P) = \sum_{i=1}^{\infty} b_i \phi_i(P) \tag{2.5a,b}$$

where we assume that the eigenfunctions $\phi_i(P)$ are normalized so as to satisfy the orthogonality relations

$$(\sqrt{m}\phi_i(P), \sqrt{m}\phi_j(P)) = \delta_{ij} \quad , \quad [\phi_i(P), \phi_j(P)] = \lambda_i \delta_{ij} \tag{2.6a,b}$$

where δ_{ij} is the Kronecker delta. We also assume that $w_1(P)$ and $w_2(P)$ are similarly normalized so that

$$\begin{aligned}(\sqrt{m}w_1^n(P), \sqrt{m}w_1^n(P)) &= (\sqrt{m} \sum_{i=1}^{\infty} a_i \phi_i(P), \sqrt{m} \sum_{j=1}^{\infty} a_j \phi_j(P)) \\ &= \sum_{i=1}^{\infty} a_i^2 = 1\end{aligned} \tag{2.7a}$$

$$\begin{aligned}(\sqrt{m}w_2^n(P), \sqrt{m}w_2^n(P)) &= (\sqrt{m} \sum_{i=1}^{\infty} b_i \phi_i(P), \sqrt{m} \sum_{j=1}^{\infty} b_j \phi_j(P)) \\ &= \sum_{i=1}^{\infty} b_i^2 = 1\end{aligned} \tag{2.7b}$$

If $w_2^n(P)$ is normalized as in Eq. (2.7b), then Λ_2^n is simply

$$\Lambda_2^n = [w_2^n(P), w_2^n(P)] = [\sum_{i=1}^{\infty} b_i \phi_i(P), \sum_{j=1}^{\infty} b_j \phi_j(P)] = \sum_{i=1}^{\infty} b_i^2 \lambda_i \tag{2.8}$$

We know that if Λ_1^n and Λ_2^n are stationary values of Rayleigh's quotient (where $\Lambda_1^n = [w_1^n(P), w_1^n(P)]$), then $w_1^n(P)$ and $w_2^n(P)$ must be orthogonal in both mass-weighted and energy inner products.[20] Therefore the equations

$$\begin{aligned}(\sqrt{m}w_1^n(P), \sqrt{m}w_2^n(P) &= (\sqrt{m} \sum_{i=1}^{\infty} a_i \phi_i(P), \sqrt{m} \sum_{j=1}^{\infty} b_j \phi_j(P)) \\ &= \sum_{i=1}^{\infty} a_i b_i = 0\end{aligned} \tag{2.9a}$$

$$[w_1^n(P),\ w_2^n(P)] = [\sum_{i=1}^{\infty} a_i\phi_i(P),\ \sum_{j=1}^{\infty} b_j\phi_j(P)]$$

$$= \sum_{i=1}^{\infty} a_i b_i \lambda_i = 0 \qquad (2.9b)$$

must be satisfied.

To determine the minimum value that Λ_2^n can reach in a Rayleigh-Ritz approximation, we must minimize $\Lambda_2^n = \sum_{i=1}^{\infty} b_i^2\lambda_i$ over the b_i's, subject to the constraints given by Eqs. (2.7b) and (2.9a,b). Hence, using the Lagrange multipliers p_1, p_2, and p_3, we can write the equations

$$\frac{\partial}{\partial b_j}\left(\sum_{i=1}^{\infty} b_i^2\lambda_i\right) = p_1 \frac{\partial}{\partial b_j}\left(\sum_{i=1}^{\infty} b_i^2 - 1\right) + p_2 \frac{\partial}{\partial b_j}\left(\sum_{i=1}^{\infty} a_i b_i\right)$$

$$+ p_3 \frac{\partial}{\partial b_j}\left(\sum_{i=1}^{\infty} a_i b_i \lambda_i\right) \quad , \quad j = 1,2,... \qquad (2.10)$$

which can be reduced to

$$2b_j\lambda_j = 2p_1 b_j + p_2 a_j + p_3 a_j \lambda_j \quad , \quad j = 1,2,... \qquad (2.11)$$

yielding

$$b_j = \frac{p_2 + p_3\lambda_j}{2(\lambda_j - p_1)}\, a_j \quad , \quad j = 1,2,... \qquad (2.12)$$

Equations (2.7b), (2.9a,b) and (2.12) must be satisfied by the coefficients b_1, b_2... and the Lagrange multipliers p_1, p_2 and p_3. Because there is an infinity of coefficients b_i and an infinite number of Eqs. (2.12), we cannot solve for the minimum value of Λ_2^n in the general case. However, it is clear from Eq. (2.7a) that the coefficients a_i (i = 1,2,...) must approach zero rapidly for increasing i. Indeed, if $\Lambda_1^n = \sum_{i=1}^{\infty} a_i^2\lambda_i$ is reasonably close to λ_1, then the coefficients a_i must approach zero very rapidly as i increases.

Let us examine the case in which a_1, a_2 and a_3 are the only nonzero coefficients a_i. In this case, it is clear from Eq. (2.12) that the minimum possible Λ_2^n occurs when b_1, b_2 and b_3 are the only nonzero coefficients b_i. Solving Eqs. (2.7b) and (2.9), we conclude that

$$b_1 = \frac{a_2 a_3(\lambda_3 - \lambda_2)}{D} \quad , \quad b_2 = -\frac{a_1 a_3(\lambda_3 - \lambda_1)}{D} \quad , \quad b_3 = \frac{a_1 a_2(\lambda_2 - \lambda_1)}{D} \tag{2.13}$$

where

$$D = [a_1^2 a_2^2(\lambda_2 - \lambda_1)^2 + a_2^2 a_3^2(\lambda_3 - \lambda_2)^2 + a_3^2 a_1^2(\lambda_3 - \lambda_1)^2]^{1/2} \tag{2.14}$$

Inserting these values into Eq. (2.8), we find that the lowest value for Λ_2^n that can be obtained by the Rayleigh-Ritz method on the basis of $w_1^n(P)$ is

$$\Lambda_2^n = b_1^2\lambda_1 + b_2^2\lambda_2 + b_3^2\lambda_3 = \lambda_2 + \frac{a_2^2(\lambda_3 - \lambda_2)(\lambda_2 - \lambda_1)(\lambda_2 - \Lambda_1)}{D^2} \tag{2.15}$$

Clearly, as a_2 approaches zero, Λ_2^n approaches λ_2, as anticipated. Hence, the presence of $\phi_2(P)$ in $w_1^n(P)$ limits the accuracy that can be achieved on Λ_2^n. This is also suggested by the fact that Eqs. (2.9) cannot be satisfied when $w_2^n(P) = \phi_2(P)$ (so that $b_2^2 = 1$ and all other b_i's are zero) and a_2 is nonzero. In attempting to calculate Λ_3^n, we expect that its accuracy would be similarly limited by the presence of $\phi_3(P)$ in $w_1^n(P)$ and $w_2^n(P)$, due to the orthogonality constraints. In general, we conclude that the accuracy of computed higher eigenvalues is limited by inaccuracies in the computed lower eigenfunctions. For this reason, it is extremely important that convergence to the lower eigenvalues and eigenfunctions be as rapid as possible. Hence, in assessing the suitability of a given set of admissible functions for estimating a

suitability of a given set of admissible functions for estimating a given higher mode by the Rayleigh-Ritz method, the question is not only whether the set of admissible functions can accurately duplicate that particular mode, but also whether the set can also duplicate all of the modes below that mode extremely well.

To illustrate the above idea, let us consider a uniform bar in axial vibration, where the bar is fixed at one end and free at the other end. The eigenvalues and eigenfunctions satisfy the differential eigenvalue problem

$$-EA \frac{d^2\phi(x)}{dx^2} = \lambda m\phi(x), \quad \phi(0) = 0, \quad \frac{d\phi(L)}{dx} = 0 \tag{2.16}$$

and are given by

$$\lambda_i = \left[\frac{(2i-1)\pi}{2}\right]^2 \frac{EA}{mL^2}, \quad \phi_i(x) = \sqrt{\frac{2}{mL}} \sin \frac{(2i-1)\pi x}{2L}, \quad i = 1,2,... \tag{2.17}$$

respectively. Here EA is the axial stiffness, m is the mass per unit length and L is the length of the bar. If we use the finite element method to approximate the eigensolution and divide the bar into ten linear elements of equal length, we obtain the computed eigenvalues in the third column of Table 2.1. On the other hand, we can approximate each eigenvalue by minimizing Rayleigh's quotient subject to constraints of orthogonality to actual lower eigenfunctions, rather than to computed ones, using the same finite element admissible functions. For the ith eigenvalue, this can be done by obtaining the i-1 exact orthogonality constraints on the vector of nodal displacements in closed form, and generating a basis of n-i+1 independent vectors that satisfy the

constraints exactly. The eigenvalue problem in terms of this reduced basis is solved for the lowest eigenvalue, which is the minimum value of Rayleigh's quotient that can be obtained with the given admissible functions subject to the exact orthogonality constraints. These values are listed in the fifth column of Table 2.1. Because double precision was used and the eigenvalue problems were of order nine or less, we can safely assume that roundoff and truncation errors were insignificant in this comparison. The third and fifth columns of Table 2.1 enable us to see the effect of inaccuracy in orthogonality constraints on eigenvalue accuracy, because the procedure outlined above yields the estimate that would be obtained for each eigenvalue on the basis of accurate lower modes. It also yields the best approximation to a given eigenvalue and eigenfunction permitted by the use of a given set of admissible functions; in general, the Rayleigh-Ritz method does not.

The fourth and sixth columns of Table 2.1 contain the percentage error obtained in the eigenvalues in the third and fifth columns, where the percentage error is defined as the difference between computed and exact eigenvalues divided by the actual eigenvalue. Comparing the error in the second eigenvalue obtained by the two procedures, we see that forty percent of the error obtained by using the finite element method would be eliminated if the lowest mode were computed exactly. The rest of the error is due to the admissible functions' inability to reproduce the second mode accurately. Looking at the error in the higher eigenvalues, we see that the error associated with inaccuracy in the orthogonality constraints is typically of the order of several percent.

From the above discussion, we can see that, for accurate estimates of higher eigenvalues, we must have (1) a sufficient total number of degrees of freedom so that minimization of the highest desired eigenvalue can be carried out with a sufficient number of active degrees of freedom and (2) accurately computed lower modes. We should be able to tell whether inaccuracy of lower modes is inhibiting convergence to higher ones by the number of active degrees of freedom required for a given level of accuracy in different eigenvalues. If the inaccuracy of lower modes is not a problem, all modes should require roughly the same number of active degrees of freedom. Otherwise, many more active degrees of freedom are necessary for higher modes than for lower ones.

This discussion has not yet addressed the key question as to which type of admissible functions is most suitable. In the next section, we examine the differences between the admissible functions used in the h-version and the p-version of the finite element method, as well as the reasons why one type of admissible functions can be expected to give superior results.

2.3 THE h-VERSION AND THE p-VERSION OF THE FINITE ELEMENT METHOD

In the h-version of the finite element method, the model is refined by refining the mesh, so that the element size decreases while the polynomial degree remains the same. In the p-version, the mesh remains unchanged while the polynomial degree in the elements is increased. In the hierarchical p-version, the added admissible functions do not affect previously computed mass and stiffness coefficients, so that the embedding property is preserved. As a result, monotonic convergence is

guaranteed by the inclusion principle.[3] On the other hand, monotonic convergence is not always guaranteed for the h-version.[21]

From a global perspective, an admissible function in the finite element method is nonzero only over a few neighboring elements sharing a common node. In the h-version, as nodes are added to refine the mesh, the elements over which the admissible functions are nonzero become smaller and smaller. By contrast, in the p-version, the added admissible functions are nonzero over elements from the original mesh, which never decrease in size. Hence, the added degrees of freedom in the p-version provide information about the displacement over a greater portion of the structure than the added degrees of freedom in the h-version, and do it with less higher mode participation, as it takes more participation of higher modes to represent admissible functions which are nonzero over smaller areas. In this regard, the p-version is similar to the classical Rayleigh-Ritz method, in which all admissible functions are global functions, i.e., they are nonzero over the entire domain of the structure. Because the classical Rayleigh-Ritz method generally requires far fewer degrees of freedom than the h-version of the finite element method for a given level of accuracy and because the h-version facilitates the analysis of complex structures with components of different types and material properties, the p-version clearly combines the most attractive features of both the classical Rayleigh-Ritz method and the h-version of the finite element method.

In yet another regard, the p-version is superior to both the h-version and the classical Rayleigh-Ritz method. The actual eigenfunctions satisfy force and moment continuity within the structure, even

at material discontinuities and at junctions of different components. This can be seen by considering an infinitesimal region from any location in the structure. If the net force and moment on the region is not exactly zero, implying lack of force and moment continuity, then as the mass of the region approaches zero, its acceleration approaches infinity, which is clearly not possible in an eigenfunction. In the classical Rayleigh-Ritz method, the admissible functions are typically continuous in all derivatives, which leads to force and moment discontinuities at material discontinuities. On the other hand, the h-version of the finite element method calls for refinement by subdividing elements over which the material properties are continuous. Because the finite element admissible functions are not continuous in derivatives higher than the derivatives essential for the problem, force and moment discontinuities are introduced when elements with continuous material properties are subdivided. By contrast, the p-version calls for the structure to be divided into elements over which the material properties are continuous. At boundaries between elements, higher derivatives can be discontinuous, so that forces and moments can be continuous. As the model is refined, hierarchical functions continuous in all derivatives are added over elements where material properties are continuous. Hence, the p-version allows higher derivatives to be discontinuous at material discontinuities, thus permitting force and moment continuity, and it preserves force and moment continuity where material properties are continuous.

The above arguments support the superiority of the p-version over the h-version, in agreement with the findings of Babuska et al., who

concluded that when convergence is asymptotic p-version convergence cannot be slower than h-version convergence, provided that mesh refinement is quasiuniform.[2] Because non-quasiuniform mesh refinement in general requires an adaptive approach,[2] and an adaptive approach would be considerably more difficult to employ in the simultaneous convergence toward a number of eigenvalues and eigenfunctions than in a single-solution problem, we must be content with the p-version as the most promising approach to eigenvalue estimation by means of the finite element method. In this approach, we simply divide the domain of the structure into a sufficient number of elements to describe its geometry, and refine the model by means of hierarchical functions until we obtain the desired level of accuracy. This assumes that the geometry of the structure can be described accurately in both versions of the finite element method.

2.4 NUMERICAL EXAMPLES

In the first example, we seek the eigenvalues of a stepped cantilever beam consisting of four segments of unit length and having the material properties shown in Figure 2.1. We propose to examine the eigenvalue convergence rates as we refine the model first by means of the h-version, and then by means of the p-version. In the h-version, we add degrees of freedom by simply subdividing the segments into more beam elements of equal length while keeping the same cubic basis functions for all elements. In the p-version, we begin with one element for each of the four segments of the beam, and then refine each element by adding up to ten hierarchical functions of the form

$$\psi_5 = a_5\xi^2(1 - \xi)^2$$

$$\psi_6 = a_6\xi^2(\tfrac{1}{2} - \xi)(1 - \xi)^2$$

$$\psi_7 = a_7\xi^2(\tfrac{1}{3} - \xi)(\tfrac{2}{3} - \xi)(1 - \xi)^2 \qquad (2.18)$$

$$\vdots$$

$$\psi_{4+j} = a_{4+j}\xi(1 - \xi)\prod_{i=0}^{j}(\tfrac{i}{j} - \xi),$$

where $\xi = (x - x_i)/(x_{i+1} - x_i)$, in which x_i and x_{i+1} are node locations. Of course, the number of elements remains the same. The coefficients $a_5, a_6, \ldots, a_{4+j}$ are scaling factors used to make the element mass matrices approximate the unit matrix closely, to prevent these matrices from becoming ill-conditioned. In using both the h-version and the p-version, the level of refinement was kept nearly constant throughout the structure, and the total number of degrees of freedom was increased from eight to forty-eight.

Figures 2.2 and 2.3 show the convergence rates obtained with the h-version and the p-version, respectively. Each line plotted on the graphs corresponds to the convergence path for one of the lowest twenty eigenvalues. The error for each eigenvalue is plotted on a logarithmic scale along the vertical axis, and the number of active degrees of freedom (the total number of degrees of freedom minus the number identifying the eigenvalue) is plotted on a logarithmic scale on the horizontal axis. The actual eigenvalues for this system can be obtained using a transfer matrix approach.

Clearly, the p-version exhibits faster convergence to the actual eigenvalues. A closer examination permits us to observe some

interesting characteristics of the convergence process. In both cases, there is a clear distinction between the nearly horizontal preasymptotic convergence with only a few active degrees of freedom, and the asymptotic range where the logarithm of the error, plotted against the logarithm of the number of active degrees of freedom, decreases more rapidly. In the p-version, this distinction is so great that the plot is reminiscent of waterfalls, with a nearly level "flow" preceding a precipitous drop. In the h-version, however, the distinction is not so marked, as the asymptotic convergence is much slower. A final observation is that in the h-version the convergence paths are roughly parallel in the asymptotic range, but spaced apart, so that more active degrees of freedom are needed to compute each successive eigenvalue to within a given level of accuracy. This indicates that the constraint of orthogonality to inaccurate lower modes is inhibiting convergence, as discussed earlier. By contrast, in the p-version, there is much less spacing between the convergence paths, indicating that approximately the same number of active degrees of freedom is required for each eigenvalue. We conclude that convergence to lower modes must be so rapid that inaccuracy in the orthogonality constraints is not inhibiting convergence significantly.

The fact that in the h-version an increasingly large number of active degrees of freedom is required for higher eigenvalues has profound implications. It suggests that sufficiently accurate estimates of higher eigenvalues may be beyond reach using the h-version of the finite element method for structures in which there can be significant participation of the higher modes. On the other hand, such higher eigenvalues

may be within easy reach using the p-version, as fewer active degrees of freedom are required for relatively accurate eigenvalues. Indeed, in this example, we found that when forty-four degrees of freedom were used, twenty eigenvalues were found to be accurate to three decimal places. This means that 45% of the computed eigenvalues were exact for all practical purposes. This level of computational accuracy is very uncommon in vibrations problems.

Although it is instructive to plot the convergence paths in Figs. 2.2 and 2.3 on logarithmic scales, because we are studying asymptotic behavior, it is important to note that such plots can be misleading representations of the computational effort involved. Indeed, because the logarithmic scale is more compressed as the number of active degrees of freedom increases, it may appear that additional degrees of freedom make little difference in the amount of computational effort required. In fact, the opposite is true: additional degrees of freedom add much more substantially to the computational effort required when the number of degrees of freedom is higher. For this reason, we see that the p-version exhibits performance far superior to that of the h-version in terms of the amount of computational effort required, perhaps to a larger extent than the plots in Figs. 2.2 and 2.3 may suggest.

As a second example, we consider a rectangular membrane sixteen units wide and twelve units long, with unit mass and unit tension in all directions. For the h-version we used linear, quadratic and cubic interpolation functions in conjunction with triangular elements. For the p-version, we used only eight triangular elements with up to quintic interpolation functions. With ξ_1, ξ_2 and ξ_3 as the standard linear

interpolation functions, the quadratic element was formed by adding three hierarchical functions, a typical one being

$$\psi_4 = a_4\xi_2\xi_3 \tag{2.19}$$

The cubic element was formed by adding three hierarchical functions of the form

$$\psi_7 = a_7\xi_2(\xi_2 - \xi_3)\xi_3 \tag{2.20}$$

and one hierarchical function of the type

$$\psi_{10} = a_{10}\xi_1\xi_2\xi_3 \tag{2.21}$$

For the quartic element, three functions of the form

$$\psi_{11} = a_{11}\xi_2(\xi_2 - 2\xi_3)(\xi_3 - 2\xi_2)\xi_3 \tag{2.22}$$

and two functions of the form

$$\psi_{14} = a_{14}\xi_1^2\xi_2\xi_3 \tag{2.23}$$

were added. Note that ψ_{10} and ψ_{14} are characterized by the fact that they are zero on the boundaries of the element. Finally, for the quintic element, three more functions with nonzero values on element sides and three more functions with a value of zero on the boundaries were added, for a total of twenty-one element degrees of freedom. As in the case of the beam element, all hierarchical functions were scaled to yield well-conditioned element mass matrices. In this two-dimensional case, care must be taken to preserve interelement continuity, because we were not able to choose a complete set of hierarchical functions that reduce to zero on element boundaries, as in the one-dimensional case. Continuity was preserved by adding "nodes" on element midsides corresponding to all hierarchical functions not equal to zero on element boundaries. Functions such as ψ_{10} and ψ_{14} could be treated as "nodeless".

Figures 2.4, 2.5 and 2.6 show the eigenvalue convergence paths for the h-version using linear, quadratic and cubic elements. Figure 2.7 shows the results for the p-version with up to quintic elements. In all cases, the maximum number of degrees of freedom was about eighty. From Fig. 2.4 it is clear that linear elements do not offer satisfactory convergence, especially by comparison with higher-order elements, and Figure 2.5 indicates that quadratic elements do not fare much better. The cubic elements used for Fig. 2.6 perform reasonably well on a few eigenvalues, but not as well as the elements used in the p-version for Fig. 2.7. Qualitatively, the features of the comparison between convergence in the h-version and in the p-version are very similar to those in the first example, the main difference being that more degrees of freedom are required for the two-dimensional problem. Again we see that in the h-version more active degrees of freedom are required for successive eigenvalues, while this effect is minimized in the p-version, indicating that inaccuracy in orthogonality constraints inhibits convergence much less in the p-version.

2.5 CONCLUSIONS

Applications of the finite element method to vibrations problems differ from static applications in that the interest lies in many solutions rather than in a single solution. To explain the decrease in accuracy of higher eigenvalues, we can recast the determination of stationary values of Rayleigh's quotient as a series of successive minimizations of Rayleigh's quotient subject to orthogonality constraints. For a given computed eigenvalue, there are two ways in

which this characterization differs from the analogous successive minimization characterization of the actual eigenvalues. The first difference is that the number of "active" degrees of freeedom in the minimization process is finite for a given computed eigenvalue, and the number of active degrees of freedom decreases for higher eigenvalues; the number is infinite for actual eigenvalues. The second is that higher eigenfunctions are constrained to be orthogonal to computed, rather than actual, lower eigenfunctions.

We can expect convergence in each successive minimization to an eigenvalue to be similar to convergence to the minimum potential energy in static applications of the finite element method. Hence, the p-version exhibits faster convergence to actual eigenvalues than the h-version, where the convergence is a function of the number of active degrees of freedom. However, the orthogonality constraints determine the values to which the computed eigenvalues are converging in each minimization, and these values are higher than the actual eigenvalues in general, due to inaccuracy in the lower computed eigenfunctions. For this reason, rapid convergence to lower eigenfunctions is extremely important in vibrations applications of the finite element method, so that convergence to actual higher eigenvalues will be inhibited as little as possible by inaccuracy in the orthogonality constraints.

The difference between the h-version and the p-version amounts to different choices of admissible functions used in the Rayleigh-Ritz method. For reasons explained above, admissible functions of the p-version are more suitable than those of the h-version. In the numerical examples presented, convergence in the p-version was significantly

better than convergence in the h-version, especially for higher eigenvalues. Plots of eigenvalue convergence paths demonstrate that in the h-version, the number of active degrees of freedom required for acceptable accuracy continues to increase for progressively higher eigenvalues, while in the p-version the number increases at a much smaller rate.

In the analysis of very flexible large structures, the computation of the response is likely to require the inclusion of a larger number of modes than for ordinary structures. For this reason, we must be able to compute a larger number of higher modes with greater accuracy. The results of this paper indicate that this is feasible using the p-version of the finite element method, while the computational effort required by the h-version may be prohibitive. In some applications, particularly in the control of flexible structures, an accurate knowledge of the structure's eigenfunctions is required. Due to the stationarity of Rayleigh's quotient in the neighborhood of an eigenfunction, the error in the eigenfunction is ordinarily one order of magnitude larger than the error in the eigenvalue. Hence, for satisfactory eigenfunction accuracy, eigenvalue errors that are not very small, say errors above one or two percent, may be unacceptable in some higher modes. For this reason, the p-version shows greater promise in modeling for structural control as well.

Table 2.1 - Eigenvalue Error Due to Orthogonality Constraints

Mode Number	Actual Eigenvalues	Finite Element Computed Eigenvalues	Percentage Error	Finite Element Eigenvalues with Ideal Orthogonality Constraints	Percentage Error
i	λ_i	Λ_i^{10}		Λ_i	
2	22.20	22.62	1.86	22.44	1.09
3	61.68	64.91	5.24	64.11	3.93
4	120.90	133.49	10.42	131.25	8.56
5	199.85	234.71	17.44	229.61	14.89
6	298.55	376.36	26.06	366.01	22.59
7	416.99	564.28	35.32	544.87	30.67
8	555.16	792.22	42.70	759.03	36.72
9	713.07	1023.09	43.48	974.85	36.71
10	890.73	1178.11	32.26	1132.42	27.13

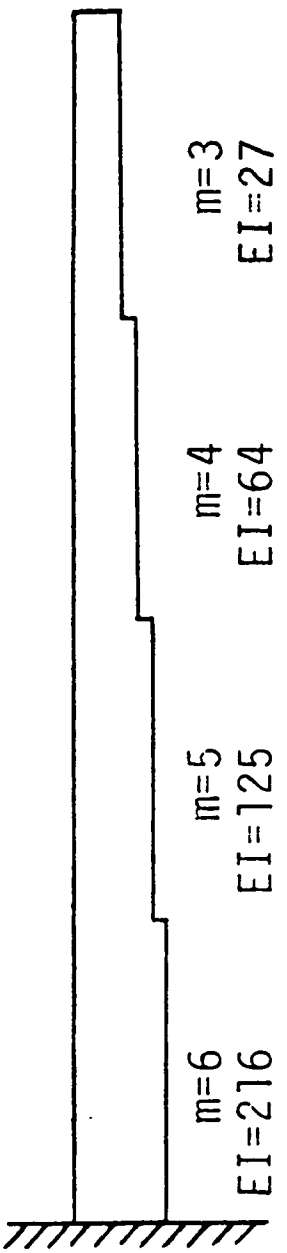

Figure 2.1. Stepped cantilever beam in flexural vibration.

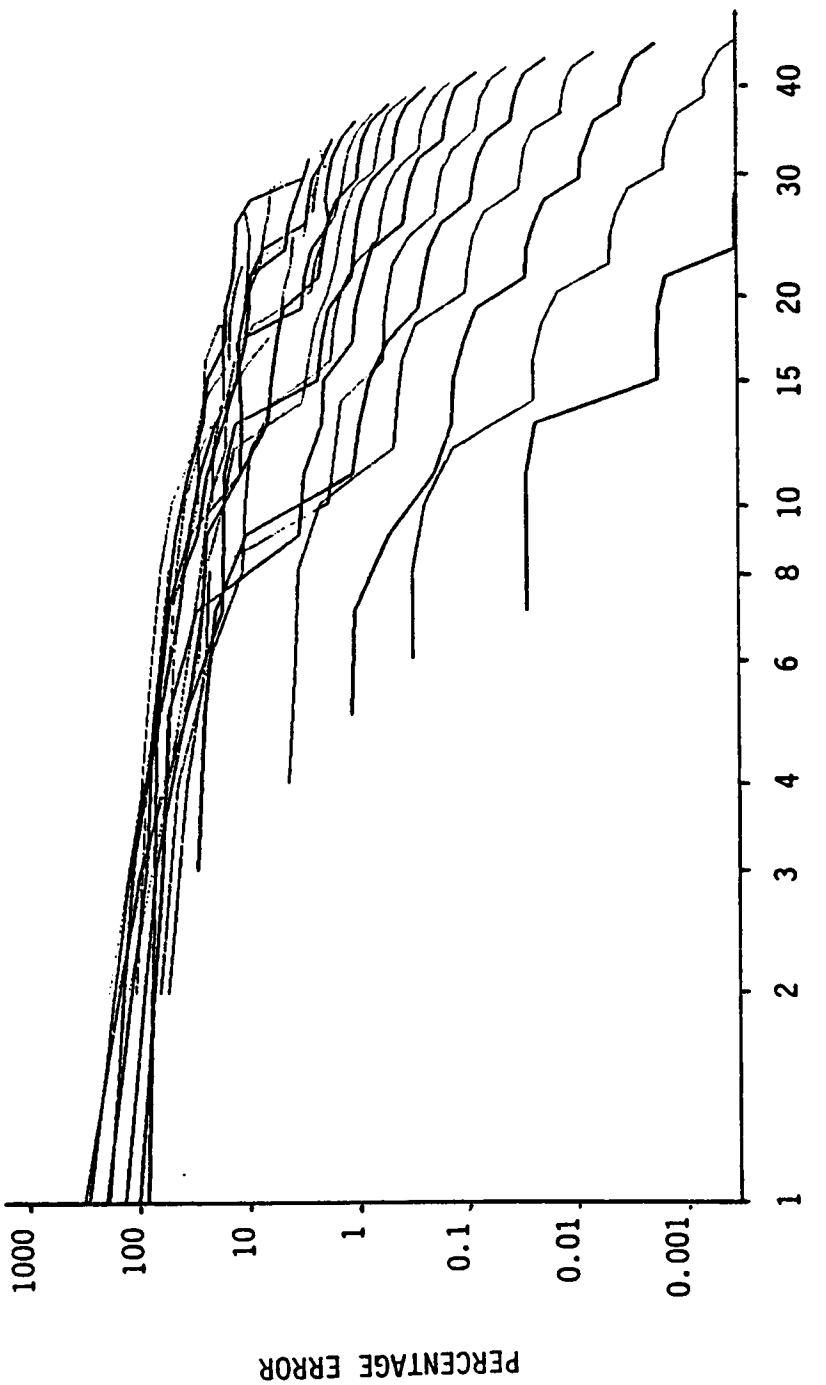

Figure 2.2. Logarithmic plots of eigenvalue convergence paths for the beam in Fig. 2.1 using the h-version.

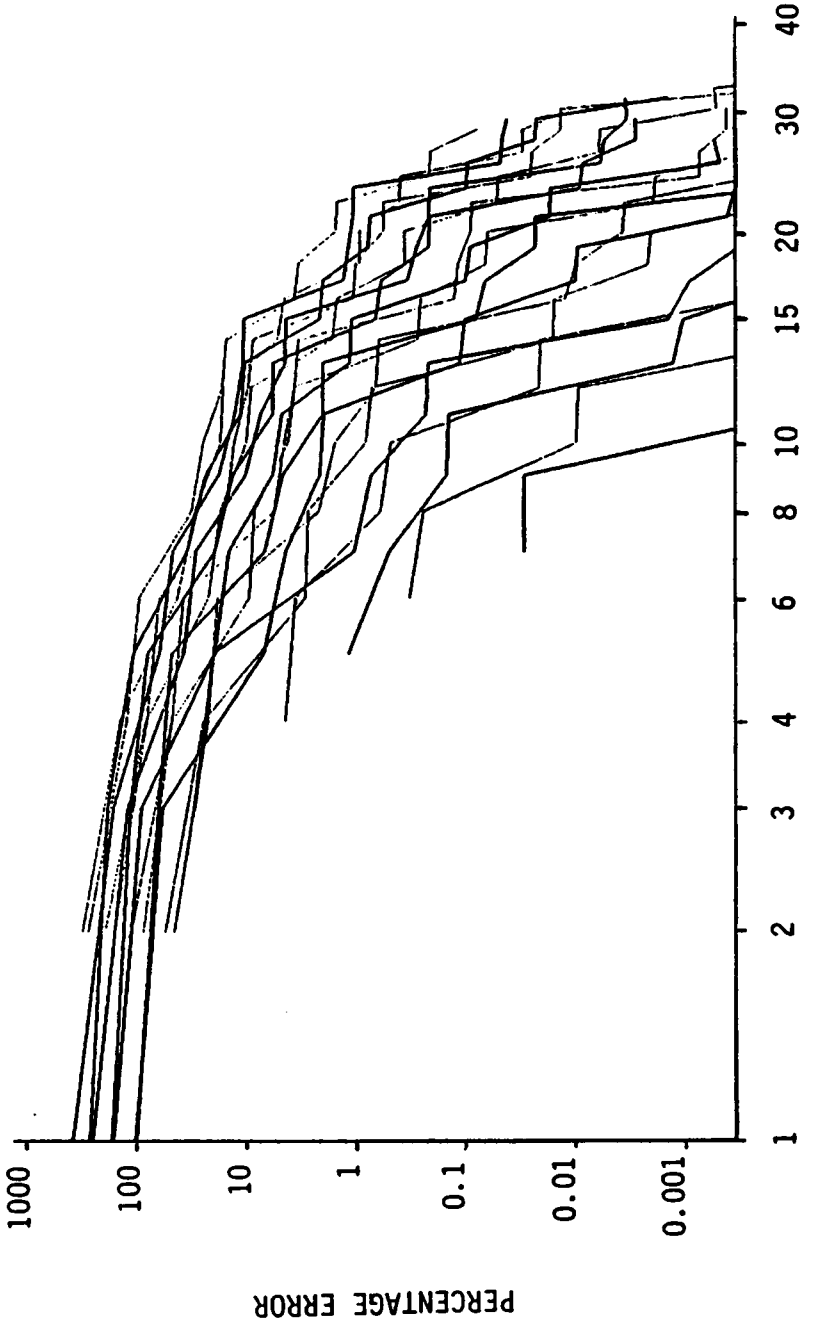

Figure 2.3. Logarithmic plots of eigenvalue convergence paths for the beam in Fig. 2.1 using the p-version.

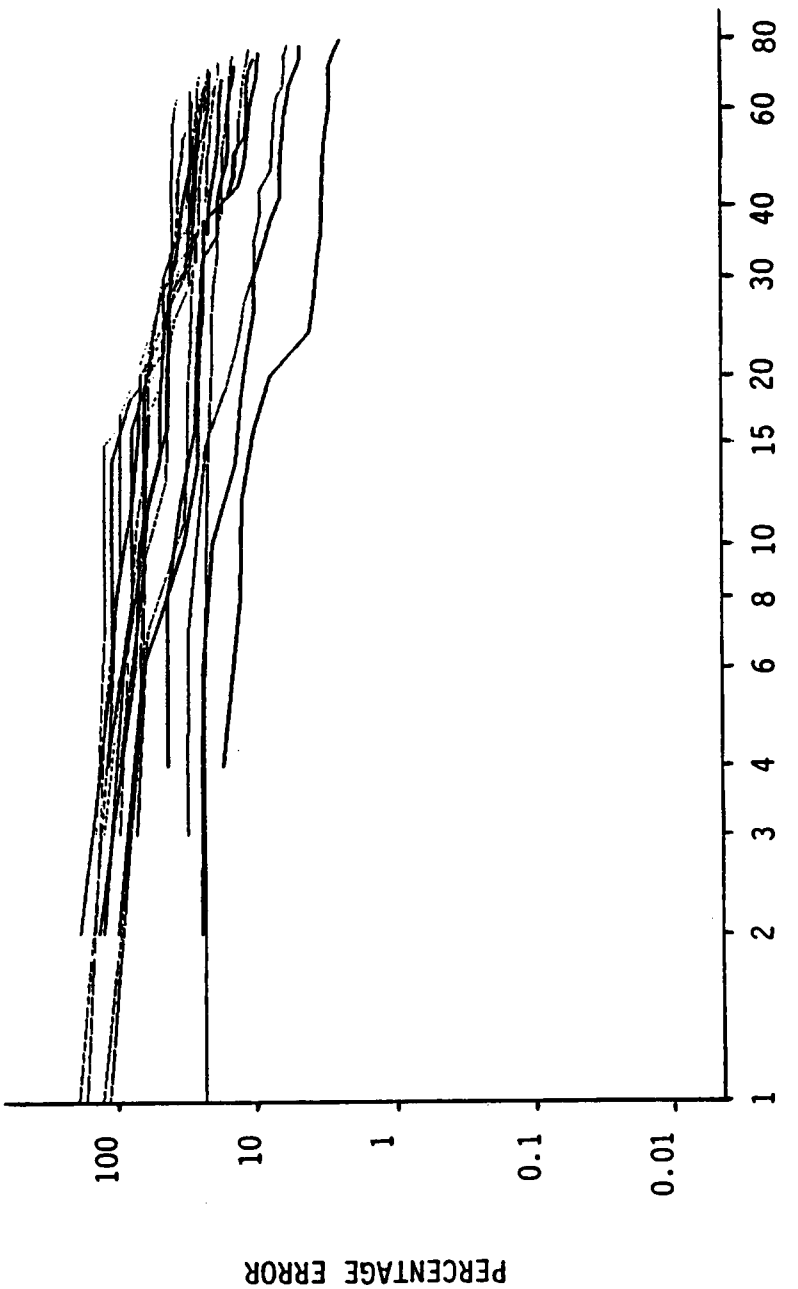

Figure 2.4. Logarithmic plots of eigenvalue convergence paths for a rectangular membrane using the h-version with linear elements.

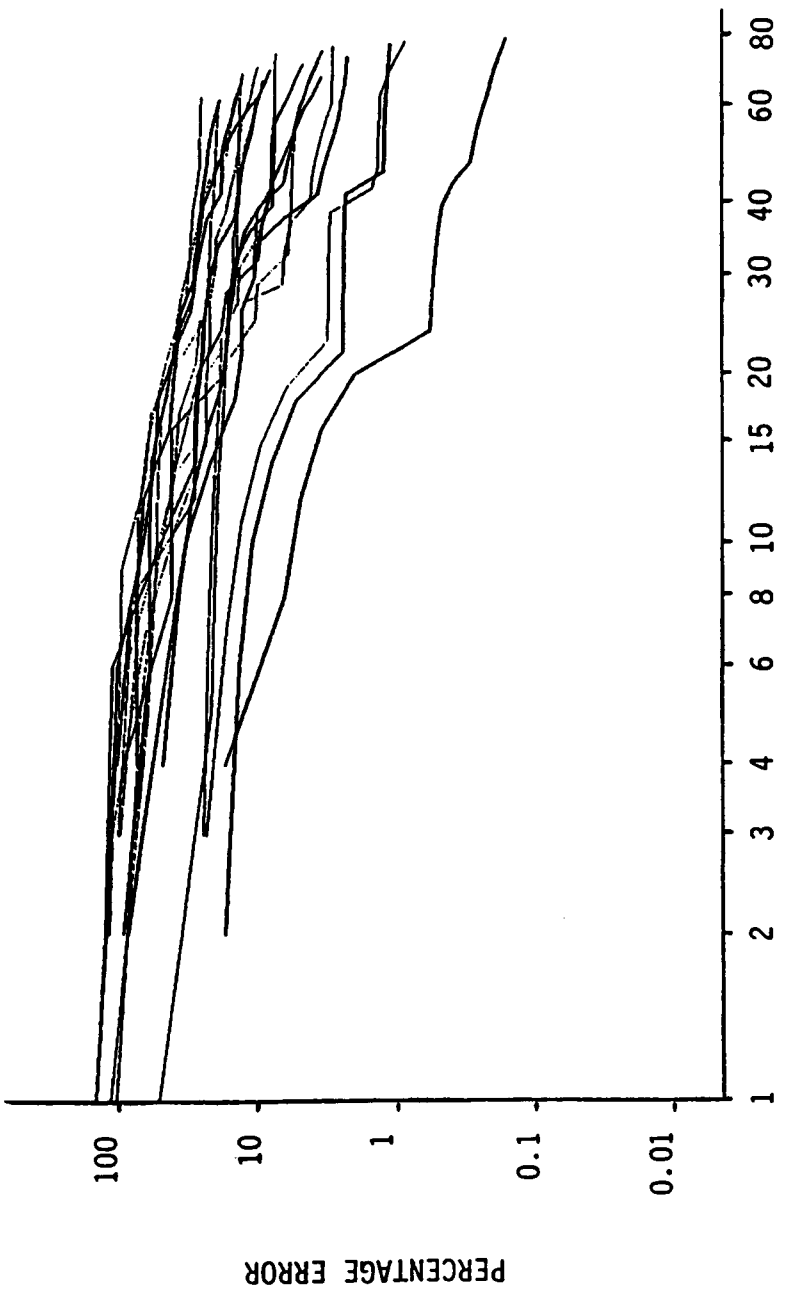

Figure 2.5. Logarithmic plots of eigenvalue convergence paths for a rectangular membrane using the h-version with quadratic elements.

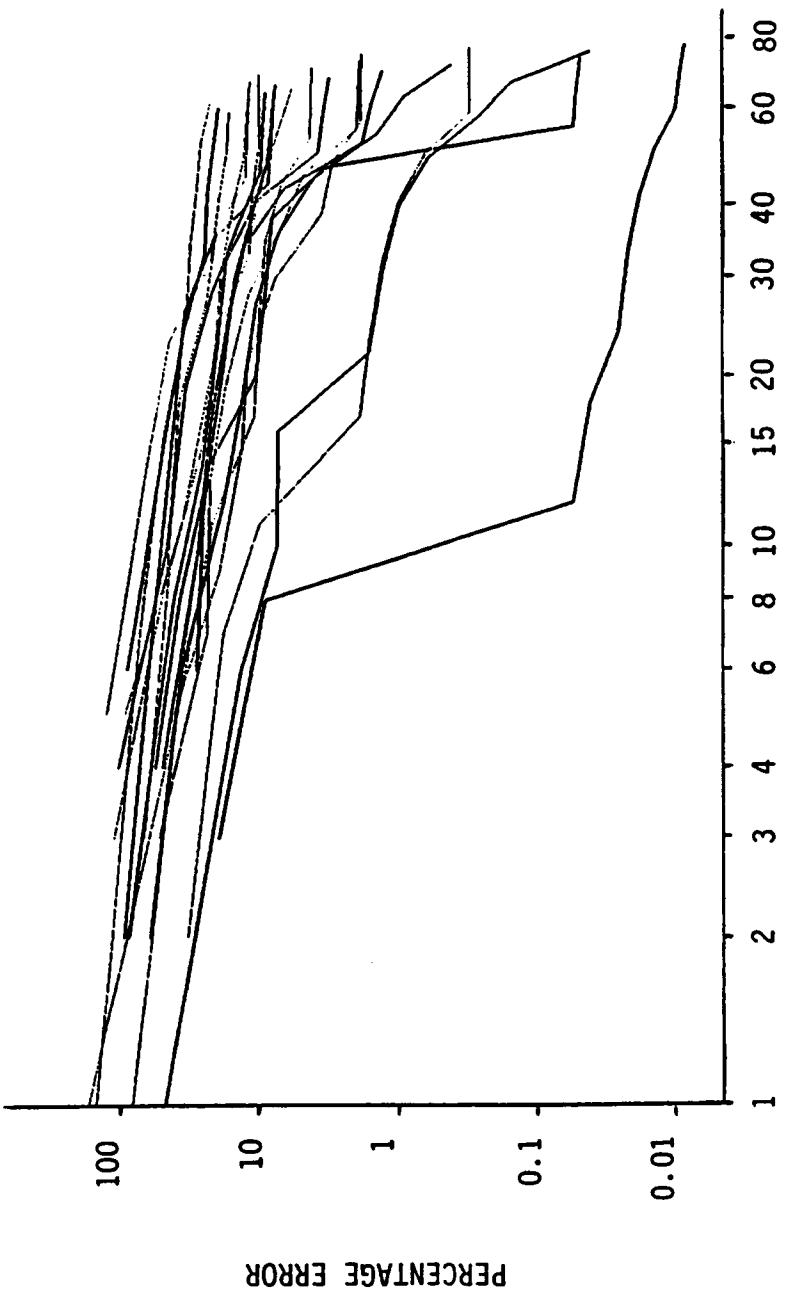

Figure 2.6. Logarithmic plots of eigenalue convergence paths for a rectangular membrane using the h-version with cubic elements.

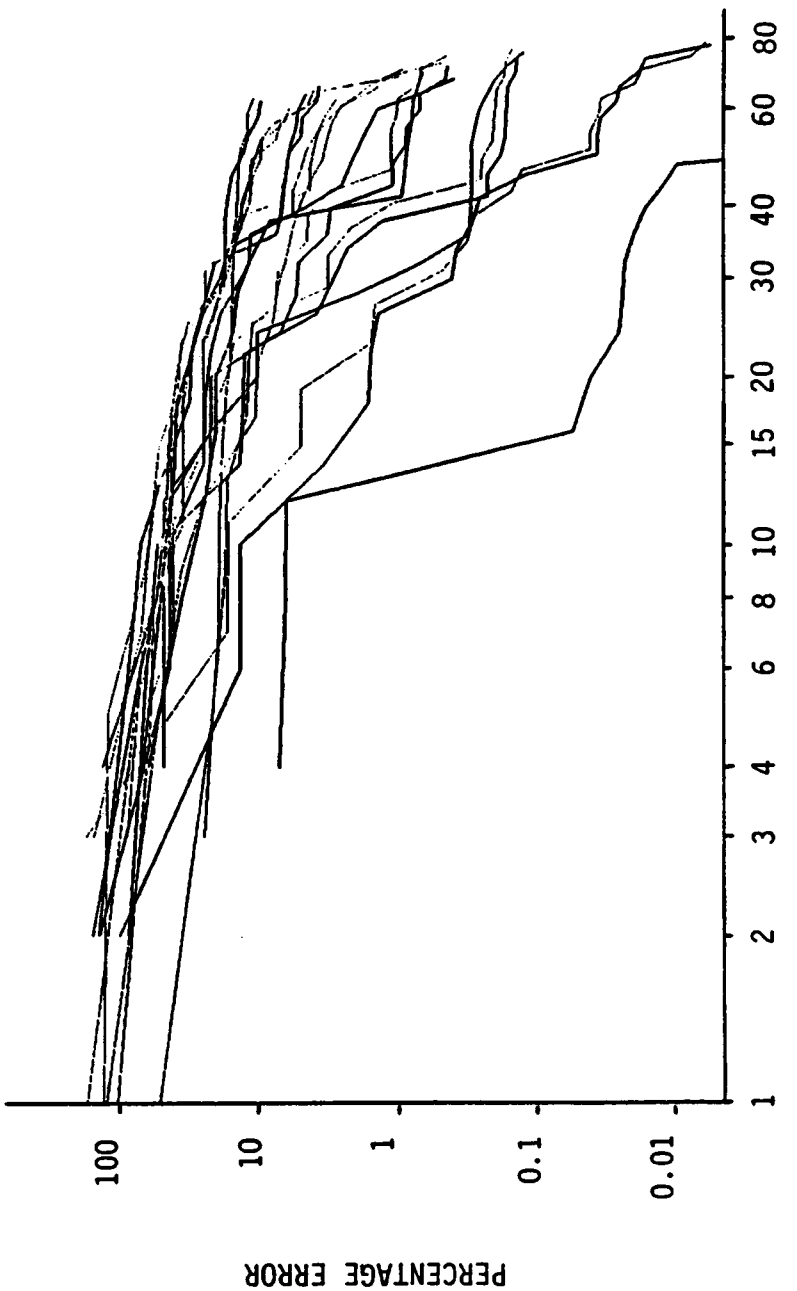

Figure 2.7. Logarithmic plots of eigenvalue convergence paths for a rectangular membrane using the p-version with up to quintic elements.

Chapter 3

SUBSTRUCTURING WITH SELF-REFINING SUPER-ELEMENTS

3.1 INTRODUCTION

In the past two decades, the dynamic analysis of large structures has received considerable attention. A number of methods have been developed for analyzing the vibration of complex structures. Of these, many fall into one of two classifications. In the component mode synthesis methods, a structure is divided into substructures and each substructure is modeled in terms of a few "component modes," or substructure displacement functions. These reduced substructure models are coupled together to form a model for the total structure, and the resulting eigenvalue problem is of much lower order than if reduction had not taken place at the substructure level.[8-16] In the subspace iteration method, the structure model is not reduced, but in a procedure related to vector iteration in the power method, a set of eigenvectors and eigenvalues corresponding to the lower modes of the structure is obtained.[5,6,22]

In the component mode synthesis methods, the accuracy of the results depends on the quality of the substructure models and on how they are coupled together. In order to ensure that the substructure models will adequately represent the motion of the substructures as part of the total structure, substructure displacement functions of several types have been used. "Constraint modes" are static responses to displacements at the interfaces between substructures, and they include the set of substructure rigid-body modes as a subset.[9] "Normal modes"

are the natural modes of vibration of the substructures with interfaces either fixed, free, or loaded in some manner to simulate the effect of the rest of the structure.[9-11] Of the normal modes used, the loaded-interface type has been shown to give superior results,[11] but the question of what the optimal interface loadings are remains. Other component modes which are directly related to the solution of some substructure response or eigenvalue problem include "attachment modes,"[12] "inertia relief modes,"[13,14] and "residual attachment modes."[12-14] "Admissible vectors" contain coefficients of local finite element admissible functions and represent substructure admissible functions which usually have no direct physical significance, except that they are often chosen based on the modes of a simpler structure similar to the one being analyzed.[15,16] Admissible vectors appear to require less computational effort to generate, but for complicated structures the selection of a suitable set may present difficulties. Regardless of the method used to generate the component modes, a poor selection can result in a model that is stiffer than the actual structure, so that structure modes can be inaccurately predicted or even skipped altogether.

The object when selecting component modes is to choose the smallest set that will yield the greatest accuracy in the most structure modes. With an ideal set, only as many component modes are needed as the number of structure modes sought. Of course, such a set cannot be selected for a substructure without knowing how it will interact with the rest of the structure. Frequently in component mode synthesis, the component modes are chosen to give as complete a set of displacement degrees of freedem as possible to the substructures, independent of the properties of the

rest of the structure. While substructure independence does have some value, taking an early estimate of the interaction with the structure into account when generating component modes can improve their quality, so that fewer of them will yield better results with a smaller structure eigenvalue problem. The method of this chapter has this feature, and the numerical results attest to the merit of such an approach.

Regarding the coupling of substructures, although some may have overlooked this, Meirovitch and Hale have pointed out that the practice of enforcing geometric compatibility between substructures at only a finite number of points on substructure interfaces can cause the computed structure eigenvalues to cease to be upper bounds for the actual eigenvalues.[15] This is because geometric compatibility may not be satisfied at some points on the interfaces, particularly if the interfaces are composed of lines or surfaces, which contain an infinite number of points. For this reason, they have introduced the concept of the "intermediate structure," which is the structure whose interface compatibility only approximates that of the real structure. Because the intermediate structure model is more flexible than the actual structure, at least at interfaces, its eigenvalues can be lower than those of the actual structure, so that the accuracy of the modal estimates obtained can again become uncertain.

By comparison with the component mode synthesis methods, the subspace iteration method can be a safer approach to the analysis of large structures. In this method, the structure is treated as a whole and in the iteration process, a set of initial trial vectors for the entire structure converges to the set of lower modes for the structure. The

method has been mechanized so that no intuition is required on the part of the analyst to generate a good set of initial trial vectors. However, large problems may require a great deal of data transfer in and out of core, greatly increasing the computational time required.

In a recent paper, Hale and Meirovitch have developed a substructure synthesis method that allows the subspace iteration method to be carried out on the substructure level.[16] An initial set of admissible vectors is chosen for each of the substructures, and the reduced structure eigenproblem is assembled and solved for estimates of the lower structure modes. Then each set of substructure admissible vectors is improved by calculating the dynamic response to the interface forces exerted by the rest of the structure as it vibrates in the computed lower modes. This technique makes the component mode synthesis approach less sensitive to the quality of initial substructure representation, as the component modes are iteratively improved. It also reduces the problems associated with the subspace iteration method for large structures, as the size of the structure eigenproblem is greatly reduced, and the substructures can be processed independently and in parallel. However, some problems still remain. In the paper by Hale and Meirovitch, the concept of the "intermediate structure" is still used, as interface compatibility between substructures is not exactly satisfied. Also, the explanation of the method and the computational procedure are quite complicated and cumbersome. The initial admissible vectors are chosen to resemble the modes of a simpler structure similar to the structure being analyzed, but for more complicated structures it may be more difficult to generate a suitable set of initial admissible

vectors. For this reason, this technique seems difficult to automate completely, as a considerable amount of intuition on the part of the analyst may still be required.

In this chapter, a different method is presented which carries out the subspace iteration method on the substructure level. This method does not require the concept of the "intermediate structure," as it provides a technique in which interface compatibility can be satisfied as well as is possible when modeling a given structure as a whole using the finite element method. Ordinarily, this can be done exactly, even when interfaces are lines or surfaces, although in some circumstances it may not prove convenient. The formulation and computational procedure for this method are much more straightforward than for the method of Hale and Meirovitch,[16] and the structure eigenvalue problem is smaller. Again, the substructures can be processed independently and in parallel. Finally, this method requires no intuition on the part of the analyst as it can be fully automated, generating its own initial trial vectors. In fact, it would be a relatively simple matter to implement the method in a form in which an analyst could simply enter data describing the structure as a whole, without being concerned with any of the substructuring details.

3.2 ENSURING EXACT INTERFACE COMPATIBILITY

In the Rayleigh-Ritz method, of which the finite element method can be considered a subset, computed eigenvalues are guaranteed to be upper bounds for structure eigenvalues if admissible functions are continuous in up to the (p-1)st derivative wherever the differential stiffness

operator is of order 2p in space.[20] In the finite element method, when conforming elements are used, the element interpolation functions are selected in such a way that this continuity will be ensured between elements.

The displacement in an element is expressed in terms of interpolation functions multiplied by nodal displacement degrees of freedom. Each of the element interpolation functions has a value of one in its corresponding nodal degree of freedom and a value of zero in all of the element's other nodal degrees of freedom, so that the element nodal degrees of freedom can vary arbitrarily and independently. Further, in the case of conforming elements, the interpolation functions must satisfy the requirement that sharing the nodal degrees of freedom associated with the boundary between two neighboring elements will automatically ensure the continuity of up to the (p-1)st displacement derivative everywhere on the boundary between these elements. For a structure modeled in terms of conforming elements, sharing nodal degrees of freedom in this manner ensures exact displacement continuity throughout the model, and it also makes assembling the structure mass and stiffness matrices a simple matter of superimposing element mass and stiffness matrices.

We exploit these properties of the conforming elements used to model a structure in order to represent substructures as conforming super-elements which can be used to model the same structure. For each substructure, we generate substructure interpolation functions in terms of element interpolation functions, with each substructure interpolation function satisfying the requirements above for conforming element inter-

polation functions. The super-elements that we construct to represent substructures have the property that when nodal degrees of freedom are shared between substructures, exact interface compatibility is ensured throughout the structure model. Again, structure mass and stiffness matrices are formed by simply superimposing super-element mass and stiffness matrices, but because these are greatly reduced in size, the structure model is much smaller. We also make use of the fact that, in the hierarchical finite element method for one-dimensional elements, elements can be refined by adding hierarchical interpolation functions which go to zero in up to the (p-1)st displacement derivative at element boundaries.[23] These functions clearly do not affect inter-element compatibility, but adding displacement degrees of freedom of this type to elements can improve their performance substantially. Hence a similar approach will allow us to add displacement degrees of freedom to the substructure models.

We assume that we are given a conforming finite element model of a structure that is composed of substructures. Within a substructure, the finite element representation of the displacement is given by

$$\underset{\sim}{u}(P,t) = \sum_{i=1}^{n_s} \underset{\sim}{\phi}_i(P) a_i(t) = \Phi(P)\underset{\sim}{a}(t) \tag{3.1}$$

in which $\underset{\sim}{u}(P,t)$ is a vector of displacements in the three Cartesian directions as a function of position and time, $\Phi(P)$ is a matrix of interpolation functions, $\underset{\sim}{a}(t)$ is a vector of nodal degrees of freedom, and n_s is the total number of nodal degrees of freedom in the substructure. If only m_s of these degrees of freedom are shared with the

rest of the structure at substructure interfaces, we can partition as follows:

$$\underset{\sim}{u}(P,t) = \sum_{i=1}^{m_s} \underset{\sim}{\phi}_i(P)a_i(t) + \sum_{i=m_s+1}^{n_s} \underset{\sim}{\phi}_i(P)a_i(t) \qquad (3.2)$$

$$= [\Phi_1(P) \vdots \Phi_2(P)] \begin{bmatrix} \underset{\sim}{a}_1(t) \\ \underset{\sim}{a}_2(t) \end{bmatrix}$$

in which $\underset{\sim}{a}_1(t)$ contains nodal degrees of freedom that are shared with the rest of the structure, and $\underset{\sim}{a}_2(t)$ contains nodal degrees of freedom which are internal to the substructure. If the structure model were not divided into substructures, displacement continuity at the locations of the substructure interfaces would be ensured by requiring that the elements on either side of the interfaces share the nodal degrees of freedom $\underset{\sim}{a}_1(t)$. Therefore, in constructing reduced substructure models, we must make sure that $\underset{\sim}{a}_1(t)$ is still shared with the rest of the structure model so that exact displacement continuity will continue to be ensured everywhere on the interfaces between substructures. We note that the interface compatibility does not depend on the entries in $\underset{\sim}{a}_2(t)$.

We can express the displacement in the substructure in terms of a reduced set of interpolation functions, each of which is a linear combination of the finite element interpolation functions. Thus the set of substructure interpolation functions $\Psi(P)$ is of the form

$$\Psi(P) = \Phi(P)C \qquad (3.3)$$

in which C is a rectangular matrix of coefficients having n_s rows. If we wish to preserve displacement continuity at the interfaces, we must have a set of functions $\Psi_1(P)$ equal in number to the set of functions $\Phi_1(P)$, which will share nodal degrees of freedom $\underset{\sim}{a}_1(t)$ with the rest of

the structure as the functions in $\Phi_1(P)$ do in the full finite element model. The functions $\Psi_1(P)$ must have the same displacement properties at the interfaces that the functions in $\Phi_1(P)$ have. Because the functions in $\Phi_2(P)$ do not affect displacement continuity at the interfaces, they can participate arbitrarily in $\Psi_1(P)$. The remaining functions $\Psi_2(P)$ in $\Psi(P)$ must not affect interface compatibility, so they must consist entirely of the functions in $\Phi_2(P)$. Hence, if we partition Eq. (3.3) in the form

$$\Psi(P) = [\Psi_1(P) \,\vdots\, \Psi_2(P)] = [\Phi_1(P) \,\vdots\, \Phi_2(P)] \left[\begin{array}{c:c} C_{11} & C_{12} \\ \hdashline C_{21} & C_{22} \end{array}\right] \tag{3.4}$$

we find that C must have the form

$$C = \left[\begin{array}{c:c} C_{11} & C_{12} \\ \hdashline C_{21} & C_{22} \end{array}\right] = \left[\begin{array}{c:c} I & 0 \\ \hdashline C_{21} & C_{22} \end{array}\right] \tag{3.5}$$

where C_{21} and C_{22} are arbitrary. It can be easily verified that the functions in $\Psi_1(P)$ satisfy the requirements for conforming element interpolation functions at the substructure interfaces. Also, the functions in $\Psi_2(P)$ satisfy the requirements for hierarchical functions mentioned above. Hence, with this super-element approach, we can allow a given set of displacement degrees of freedom for substructures while ensuring exact interface compatibility throughout the structure, so that the "intermediate structure" concept can be discarded. Note that this requires discretization of the entire structure with conforming finite elements. For any other discretization procedure in the context of the component mode synthesis method, the intermediate structure concept remains valid.

In terms of the substructure interpolation functions in $\Psi(P)$, the displacement is represented in the substructure in the form

$$\underset{\sim}{u}(P,t) = \Psi(P)\underset{\sim}{b}(t) = [\Psi_1(P) \,\vdots\, \Psi_2(P)] \begin{bmatrix} \underset{\sim}{b}_1(t) \\ \hline \underset{\sim}{b}_2(t) \end{bmatrix} \tag{3.6}$$

Here, $\underset{\sim}{b}_1(t)$ is shared with the rest of the structure and must be equal to $\underset{\sim}{a}_1(t)$ in Eq. (3.2). The question of what displacement degrees of freedom are spanned by the functions in $\Psi(P)$ remains. If we are given a set of component modes for which the matrix of coefficients for the finite element functions $\Phi(P)$ is A, a matrix C of the form in Eq. (3.5) can be obtained from A by means of the linear transformation

$$C = \left[\begin{array}{c|c} I & 0 \\ \hline C_{21} & C_{22} \end{array}\right] = AZ = \left[\begin{array}{c|c} A_{11} & A_{12} \\ \hline A_{21} & A_{22} \end{array}\right] \left[\begin{array}{c|c} Z_{11} & Z_{12} \\ \hline Z_{21} & Z_{22} \end{array}\right] \tag{3.7}$$

in which Z is given by

$$Z = \left[\begin{array}{c|c} A_{11}^{-1} & -A_{11}^{-1}A_{12} \\ \hline 0 & I \end{array}\right] \tag{3.8}$$

We note that ordinarily the columns in A can be rearranged so that A_{11} is nonsingular. Hence, this technique allows us to represent substructures as super-elements in which interface compatibility is satisfied exactly and nearly any desired set of component modes can be spanned with the set of displacement degrees of freedom. One m_s-dimensional matrix inverse needs to be computed, but its accuracy is not crucial to compatibility if we simply set C_{11} and C_{22} equal to I and 0, respectively. With this approach, only the accuracy with which $\Psi(P)$ spans the desired set of component modes depends on the accuracy of this inverse.

The reduced substructure mass and stiffness matrices M'_{ss} and K'_{ss} are obtained from the finite element mass and stiffness matrices M_{ss} and K_{ss} by means of the familiar transformations

$$M'_{ss} = C^T M_{ss} C, \quad K'_{ss} = C^T K_{ss} C \tag{3.9a,b}$$

and now M'_{ss} and K'_{ss} can be assembled into the structure mass and stiffness matrices in the usual manner for element matrices. We note that this approach adds a degree of freedom to the structure model for each of the functions in $\Psi_2(P)$, but not for the functions in $\Psi_1(P)$ since these share coefficients with the rest of the structure already.

It remains for us to discuss the nature of interface compatibility when non-conforming elements are used in the structure model. This question is relevant because in some cases it may be more convenient to use non-conforming elements than conforming elements. Clearly, if non-conforming elements are used at the interfaces, this method will not guarantee exact displacement continuity at the interfaces. However, this method will preserve whatever compatibility is present in the finite element model of the structure as a whole. Hence the eigenvalues computed by this method will continue to be upper bounds for the eigenvalues that would be computed for a given finite element model of the structure as a whole.

3.3 EIGENANALYSIS PROCEDURE FOR THE STRUCTURE

By the method just described, the substructures making up a given structure can be modeled as super-elements with a given set of displacement degrees of freedom. To analyze the structure as a whole using the method of this paper, we begin by selecting a set of trial vectors for

each substructure and constructing reduced super-element models possessing these displacement degrees of freedom. These super-elements are assembled together to form a reduced-order structure model, from which estimates for the lower structure eigenvalues and eigenvectors are obtained. The structure model contains only the interface degrees of freedom shared by various substructures, and degrees of freedom corresponding to internal substructure interpolation functions $\Psi_2(P)$ in Eq. (3.6). Hence, the computed eigensolution for the structure model yields estimates for the interface motion of the lower structure modes. With this information, the dynamic response of each substructure to interface motion in the lower approximate structure modes can be obtained. These response vectors form a new set of substructure displacement degrees of freedom. The super-elements are refined so that these new degrees of freedom replace the former ones, and the structure model is assembled again and solved. Iteration between structure and substructure levels can occur until the model has converged to the lower structure modes.

In this method, since the trial vectors are automatically improved by the iteration process, the emphasis is on selecting initial trial vectors with a minimum of computational effort, rather than on selecting initial trial vectors of good quality. The method automatically generates and solves the substructure eigenvalue problem that the component modes should satisfy, so we need not solve a substructure eigenvalue problem to obtain initial trial vectors. As it happens, the set of component modes known as constraint modes must be calculated for each substructure for use in obtaining substructure response vectors for super-element refinement, so they are available as initial trial vectors at no

additional computational expense. In the numerical examples in this paper, these constraint modes were used, sometimes supplemented by trial vectors chosen in a manner similar to that used by Bathe in the subspace iteration method,[22] as these can also be obtained at very little expense.

3.4 DETERMINING SUBSTRUCTURE RESPONSE TO INTERFACE MOTION

After the reduced structure model is assembled and solved for approximations of the lower structure modes, the estimates thus obtained of the interface motion in the lower modes are used to refine the sets of substructure displacement degrees of freedom. An efficient method for obtaining the dynamic response of substructures to interface motion as prescribed by the structure eigensolution is presented in the following.

In terms of the finite element model of Eq. (3.2), the motion of each substructure is governed by the equation

$$M_{ss}\ddot{\underset{\sim}{a}}(t) + K_{ss}\underset{\sim}{a}(t) = \left[\begin{array}{c|c} M_{11} & M_{12} \\ \hline M_{21} & M_{22} \end{array}\right]\left[\begin{array}{c} \ddot{\underset{\sim}{a}}_1(t) \\ \hline \ddot{\underset{\sim}{a}}_2(t) \end{array}\right] + \left[\begin{array}{c|c} K_{11} & K_{12} \\ \hline K_{21} & K_{22} \end{array}\right]\left[\begin{array}{c} \underset{\sim}{a}_1(t) \\ \hline \underset{\sim}{a}_2(t) \end{array}\right] = \left[\begin{array}{c} \underset{\sim}{f}(t) \\ \hline \underset{\sim}{0} \end{array}\right] \quad (3.10)$$

in which M_{ss} and K_{ss} are the substructure mass and stiffness matrices, obtained by the finite element method, $\underset{\sim}{a}_1(t)$ contains interface displacements from the structure eigensolution, $\underset{\sim}{a}_2(t)$ contains internal displacements, and $\underset{\sim}{f}(t)$ contains interface forces exerted on the substructure by the rest of the structure. The lower partitioned set of equations is sufficient to determine $\underset{\sim}{a}_2(t)$, so we need not know what $\underset{\sim}{f}(t)$ is. For the ith structure mode, the interface displacements

$\underset{\sim}{a}_{1i}(t)$ are a portion of the ith structure eigenvector, and the interface accelerations are related to $\underset{\sim}{a}_{1i}(t)$ by

$$\ddot{\underset{\sim}{a}}_{1i}(t) = - \lambda_i \underset{\sim}{a}_{1i}(t) \tag{3.11}$$

where λ_i is the ith structure eigenvalue, because the substructure is undergoing harmonic motion. Similarly, $\ddot{\underset{\sim}{a}}_{2i} = - \lambda_i \underset{\sim}{a}_{2i}(t)$, so the lower set of equations in Eq. (3.10) becomes

$$\{- \lambda_i [M_{21} \vdots M_{22}] + [K_{21} \vdots K_{22}]\} \begin{bmatrix} \underset{\sim}{a}_{1i}(t) \\ \hdashline \underset{\sim}{a}_{2i}(t) \end{bmatrix} = \underset{\sim}{0} \tag{3.12}$$

which can be written

$$(K_{22} - \lambda_i M_{22}) \underset{\sim}{a}_{2i} = (\lambda_i M_{21} - K_{21}) \underset{\sim}{a}_{1i} \tag{3.13}$$

as the time dependence can be neglected. In the spirit of the power method, we can solve Eq. (3.13) by the iterative approach

$$\underset{\sim}{a}_{2i}^{(k+1)} = K_{22}^{-1} \{[\lambda_i M_{21} - K_{21}] \underset{\sim}{a}_{1i} - \lambda_i M_{22} \underset{\sim}{a}_{2i}^{(k)}\} \tag{3.14}$$

in which $\underset{\sim}{a}_{2i}^{(k)}$ and $\underset{\sim}{a}_{2i}^{(k+1)}$ are the kth and (k+1)st iterations for $\underset{\sim}{a}_{2i}$. We note that K_{22} cannot be singular if the substructure is properly attached to the structure.

The convergence rate for the iterative procedure of Eq. (3.14) is worth examining. To this end, let

$$\underset{\sim}{a}_{2i} = U \underset{\sim}{q} \tag{3.15}$$

where U is the square matrix whose columns are eigenvectors of the constrained-interface substructure eigenvalue problem $K_{22}U = M_{22}U\Gamma$, normalized so that $U^T M_{22} U = I$, and $\underset{\sim}{q}$ is a vector of modal coordinates for the constrained-interface substructure. Premultiplying Eq. (3.13) by U^T and using Eq. (3.15) yields

$$(\Gamma - \lambda_i I) \underset{\sim}{q} = U^T [\lambda_i M_{21} - K_{21}] \underset{\sim}{a}_{1i} = \underset{\sim}{Q} \tag{3.16}$$

where Γ is the diagonal matrix of eigenvalues for the constrained-interface substructure and $\underset{\sim}{Q}$ is a vector of modal forces. Letting γ_j be the jth eigenvalue in Γ, the solution for q_j in Eq. (3.16) is simply

$$q_j = \frac{Q_j}{\gamma_j - \lambda_i} \tag{3.17}$$

The iterative procedure of Eq. (3.14) in modal coordinates becomes, from Eq. (3.16),

$$\underset{\sim}{q}^{(k+1)} = \Gamma^{-1}[\underset{\sim}{Q} + \lambda_i \underset{\sim}{q}^{(k)}] \tag{3.18}$$

so that

$$q_j^{(k+1)} = 1/\gamma_j(Q_j + \lambda_i q_j^{(k)}) \tag{3.19}$$

If

$$q_j^{(k)} = \frac{Q_j}{\gamma_j - \lambda_i} + e_j \tag{3.20}$$

where e_j is the error in the jth mode, we obtain in the (k+1)st iteration

$$\begin{aligned} q_j^{(k+1)} &= 1/\gamma_j[Q_j + \lambda_i(\frac{Q_i}{\gamma_j - \lambda_i} + e_j)] \\ &= \frac{Q_j}{\gamma_j}[1 + \frac{\lambda_i}{\gamma_j - \lambda_i}] + \frac{\lambda_i}{\gamma_j} e_j \\ &= \frac{Q_j}{\gamma_j - \lambda_i} + \frac{\lambda_i}{\gamma_j} e_j \end{aligned} \tag{3.21}$$

Hence the error in the jth mode is multiplied by λ_i/γ_j in each iteration. Because the constrained-interface substructure is much stiffer than the total structure, γ_j is much larger than λ_i so that convergence is extremely rapid. Indeed, in the numerical examples in this chapter <u>one</u> iteration was sufficient.

3.5 COMPUTATIONAL PROCEDURE

The computational procedure for this method is described in the outline below, where it is assumed that the m lower modes are sought. The simplicity of the method is readily apparent.

1. For each substructure:
   (a) Assemble and store M_{ss} and K_{ss}, which can be partitioned as in Eq. (3.10).
   (b) Decompose K_{22} and calculate and store $D_1 = K_{22}^{-1}M_{21}$, $D_2 = K_{22}^{-1}K_{21}$, and $D_3 = K_{22}^{-1}M_{22}$ for use in 3(c) below.
   (c) For starting vectors, let

$$C = \left[\begin{array}{c:c} I & 0 \\ \hdashline C_{21} & C_{22} \end{array}\right] = \left[\begin{array}{c:c} I & 0 \\ \hdashline -D_2 & V \end{array}\right]$$

   where V contains vectors chosen as in the subspace iteration method (see discussion below). The left part of C contains "constraint modes." Store C_{21} and C_{22} for use in 3(b) below.
   (d) Using Eqs. (3.9a,b), calculate super-element matrices M'_{ss} and K'_{ss} and assemble them into the reduced structure matrices M and K.

2. On the structure level, find the lower m eigenvalues and eigenvectors to solve $KX = MX\Lambda$, where Λ is square and diagonal and X is rectangular.
3. On the substructure level:
   (a) Extract the substructure degrees of freedom X_{ss} from X. Each of the m columns of X_{ss} corresponds to $\underset{\sim}{b}$ in Eq. (3.6).

(b) Obtain

$$A = \begin{bmatrix} A_1 \\ A_2 \end{bmatrix} = \left[\begin{array}{c|c} I & 0 \\ \hline C_{21} & C_{22} \end{array}\right] X_{ss}$$

Each column of A corresponds to $\underset{\sim}{a}$ in Eq. (3.2). Note that A_1 can simply be partitioned from X_{ss}.

(c) As in Eq. (3.14), carry out the super-element refinement

$$A_2' = D_1 A_1^{\Lambda} - D_2 A_1 - D_3 A_2^{\Lambda}$$

(d) Carry out the linear transformation

$$C = \left[\begin{array}{c|c} I & 0 \\ \hline C_{21} & C_{22} \end{array}\right] = \begin{bmatrix} A_1 \\ \hline A_2' \end{bmatrix} Z$$

of Eq. (3.7) to ensure interface compatibility, interchanging columns of A if necessary (see discussion below). Store C_{21} and C_{22}.

(e) Again, use Eqs. (3.9a,b) to calculate super-element matrices, and assemble them into the structure matrices.

Alternate between parts 2 and 3 until the desired level of accuracy is obtained.

The first vector in V of 1(c) consists of the quotients m_{ii}/k_{ii}, where m_{ii} and k_{ii} are the diagonal entries in M_{22} and K_{22}. These are scaled so that super-element mass matrices are well-conditioned. The other vectors are simply unit vectors with entries of one in locations where the ratio m_{ii}/k_{ii} is largest. This is analogous to a procedure used to establish starting vectors in the subspace iteration method.[22]

For the linear transformation in 3(d), a maximum-pivot-strategy matrix inversion subroutine was modified to generate a matrix Z which performs the necessary elementary operations on the columns of A so tht

C will be of the proper form. With the maximum-pivot feature, the columns of A are reordered, in effect, so that the square submatrix of A_1 yielding the best inverse becomes A_{11} in Eq. (3.7). We have not yet formally addressed the case in which fewer structure modes are sought than the number of interface degrees of freedom for a given substructure, i.e., $m < m_s$. In this case A has m columns and C must have m_s columns, with the upper m_s rows being the identity matrix. Here the $m \times m_s$ transformation matrix Z consist of the inverse of the "best" $m \times m$ submatrix of the upper m_s rows of A, with zero columns inserted in locations corresponding to rows of A_1 not containing pivots. Hence, if the upper square portion of C is simply set equal to the identity matrix and the lower portion is A_2Z, C spans the subspace spanned by A.

The operations in part 3 of the computational procedure are performed independently for each of the substructures, so that these tasks can be carried out simultaneously for all of the substructures on machines capable of parallel processing. This feature and the rapid convergence of the response vectors mentioned in the previous section are two major reasons for using this method rather than the subspace iteration method. A third is the decrease in storage requirements at any time during the process.

3.6 NUMERICAL EXAMPLES

For the first numerical example, we consider the positive semi-definite structure shown in Fig. 3.1. The structure is composed of two rectangular frames which are diagonally braced (substructures I and

III), spaced apart by a three-longeron truss (substructure II). All of the joints in substructures I and III are assumed to be rigid and the members are modeled as thin-walled tubular grid elements with the properties EI = 20.0, EA = 4000., GJ = 15.385, m = 4.0, and I_m = 0.04. Here, EI, EA, and GJ are bending, axial, and torsional stiffnesses, respectively, m is the mass per unit length, and I_m is the mass moment of inertia about each member's axis, per unit length. Substructure II is constructed entirely with pin joints, on the other hand, and is attached to each of the other substructures by means of three pin joints. The members of substructure II are modeled as thin-walled tubular spar elements having one-half the diameter and the wall thickness of the members comprising substructures I and III. Material properties for the spar elements in substructure II are EA = 1000, m = 1. The structure has a total of 93 degrees of freedom.

Substructures I and III each share nine displacement degrees of freedom with substructure II, for a total of eighteen interface degrees of freedom. The structure has six rigid body modes, so that if we seek estimates for the lower ten elastic modes, we must have m = 16 for each of the substructures. This requires seven internal degrees of freedom for each of substructures I and III, for a total of thirty-two degrees of freedom in the structure eigenproblem. For comparison, the method of Reference 16 would require a structure eigenproblem of order forty-eight to obtain the ten lower flexible modes.

The first column of Table 3.1 contains the exact nonzero eigenvalues obtained for the structure as a whole. The following columns contain nonzero eigenvalues obtained in the solution of successive

reduced structure eigenproblems. Clearly, the eigenvalues obtained before substructure trial vectors are improved from the very simple initial set are not very accurate. But the eigenvalues obtained from the second, third and fourth structure eigenproblems demonstrate the rapid convergence of this method. Indeed, the lower seven nonzero eigenvalues from the fourth structure eigenproblem are accurate to within three places. After only one improvement of the substructure vectors, the lower two nonzero eigenvalues are correct to five places, and the lower seven nonzero eigenvalues have less than one percent error. It is important to note that this is without any effort on the part of the analyst to select "good" initial component modes.

For a second numerical example, we consider the helicopter tail-boom structure analyzed in Ref. 5 and shown in Fig. 3.2. This is an open truss positive definite structure with 108 truss members, 28 joints and 72 degrees of freedom. All members have the same material properties of $EA = 10.5 \times 10^{6}$ and $m = 2.588 \times 10^{-4}$.

The structure is conveniently divided into three substructures at locations A-A and B-B (see Fig. 3.2). There are twelve interface degrees of freedom at each division, for a total of twenty-four interface degrees of freedom in the structure. Without adding any internal degrees of freedom to substructures, we can find the lowest twelve structure modes with a structure eigenproblem of order twenty-four. Here, the method of Ref. 16 would require a structure eigenproblem of order sixty. Table 3.2 contains the lowest twelve exact eigenvalues for the structure as a whole and the estimates for the lowest twelve eigenvalues obtained in the first three reduced structure

eigenproblems. After the first improvement of trial vectors the first five eigenvalues are correct to five places, and the next three have less than 0.4% error. After another iteration the first six eigenvalues are correct to six places. Again, these results were obtained without any particular effort to select initial trial vectors of good quality.

3.7 CONCLUSIONS

In this chapter, a new method is presented for carrying out an improved form of subspace iteration on the substructure level. It is not afflicted with problems associated with similar methods which have been developed in the past, as the compatibility present in the finite element model of the structure as a whole is preserved, and the computational procedure for the method is much more streamlined. The convergence rate for this method is excellent, as demonstrated by the numerical examples. This is in spite of the fact that initial trial vectors were generated automatically at virtually no computational expense above that necessary for the trial vector improvement process on the substructure level.

There is no apparent reason why this method cannot be totally automated. Indeed, the only part of the method that was not automated in the examples for this paper was the choice of where to divide the structures into substructures. With skyline information available for the structure as a whole, this should also be easy to automate. Hence, it appears that the method can be implemented in a form in which an analyst can simply prepare the data describing the structure as a whole without concern for substructuring details. In this form, this method

offers three significant advantages over the standard subspace iteration method: the ability to process substructures in parallel, a faster convergence rate when the iteration is carried out on the substructure level, and reduced core storage requirements.

The component mode synthesis methods offer the capability of designing various components of a structure independently of one another. This method preserves this capability and even enhances it. Based on a preliminary design for each of the components, the method can be used to assemble the reduced structure model and efficiently obtain a good set of component modes and a good approximation of the interface motion in each of the structure's lower modes with only one improvement of the initial trial vectors for the components. With this data, the component modes can be improved independently for each component as design changes are made. If changes are substantial, the estimates for interface motion can be improved by assembling the altered super-element matrices together again and re-solving the reduced structure eigenproblem.

In sum, the method presented here offers a number of advantages over existing component mode synthesis and subspace iteration methods in allowing for exact compatibility throughout the structure model, iterative improvement of substructure trial vectors so that an initial set can be generated automatically and economically, faster convergence when subspace iteration is carried out on the substructure level, and parallel processing of substructures.

Table 3.1 Computed Nonzero Eigenvalues for the Structure in Figure 3.1

Exact Eigenvalues	Eigenvalues Computed from Reduced Structure Eigenproblems			
	First Eigenproblem	Second Eigenproblem	Third Eigenproblem	Fourth Eigenproblem
0.38962354E-02	0.45979363E-02	0.38962377E-02	0.38962354E-02	0.38962354E-02
0.63739073E-01	0.73921460E-01	0.63739341E-01	0.63739101E-01	0.63739088E-01
0.88234673E-01	0.14550932E+00	0.88259295E-01	0.88236477E-01	0.88235366E-01
0.14414122E+00	0.27638192E+00	0.14433102E+00	0.14414819E+00	0.14414441E+00
0.18342189E+00	0.43954679E+00	0.18438150E+00	0.18352517E+00	0.18346489E+00
0.20869841E+00	0.65449295E+00	0.20876625E+00	0.20870027E+00	0.20869968E+00
0.23543992E+00	0.97453193E+00	0.23749514E+00	0.23548173E+00	0.23546245E+00
0.38690624E+00	0.12684831E+01	0.40531417E+00	0.38755807E+00	0.38727872E+00
0.50425149E+00	0.16324224E+01	0.51298943E+00	0.50468874E+00	0.50446924E+00
0.65441061E+00	0.17445160E+01	0.66171124E+00	0.65557118E+00	0.65486285E+00

Table 3.2 Computed Eigenvalues for a Helicopter Tail Boom

Exact Eigenvalues	Eigenvalues Computed from Reduced Structure Eigenproblems		
	First Eigenproblem	Second Eigenproblem	Third Eigenproblem
0.18802306E+05	0.19027203E+05	0.18802306E+05	0.18802306E+05
0.21126307E+05	0.21372486E+05	0.21126308E+05	0.21126307E+05
0.40750934E+06	0.46308348E+06	0.40751066E+06	0.40750969E+06
0.43704323E+06	0.47270108E+06	0.43704602E+06	0.43704330E+06
0.45531624E+06	0.52607062E+06	0.45531814E+06	0.45531646E+06
0.15930000E+07	0.16510430E+07	0.15930035E+07	0.15930013E+07
0.20446687E+07	0.29945353E+07	0.20458624E+07	0.20452590E+07
0.22619709E+07	0.32148129E+07	0.22633355E+07	0.22621885E+07
0.23117166E+07	0.35742933E+07	0.23202245E+07	0.23118595E+07
0.56245722E+07	0.20010764E+08	0.59675289E+07	0.56462276E+07
0.57624179E+07	0.23525317E+08	0.65486958E+07	0.58433623E+07
0.63261552E+07	0.24604060E+08	0.70571664E+07	0.63884892E+07

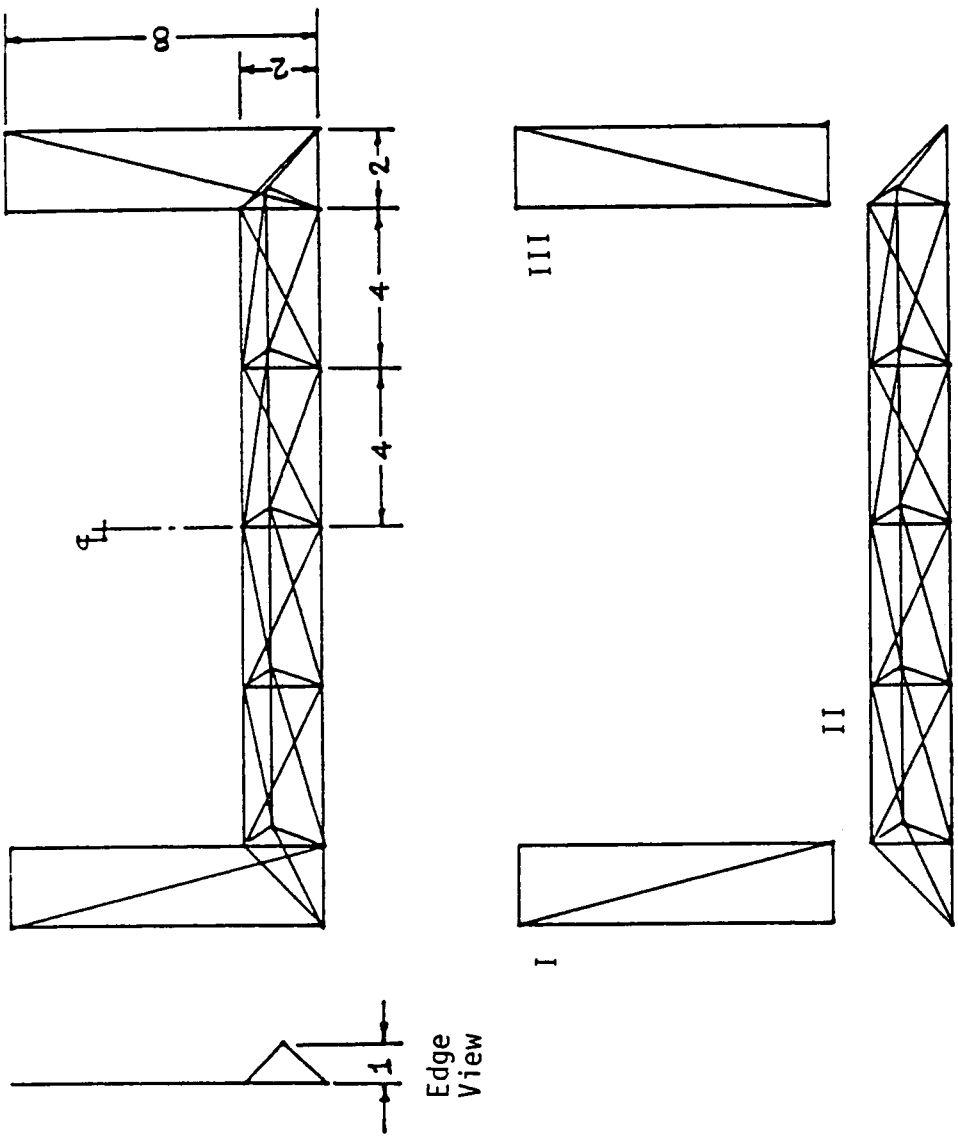

Figure 3.1. Assembled and disassembled views of the structure used in the first numerical example.

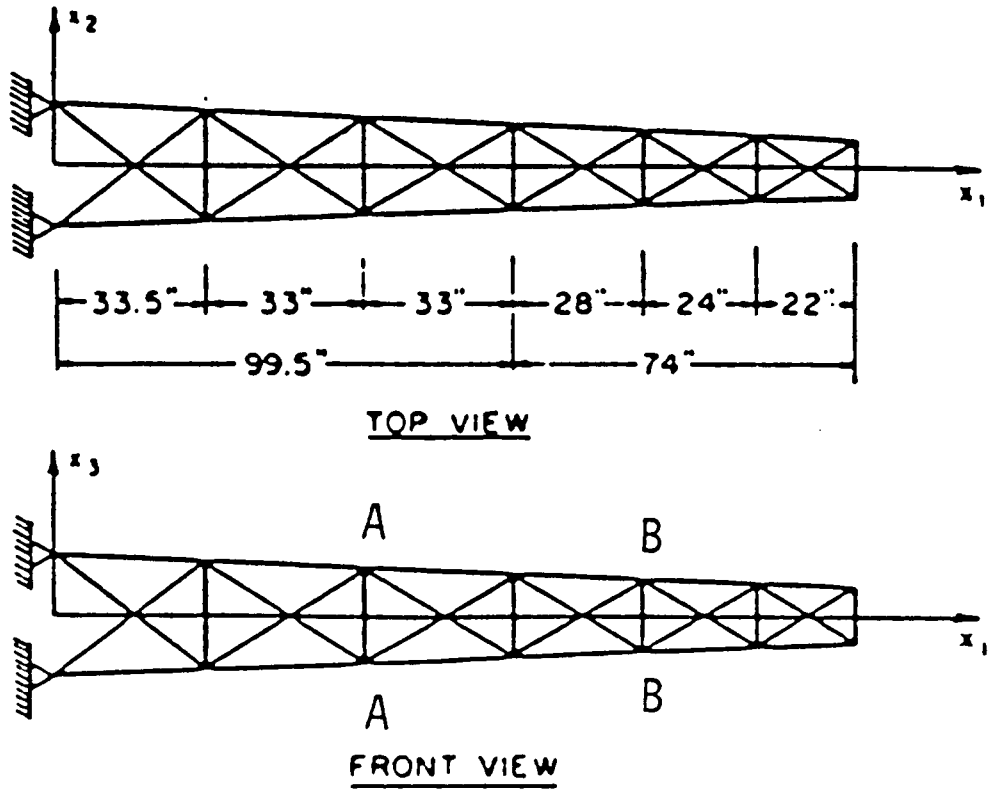

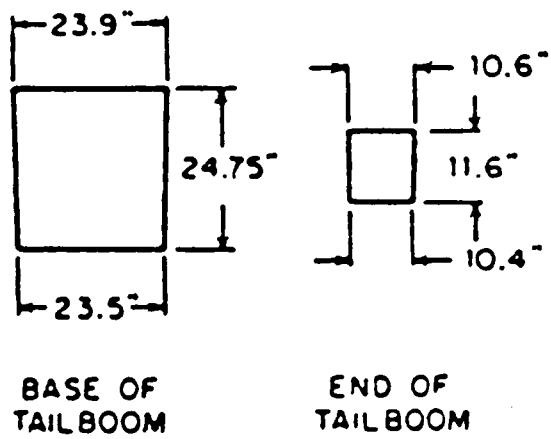

Figure 3.2. Helicopter tail boom used in the second numerical example.

Chapter 4

CONTROL OF TRAVELING WAVES IN FLEXIBLE STRUCTURES

4.1 INTRODUCTION

Traveling waves are a type of disturbance in flexible structures in which a localized pulse or "ripple" passes through a structure. This behavior is observed even though we may be accustomed to thinking in terms of structures vibrating in their natural modes of vibration. Indeed, there is a certain equivalence between motion in the form of traveling waves and vibration in a structure's natural modes. On the one hand, any disturbance in a structure, including traveling waves, can be described in terms of the structure's natural modes, if enough modes are retained in the description, because the structure's natural modes form a complete set, capable of describing any motion of the structure to any degree of accuracy. On the other hand, simple harmonic vibration in one of a structure's natural modes can be thought of as standing wave motion and described in terms of a pair of wave profiles simultaneously traveling in opposite directions. When the interest lies in damping out wave motion in a flexible structure, the question arises as to what type of control approach will be most effective and appropriate.

In modal control, a structure is controlled by controlling its modes. In practice, once the modes of a structure are known, the control task is carried out by estimating modal displacements and velocities from sensor measurements, constructing modal feedback control forces from these estimates, and obtaining actuator control forces from the modal forces by means of a linear transformation. Practical

limitations on the number of sensors and actuators to be used limit the number of modes that can be observed accurately and controlled independently. The modes of a structure are global functions, defined over the entire domain of the structure. Hence, the question can be raised as to the suitability of representing localized disturbances such as traveling waves in terms of a limited number of global functions, and controlling such disturbances by means of a finite number of modal forces, each of which must be global in nature. One can envision a modal control system which senses a traveling wave, translates this into a set of modal coordinates, and synthesizes modal control forces which call for actuator forces to be exerted in areas of the structure not yet reached by the disturbance. Such a system would clearly be less than ideal. On the other hand, it is conceivable that a modal approach would result in actuator forces that are concentrated around the disturbance, if the modal forces called for tend to reinforce each other near the disturbance and cancel in areas farther from the disturbance. We will investigate which is the case for two structures: a string in transverse vibration and a beam in bending.

Another approach which appears attractive for wave control is that of direct feedback control, in which actuator forces are simply proportional to the local velocity and displacement of the structure. Such an approach would clearly be simpler to implement, as there is no need to estimate modal coordinates in order to obtain the feedback control forces. Indeed, in this approach the control system simply responds to any motion of the structure at actuator locations, without concern for which modes are excited. In the case of traveling waves, it is clear

that this approach will not call for actuators to be active in undisturbed locations in the structure. Control gains can be obtained by approximating the results of an optimal control approach based on a reduced order model, described later in this chapter. An advantage of direct feedback control is that it is inherently stable, only drawing energy out of the structure when velocity feedback is used alone.[19] We will also investigate the performance of direct feedback control on wave motion in the structures described above, and compare it with the results obtained for modal control.

4.2 MODAL CONTROL

Consider a distributed parameter system whose behavior is governed by the partial differential equation of motion[20]

$$Lu(P,t) + m(P)\frac{\partial^2 u(P,t)}{\partial t^2} = f(P,t) \tag{4.1}$$

subject to the boundary conditions $B_i u(P,t) = 0$, $i = 1,2,\ldots,p$. Here, L is a linear, self-adjoint differential operator of order 2p, u(P,t) is the displacement, a function of the position P and time t, m(P) is the distributed mass and f(P,t) is the distributed force. The B_i's are also linear differential operators. The solution of the associated eigenvalue problem consists of a denumerably infinite set of eigenvalues Λ_k and the corresponding eigenfunctions $\phi_k(P)$ $(k = 1,2,\ldots)$. The eigenvalues are the squares of the natural frequencies ω_k of the system, $\Lambda_k = \omega_k^2$, and the eigenfunctions are orthogonal and can be normalized so as to satisfy $\int_D m(P)\phi_k(P)\phi_\ell(P)dD = \delta_{k\ell}$, $\int_D \phi_k(P)L\phi_\ell(P)dD = \Lambda_k\delta_{k\ell} = \omega_k^2\delta_{k\ell}$ where $\delta_{k\ell}$ is the Kronecker delta.

By the expansion theorem,[20] the displacement of the structure can be expressed in terms of its modes by

$$u(P,t) = \sum_{r=1}^{\infty} \phi_k(P) u_k(t) \tag{4.2}$$

where $u_k(t)$ are the modal displacements. Using the standard approach, we obtain the decoupled modal ordinary differential equations of motion

$$\ddot{u}_k(t) + \omega_k^2 u_k(t) = f_k(t), \quad k = 1,2,... \tag{4.3}$$

where

$$f_k(t) = \int_D \phi_k(P) f(P,t) dD, \quad k = 1,2,... \tag{4.4}$$

are the modal forces. In the independent modal-space control method (IMSC), each modal force depends only on the corresponding modal displacement and velocity.[17] Hence, for linear feedback,

$$f_k(t) = f_k[u_k(t), \dot{u}_k(t)] = - g_k u_k(t) - h_k \dot{u}_k(t) \tag{4.5}$$

where g_k and h_k are modal control gains.

Implementation of modal control without spillover requires a distributed control having the expression

$$f(P,t) = \sum_{k=1}^{\infty} m(P)\ \phi_k(P)\ f_k(t) \tag{4.6}$$

If the control is to be carried out by means of m discrete point actuators, the distributed control force can be written as

$$f(P,t) = \sum_{j=1}^{m} F_j(t) \delta(P - P_j) \tag{4.7}$$

and, from Eq. (4.4), each modal force is given by

$$f_k(t) = \int_D \phi_k(P) \sum_{j=1}^{m} F_j(t) \delta(P - P_j) dD = \sum_{j=1}^{m} F_j(t) \phi_k(P_j) \tag{4.8}$$

Letting $\underset{\sim}{f}$ be the vector of modal forces and $\underset{\sim}{F}$ the vector of actual forces, we can write

$$\underset{\sim}{f} = B\underset{\sim}{F} \tag{4.9}$$

where the matrix $B = [B_{kj}] = [\phi_k(P_j)]$ is known as the modal participation matrix. We can obtain the vector of actual forces from the vector of modal forces by writing

$$\underset{\sim}{F} = B^{\dagger}\underset{\sim}{f} \tag{4.10}$$

where $B^{\dagger}$ is the pseudo-inverse of B. If there are as many discrete actuators as controlled modes, then B is a square matrix. Then, assuming that B is nonsingular, Eq. (4.10) reduces to

$$\underset{\sim}{F} = B^{-1}\underset{\sim}{f} \tag{4.11}$$

To generate the modal forces, we need the modal displacements and velocities. We can extract them from the displacement and velocity profiles using the expansion theorem

$$u_k(t) = \int_D M(P)\phi_k(P)u(P,t)dD$$

$$\dot{u}_k(t) = \int_D M(P)\phi_k(P)\dot{u}(P,t)dD \tag{4.12}$$

If we use n discrete sensors, then we can interpolate between the sensor measurements to obtain the approximations $\hat{u}(P,t)$ and $\hat{\dot{u}}(P,t)$. Then, we compute $\hat{u}_k(t)$ and $\hat{\dot{u}}_k(t)$ by inserting $\hat{u}(P,t)$ and $\hat{\dot{u}}(P,t)$ in Eqs. (4.12). Alternatively, we note that at the sensor locations P_i,

$$u(P_i,t) = \sum_{r=1}^{\infty} \phi_r(P_i)u_r(t) = \underset{\sim}{\phi}^T(P_i)\underset{\sim}{u}(t) \quad i = 1,2,\ldots,n \tag{4.13}$$

where $\underset{\sim}{\phi}^T(P_i)$ is the infinite-dimensional vector of eigenfunctions evaluated at $P = P_i$ and $\underset{\sim}{u}(t)$ is the infinite-dimensional modal vector.

Introducing the measurement vector $\underset{\sim}{y}(t)$ with components $y_i(t) = u(P_i, t)$, we can rewrite Eqs. (4.13) as

$$\underset{\sim}{y}(t) = \Phi^T \underset{\sim}{u}(t) \tag{4.14}$$

Then, if we truncate the modal vector $\underset{\sim}{u}(t)$ so that its dimension is equal to the number of sensors, we can estimate the modal displacement vector from

$$\hat{\underset{\sim}{u}}(t) = (B_s^T)^{-1} \underset{\sim}{y}(t) \tag{4.15a}$$

where B_s is a square truncated matrix Φ and it represents the sensor participaOion matrix. This is equivalent to using the lowest n modes to represent the displacement profile. Similarly, the estimated modal velocity vector is

$$\hat{\dot{\underset{\sim}{u}}}(t) = (B_s^T)^{-1} \dot{\underset{\sim}{y}}(t) \tag{4.15b}$$

Finally, the modal equations of motion become

$$\ddot{u}_k + \omega_k^2 u_k = f_k = -g_k \hat{u}_k - h_k \hat{\dot{u}}_k \tag{4.16}$$

In this study, we use gains that minimize the performance functional

$$J = \int_0^\infty \{ \int_D [m(P)\dot{u}^2(P,t) + u(P,t)Lu(P,t) + rf^2(P,t)] dD \} dt \tag{4.17}$$

Using the expansion theorem, the minimization can be carried out for each mode independently resulting in the gains[17]

$$g_k = -\omega_k^2 + \omega_k (\omega_k^2 + \frac{1}{r})^{1/2}$$

$$h_k = [-2\omega_k^2 + \frac{1}{r} + 2\omega_k (\omega_k^2 + \frac{1}{r})^{1/2}]^{1/2} \tag{4.18}$$

If we have damping in the system, the partial differential equation of motion becomes

$$Lu(P,t) + C \frac{\partial u(P,t)}{\partial t} + m(P) \frac{\partial^2 u(P,t)}{\partial t^2} = f(P,t) \tag{4.19}$$

where C is a differential operator. If, for some constants α_1 and α_2, we have

$$C = \alpha_1 L + \alpha_2 m(P) \tag{4.20}$$

then the modal equations of motion become

$$\ddot{u}_k + (\alpha_1 \omega_k^2 + \alpha_2)\dot{u}_k + \omega_k^2 u_k = f_k \tag{4.21}$$

so that the equations remain uncoupled. This special case of damping is known as proportional damping.

4.3 DIRECT FEEDBACK CONTROL

In direct feedback control, the distributed control force is again given by Eq. (4.7), in which each actuator force $F_j(t)$ is now given by

$$F_j(t) = - g_j y(P_j,t) - h_j \dot{y}(P_j,t) \tag{4.22}$$

in which g_j and h_j are displacement and velocity gains and $y(P_j,t)$ and $\dot{y}(P_j,t)$ are the measured displacement and velocity at the actuator location. In matrix form, Eq. (4.22) becomes

$$\underset{\sim}{F} = - G\underset{\sim}{y}(t) - H\dot{\underset{\sim}{y}}(t) \tag{4.23}$$

in which G and H are m-dimensional square matrices and $\underset{\sim}{y}(t)$ and $\dot{\underset{\sim}{y}}(t)$ are vectors of displacement and velocities of the structure at actautor locations. For direct feedback control, G and H are diagonal, but for a more general feedback control they can be fully populated.

We need to determine values for the entries in G and H. To this end, we will take an optimal control approach for controlling a simplified model of the system. To form such a model, we will assume first that the displacement in the structure can be described in terms of the m lowest modes, since these are the modes which are the most easily excited and the most persistent in the presence of structural damping.

Hence we have, as a simplified approximation,

$$u(P,t) = \sum_{r=1}^{m} \phi_k(P)u_k(t) \tag{4.24}$$

and the m modal equations of motion become from Eqs. (4.3) and (4.9), in vector form,

$$\ddot{\underset{\sim}{u}}(t) + \Lambda\underset{\sim}{u}(t) = \underset{\sim}{f}(t) = \Phi_m\underset{\sim}{F}(t) \tag{4.25}$$

in which $\underset{\sim}{u}$ and $\ddot{\underset{\sim}{u}}$ are vectors of modal displacements and accelerations, Λ is a square diagonal matrix of the lowest m eigenvalues, and Φ_m is the m-dimensional modal participation matrix. From Eq. (4.14), the displacement vector $\underset{\sim}{y}(t)$ is given by

$$\underset{\sim}{y}(t) = \Phi_m^T\underset{\sim}{u}(t) \tag{4.26}$$

After multiplying on the left by Φ_m^{-1} and making use of Eq. (4.26), Eq. (4.25) becomes, in terms of $\underset{\sim}{y}(t)$ and $\ddot{\underset{\sim}{y}}(t)$,

$$M\ddot{\underset{\sim}{y}}(t) + K\underset{\sim}{y}(t) = \underset{\sim}{F}(t) \tag{4.27}$$

where the mass and stiffness matrices are given by

$$M = \Phi_m^{-1}(\Phi_m^{-1})^T, \quad K = \Phi_m^{-1}\Lambda(\Phi_m^{-1})^T \tag{4.28a,b}$$

The optimal control problem for this model can be cast in standard form by letting

$$\underset{\sim}{x} = [\underset{\sim}{y}^T\,\vdots\,\dot{\underset{\sim}{y}}^T]^T \tag{4.29}$$

and writing Eq. (4.27) as

$$\dot{\underset{\sim}{x}} = A\underset{\sim}{x} + B\underset{\sim}{F} \tag{4.30}$$

in which

$$A = \left[\begin{array}{c:c} 0 & I \\ \hdashline -M^{-1}K & 0 \end{array}\right], \quad B = \left[\begin{array}{c} 0 \\ \hdashline M^{-1}I \end{array}\right] \tag{4.31a,b}$$

Then, with the performance index

$$J = \int_0^\infty (\underset{\sim}{x}^T Q \underset{\sim}{x} + \underset{\sim}{F}^T R \underset{\sim}{F}) dt \tag{4.32}$$

where

$$Q = \left[\begin{array}{c|c} K & 0 \\ \hline 0 & M \end{array}\right] \tag{4.33}$$

and R is a control effort weighting matrix, the optimal control is given by

$$\underset{\sim}{F} = - R^{-1} B^T P \underset{\sim}{x} = - G \underset{\sim}{y} - H \dot{\underset{\sim}{y}} \tag{4.34}$$

where P satisfies the matrix Riccati equation[24]

$$Q - PBR^{-1}B^T P + A^T P + PA = 0 \tag{4.35}$$

As we noted above, in general G and H in Eq. (4.24) are fully populated, but in applications such as this one in which damping of a structure's vibration is the control objective, the diagonal entries in the velocity gain matrix H are ordinarily several orders of magnitude greater than the off-diagonal entries. Also, the displacement gains G are ordinarily sufficiently small that their contribution to the control forces is negligible. Hence we obtain something very close to direct feedback control as the solution to the control problem, and the simplification in implementation resulting from ignoring the off-diagonal entries in the gain matrices justifies the use of simple direct feedback control.

An important but often neglected step in the design of any structural control system is that of simulating the performance of the controls on the actual distributed structure rather than on the model used for designing the controls. We will do this in the next section to check the simplifications we made, which include using a simpler reduced

model with no damping to obtain control gains and neglecting the less significant entries in the gain matrices to obtain direct feedback control.

4.4. CONTROL OF TRAVELING WAVES

In this section, we examine the possibility of using IMSC and direct feedback control to control traveling waves in flexible structures. In each case, we begin with initial conditions describing a single, localized traveling disturbance in the structure. Because the modes of a distributed system form a set that is complete in energy, any disturbance can be expressed as a linear combination of the modes, provided a sufficiently large number of modes is included. Hence, we will use a modal approach to model the structures studied here, with eighty modes included in each simulation.

We consider first the wave motion in a second-order system, such as a string in transverse vibration, a bar in axial vibration, or a shaft in torsional vibration. Then, we consider traveling waves in fourth-order systems, such as a beam in bending vibration. In the first case, the waves travel through the system without changing shape; in the second, the system is dispersive, so that the wave changes shape as it travels. For both types of systems, we assume that there is internal damping present in the system, and that this damping is proportional to the local rate of strain in the material. In each case, we consider first the globally optimal solution to the control problem obtained by using distributed actuators. Although implementation of control by means of distributed actuators is not within the state of the art, the

globally optimal solution is valuable because it shows us qualitatively what the optimal control force distribution looks like. Then, we consider control of the wave motion using a finite number of discrete actuators, where we use modal and direct feedback approaches. In the first case only a limited number of the lower modes will be controlled. A comparison of the results obtained will demonstrate the effectiveness of the two methods in controlling waves with only a finite number of discrete actuators.

i. Second-Order Systems

We consider a second-order system in the form of a string in transverse vibration. Assuming that the system is undamped, the free vibration is governed by the partial differential equation[25]

$$- T \frac{\partial^2 u(x,t)}{\partial x^2} + m \frac{\partial^2 u(x,t)}{\partial t^2} = 0 \tag{4.36}$$

where $u(x,t)$ is the transverse displacement, T is the tension and m is the mass per unit length. Here the differential operator L is equal to $- T \partial^2/\partial x^2$. It is assumed in Eq. (4.36) that both T and m are constant.

If the string is of infinite length, it is easy to show that the solution of Eq. (4.36) can be written in the form[25]

$$u(x,t) = F_1(x - vt) + F_2(x + vt) \tag{4.37}$$

where F_1 and F_2 are wave profiles traveling to the right and to the left, respectively, with the wave velocity

$$v = \sqrt{T/m} \tag{4.38}$$

If the string is finite and fixed at both ends, then $u(x,t)$ must satisfy the boundary conditions

$$u(0,t) = u(L,t) = 0 \tag{4.39}$$

The natural frequencies are

$$\omega_k = k\pi\sqrt{T/mL^2}\ , \quad k = 1,2,... \tag{4.40}$$

and the associated normalized eigenfunctions are

$$\phi_k(x) = \sqrt{\frac{2}{mL}} \sin \frac{k\pi x}{L}\ , \quad r = 1,2,... \tag{4.41}$$

According to the expansion theorem, Eq. (4.2), the displacement of the string can be represented by a linear combination of these eigenfunctions. Alternatively, at any instant in time, the motion can be described by Eq. (4.37) in terms of traveling waves, as long as the boundary conditions are satisfied. These boundary conditions determine how the wave is reflected at the ends of the string.

Next, we add an external distributed force and distributed damping that is proportional to the local strain rate, so that the partial differential equation of motion becomes

$$-T\frac{\partial^2 u(x,t)}{\partial x^2} - C\frac{\partial^3 u(x,t)}{\partial x^2 \partial t} + m\frac{\partial^2 u(x,t)}{\partial t^2} = f(x,t) \tag{4.42}$$

where C is assumed to be constant. Because damping is of the proportional type,[20] the eigenfunctions of the damped system are the same as the eigenfunctions of the undamped system, although the eigenvalues are different. Hence, inserting Eq. (4.2) with P = x into Eq. (4.42), multiplying by $\phi_\ell(x)$, integrating over the length of the string and making use of the orthogonality relations, we obtain the independent ordinary differential equations of motion

$$\ddot{u}_k(t) + (C\omega_k^2/T)\dot{u}_k(t) + \omega_k^2 u_k(t) = f_k(t), \quad r = 1,2,... \tag{4.43}$$

where $f_k(t) = \int_0^L \phi_r(x)f(x,t)\,dx$ is the $\underline{k}$th modal force. Here we note that the damping factor is proportional to the natural frequency, $\zeta_k = (C/2T)\omega_k$ $(r = 1,2,...)$. Hence, we expect the higher modes to decay more rapidly than the lower modes, which is confirmed by the observed behavior.

One way of generating a traveling wave in a string is by quickly moving one of the end supports. If this is done to the left support, the boundary conditions of Eq. (4.38) become

$$u(0,t) = w_1(t), \; u(L,t) = 0 \tag{4.44}$$

where $w_1(t)$ is the vertical displacement of the left support. In order to represent the motion of the string in terms of the modes in Eq. (4.40), it is necessary to write the partial differential equation in terms of the displacement relative to the static response to the support displacements. This procedure is well known and is developed more extensively in the next chapter, as there the support motion persists while the control task is being carried out. Because in this chapter we are merely using this approach to generate initial conditions, we will dispense with the details and simply present the modal initial conditions for the string with a support motion of the form

$$w_1(t) = \begin{cases} \frac{1}{2}(1 - \cos\frac{2\pi t}{T}), & -T \le t \le 0 \\ 0, & t < -T, \; t > 0 \end{cases} \tag{4.45}$$

In this case, the initial conditions become

$$u_k(0) = \frac{2\sqrt{2\pi}}{k}\left[\frac{(1-e^{-\zeta_k\omega_k T}\cos\omega_{dk}T)(4\pi^2-\omega_k^2T^2) + (\zeta_k/\sqrt{1-\zeta_k^2})(e^{-\zeta_k\omega_k T}\sin\omega_{dk}T)}{\omega_k^4T^4 - 2(2\pi)^2\omega_k^2T^2(1-2\zeta_k^2) + (2\pi)^4}\right.$$

$$\left.\times(4\pi^2 + \omega_k^2T^2)\right] \tag{4.46a}$$

$$\dot{u}_k(0) = -\frac{2\sqrt{2\pi}}{k}\left[\frac{(1-e^{-\zeta_k\omega_k T}\cos\omega_{dk}T)8\pi^2\zeta_k\omega_k + (\omega_k/\sqrt{1-\zeta_k^2})(e^{-\zeta_r\omega_k T}\sin\omega_{dk}T}{\omega_k^4T^4 - 2(2\pi)^2\omega_k^2T^2(1-2\zeta_k^2) + (2\pi)^4}\right.$$

$$\left.\times(4\pi^2(2\zeta_k^2 - 1) + \omega_k^2T^2)\right] \tag{4.46b}$$

where

$$\omega_{dk} = \omega_k\sqrt{1 - \zeta_k^2} \tag{4.47}$$

For simplicity, we choose the string to have a length, tension and mass per unit length equal to unity. This gives a wave speed equal to unity, from Eq. (4.38). Hence, to generate a ripple of width λ, we choose T in Eq. (4.45) equal to λ.

We will base our evaluation of control performance partially on the performance index for the control task, given in Eqs. (4.17) and (4.32). Noting that the performance index of Eq. (4.17) cannot be evaluated when the control force distribution consists of Dirac delta functions, we will use a control force distribution of the form

$$f(x,t) = \sum_{i=1}^{m} F_i(t)\gamma(x - x_i) \tag{4.48}$$

where $\gamma(x - x_i)$ is given by

$$\gamma(x - x_i) = \frac{1}{\varepsilon}\,[U(x - (x_i - \varepsilon/2)) - U(x - (x_i + \varepsilon/2))] \qquad (4.49)$$

with $U(x)$ as the Heaviside step function, so that $\gamma(x - x_i)$ is simply a rectangular force of width ε, centered at x_i, with unit area. In these examples we choose $\varepsilon/L = 0.01$. Because

$$\int_0^L rf^2(x,t)dx = \frac{r}{\varepsilon}\sum_{i=1}^{m} F_i^2(t) \qquad (4.50)$$

we can evaluate the cost of the control effort when these discrete actuators are used by forming the product $\underset{\sim}{F}^T R \underset{\sim}{F}$, in which the matrix R is simply given by $R = (r/\varepsilon)I$, where I is the identity matrix. Finally, we must replace B in Eq. (4.11) and Φ_m in Eq. (4.25) by a modified modal participation matrix $\hat{\Phi}$, given by

$$\hat{\Phi}_{kj} = \int_0^L \phi_k(x)\gamma(x - x_j)dx = \int_{x-\varepsilon/2}^{x+\varepsilon/2} \sqrt{\frac{2}{mL}} \sin\frac{k\pi x}{L}\,(\frac{1}{\varepsilon})dx \qquad (4.51)$$

$$= \phi_k(x_j)\cdot[(\sin\frac{k\pi\varepsilon}{2L})/(\frac{k\pi\varepsilon}{2L})]$$

Figure 4.1 shows the motion of the string with the above initial conditions and with $\lambda = 0.1L$. Here, eighty modes were used to model the string. The value of C was chosen so as to give 0.1% damping in the fundamental mode, and no control forces were applied. The effect of the damping is to decrease the energy in the highest modes rather quickly, so that the disturbance profile loses its initial sharpness and its amplitude decreases.

Next, we consider a distributed control force with a control effort weighting factor of $r = 0.2$ in the performance index, Eq. (4.17). All of the modeled modes are controlled. The results are shown in Fig. 4.2. We observe from Fig. 4.2 that the control is localized at the wave, although the control force is a linear combination of modal forces and

each of the modal forces is distributed over the entire domain. This demonstrates that IMSC in its purest form, with distributed actuators, can control localized disturbances quite satisfactorily, because the control force tends to concentrate around the disturbance and it travels with the wave.

We also observe from Fig. 4.2 that the optimal control force is very nearly equal to a scalar multiple of the velocity, which is consistent with the fact that energy dissipation is the control objective. This control force causes the wave to essentially retain its shape as the amplitude decreases. We can vary the rate of decay of the wave by varying r. In this example, we selected the value of r so as to be able to monitor the effect of the controls on the system as the wave travels one complete circuit on the string. In general, r represents a penalty on the control and is chosen by the analyst so as to produce desired system performance.

Figure 4.3 shows results obtained by using nine discrete actuators and nineteen discrete sensors, all equally spaced, to control the lowest nine modes of the string. Here r = 0.002. The sensors measure the actual displacement and velocity of the string at each sensor location. Then, these measurements are used in conjunction with Eqs. (4.15) to estimate the corresponding modal displacements and velocities. The use of more sensors than actuators allows much of the motion due to uncontrolled modes to be filtered out. The modal control forces are calculated from the estimated modal displacements and velocities using the gains prescribed by Eqs. (4.18), and the actual actuator forces are calculated using Eq. (4.11). In this example, we continue to model the

lowest eighty modes, so that we expect to see residual energy in uncontrolled modes, observation spillover from uncontrolled modes and control spillover into uncontrolled modes, at least to some degree. Here, we still consider the effects of damping as in the previous two cases. The use of discrete actuators causes the wave to lose its initial smooth shape with time, although the disturbance can still be identified as it travels. Examining the plot corresponding to t = 0, it is clear that, as long as the disturbance in the system is still localized, the control force tends to accompany the disturbance. Comparing the rate of energy dissipation with the damped but uncontrolled case of Fig. 4.1, we observe that controlling only the lowest nine modes increases the energy dissipation substantially. In the time increment between t = 0 and t = 0.4, damping causes a 49% loss of energy in the uncontrolled case, while the discrete actuator controls dissipate an additional 14% by operating on the lowest nine modes. As time progresses, the controls become essentially inactive, indicating that motion in the lowest nine modes has been annihilated. The strain rate damping then causes the remaining energy to decay. The energy in the string decreases to a level of one percent of the energy of the initial conditions at t = 4.35, with a performance index of 52.33.

In Fig. 4.4, we have plots of the modal contributions $\underset{\sim}{b}_k f_k(t)$ to the actuator force vector $\underset{\sim}{F}(t)$ at t = 0, where the vectors $\underset{\sim}{b}_k$ are the columns of $B^{\dagger}$ in Eq. (4.10), or of B^{-1} in Eq. (4.11). In this case, $\hat{\Phi}$ was used. Also, in each of these plots, we have sketched the corresponding mode shape, to give an idea what the contributions would have been if the actuators were distributed devices, instead of point

actuators. The last plot represents $\sum_{k=1}^{m} \underset{\sim}{b}_k f_k(t)$ at t = 0, which is recognized from Eq. (4.10) as the actual actuator force vector $\underset{\sim}{F}(t)$ at t = 0. This figure brings out the fact that, although the modal forces are active at points far away from the disturbance, these modal forces tend to cancel out at these points. Hence, the actual forces, as exerted by the actuators, tend to be concentrated in the vicinity of the disturbance.

Figure 4.5 contains plots of the controlled response of the string when direct feedback is used. Again, r = 0.002. Here nine actuators and only nine colocated sensors are used, equally spaced. As expected, the actuators are only active exactly at the location of the disturbance, and no control effort is expended where there is no disturbance. In IMSC, this is only approximately true, and there is some wasted control effort due to the actuator activity away from the disturbance. Another difference is that the actuators continue to be active longer than in IMSC, because they respond to motion in any mode, and not just in a few targeted for control. In this case the energy in the string was reduced to only one percent of its initial value at t = 2.62 with a cost of only 33.96. Noting that the cost for IMSC was 57% higher, we conclude that the direct feedback approach is clearly superior. This is due to the fact that direct feedback does not limit its attention to the lower modes, and its control effort is more strictly confined to the neighborhood of the disturbance. Further experiments indicate that as the level of structural damping decreases, the superiority of direct feedback increases. This is in spite of the fact that only half as many sensors are required for direct feedback control.

ii. FOURTH-ORDER SYSTEMS

The motion of beams in undamped free vibration is governed by the fourth-order partial differential equation[25]

$$EI \frac{\partial^4 u(x,t)}{\partial x^4} + m \frac{\partial^2 u(x,t)}{\partial t^2} = 0 \tag{4.52}$$

where EI is the bending stiffness and m is the mass per unit length, both assumed to be constant. Here, $L = EI\, \partial^4/\partial x^4$. Equation (4.52) admits a solution in the form of the wave motion

$$u(x,t) = \cos \frac{2\pi}{\lambda} (x - vt) \tag{4.53}$$

where λ is the wavelength and

$$v = \frac{2\pi}{\lambda} \sqrt{EI/m} \tag{4.54}$$

is the wave velocity. Hence, if a given wave profile is resolved into sinusoidal components by Fourier analysis, each wave component will travel with a different velocity. It follows that the wave profile changes shape as it travels, so that the beam is dispersive.[25]

If the beam is of length L with pinned ends, then the displacement must satisfy the boundary conditions

$$u(0,t) = u(L,t) = \frac{\partial^2 u(0,t)}{\partial x^2} = \frac{\partial^2 u(L,t)}{\partial x^2} = 0 \tag{4.55}$$

The natural frequencies are

$$\omega_k = (k\pi)^2 \sqrt{\frac{EI}{mL^4}} \qquad r = 1,2,\ldots \tag{4.56}$$

and the associated normalized eigenfunctions are the same as for the string, Eq. (4.41).

In the presence of distributed damping proportional to the local strain rate and a distributed control force, the partial differential

equation of motion becomes[26]

$$EI \frac{\partial^4 u(x,t)}{\partial x^4} + C \frac{\partial^5 u(x,t)}{\partial x^4 \partial t} + m \frac{\partial^2 u(x,t)}{\partial t^2} = f(x,t) \qquad (4.57)$$

where C is the damping coefficient. The modal equations of motion can be obtained by the same approach as for the string, and the equations are nearly identical to Eqs. (4.43). However, in this case the damping factors are given by $\zeta_k = (C/2EI)\omega_k$, and the damping factor for each mode is proportional to the square of the mode number, because it is still proportional to the natural frequency. Hence, for a beam with strain rate damping, the higher modes decay much faster than the lower modes.

We will generate a traveling wave on this pinned-pinned beam by imparting to the left support the vertical motion given in Eq. (4.45). This results in the same initial conditions as are given in Eqs. (4.46). Again, we set the values of m, EI, and L equal to one. However, in this case, to get a "ripple" of nominal width λ, we must choose $T = \lambda^2/2\pi$ because this is how long a wave of wavelength λ would take to "pass through" the left support onto the beam, according to Eq. (4.54), and λ is the wavelength of the dominant Fourier component of such a "ripple." Again, we choose $\lambda = 0.1L$.

Figure 4.6 shows the uncontrolled motion of the beam with these initial conditions, with C chosen so that the damping factor in the first mode is again equal to about 0.1%. The dispersive nature of the beam is obvious from the change in the wave profile. Indeed, even at the start the wave profile looks different from that of the string as

some of the higher Fourier components break away more quickly. However, the nominal width that we chose for the "ripple" is still evident.

An aspect of this damped wave motion that is particularly worthy of note is the rapid initial dissipation of energy from the higher modes. Indeed, at t = 0.006 only about one thirtieth of the initial energy remains. At t = 0.012 only about one ninetieth remains, and from there the decay is more gradual, as the lower modes take much longer to decay.

Figure 4.7 shows the globally optimal control with distributed actuators. Again, the control force looks like the negative of the velocity. Here r was chosen as r = 0.0001. Figure 4.8 contains plots of IMSC with nine discrete actuators and nineteen discrete sensors, identical to those used in the case of the string, with r = 0.0001. Again we see that the control forces tend to be concentrated near the disturbance, although there is some effort expended elsewhere on the beam. We note that the actuators are still working when the beam has almost come to rest, whereas in the case of the string there was still a significant amount of energy in the system when the actuators stopped working. This indicates that the lower modes in the beam linger the longest because the higher ones are damped out so quickly. The performance index at the completion of the control task is 99.00.

In Fig. 4.9 we see the response of the direct feedback control system, which again uses nine colocated pairs of actuators and sensors. Here again the actuators away from the wave are completely inactive, as expected. But comparing the scale on the force axis with the one in Fig. 4.8, we see that the actuator forces in this case are much greater, at least initially. The performance index for the direct feedback

approach is 259.67, or 162% higher than that obtained with IMSC. The explanation for this is that considerable effort was expended in response to the high velocities initially present in the beam, and a large portion of these high velocities was contributed by higher modes which would have simply decayed rapidly on their own. In the case of IMSC, the contributions of higher modes were filtered out rather effectively so that the actuators could control the lower nine modes. Hence, in the case of the beam, IMSC proved to be the superior control technique because of the greater separation of natural frequencies and damping factors in the fourth-order case. The model used to design the direct feedback control system proved to be too simplistic to account for the variety of modes with their widely varying damping factors.

4.6 CONCLUSIONS

The numerical examples presented here give considerable insight into the question of what control strategy will be most effective for controling traveling waves in structures. To summarize briefly, when there is a small amount of material damping in a structure, modal control is attractive because the lower modes are targeted for control and higher modes are damped out more quickly on their own, as the modal damping factors are proportional to modal frequencies. However, when the modal frequencies are closely spaced, as in the case of the string, direct feedback control becomes more attractive because the number of modes from which energy can be dissipated is much greater than the number of actuators, which is the limit on the number of modes that can be controlled using IMSC. We have also seen that in IMSC, despite the

fact that a global approach to control is taken, the actuator forces do tend to concentrate near a localized disturbance such as a traveling wave.

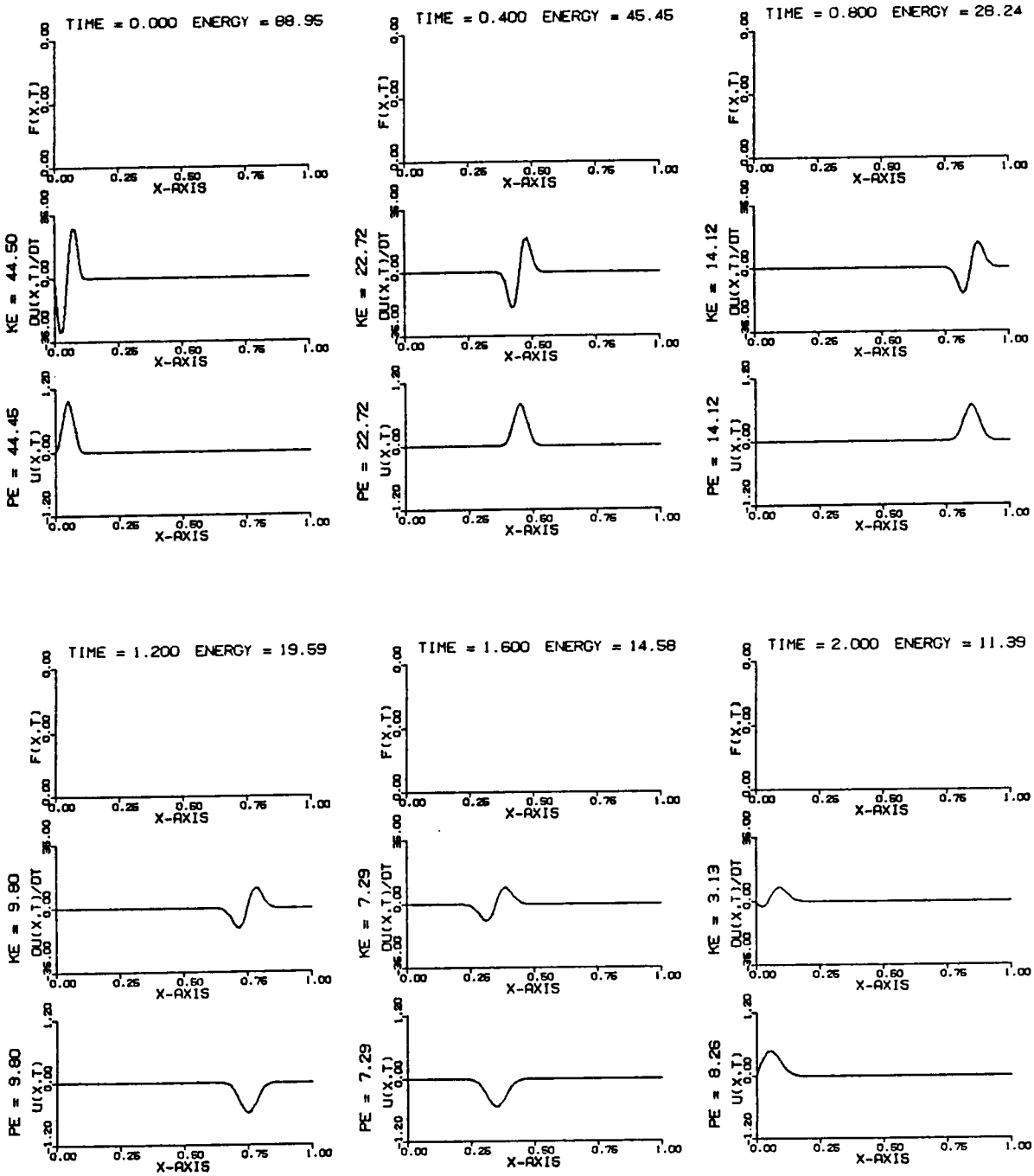

Figure 4.1. Uncontrolled damped wave motion in a string.

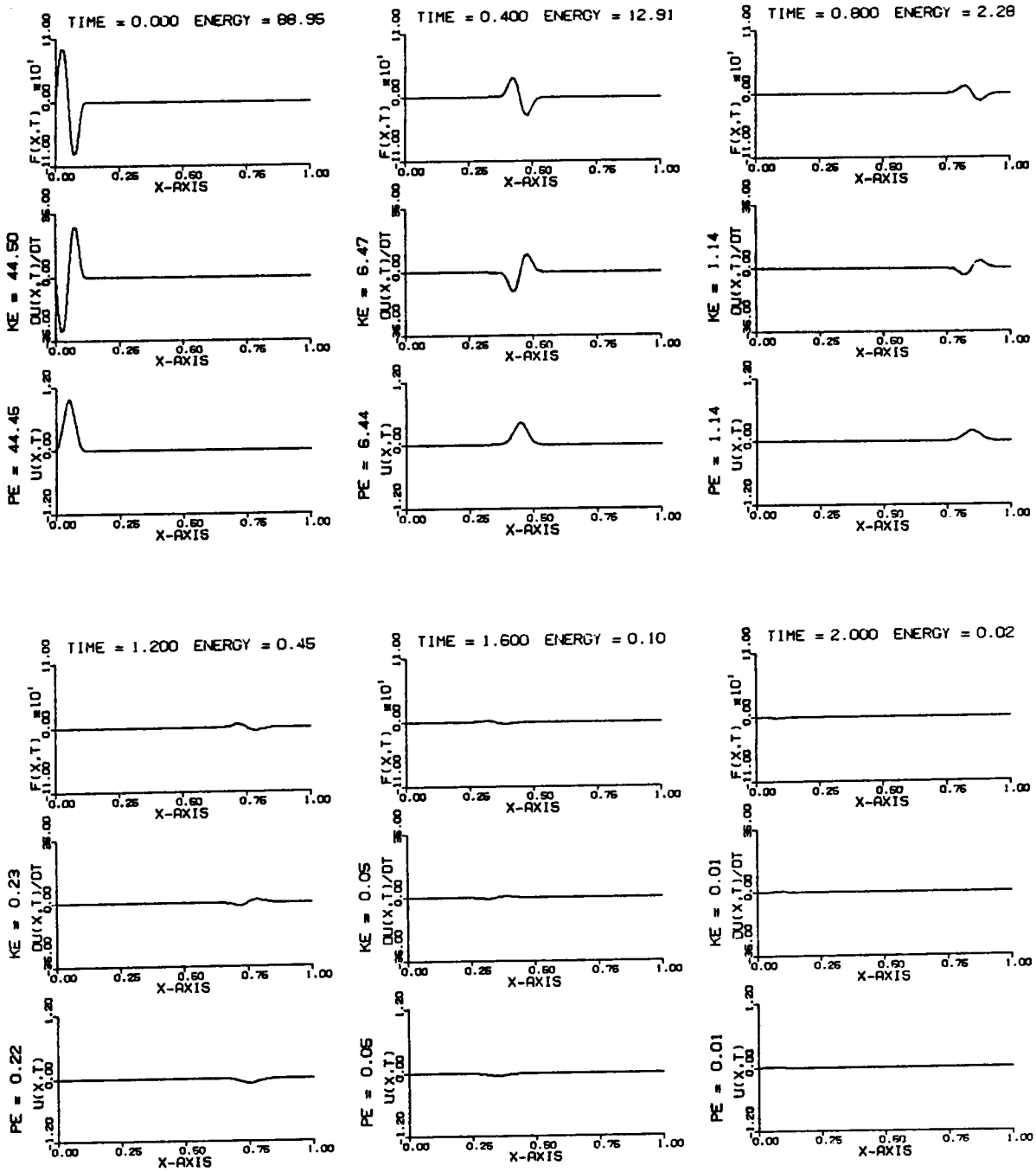

Figure 4.2. Globally optimal (distributed) control of wave motion in a string.

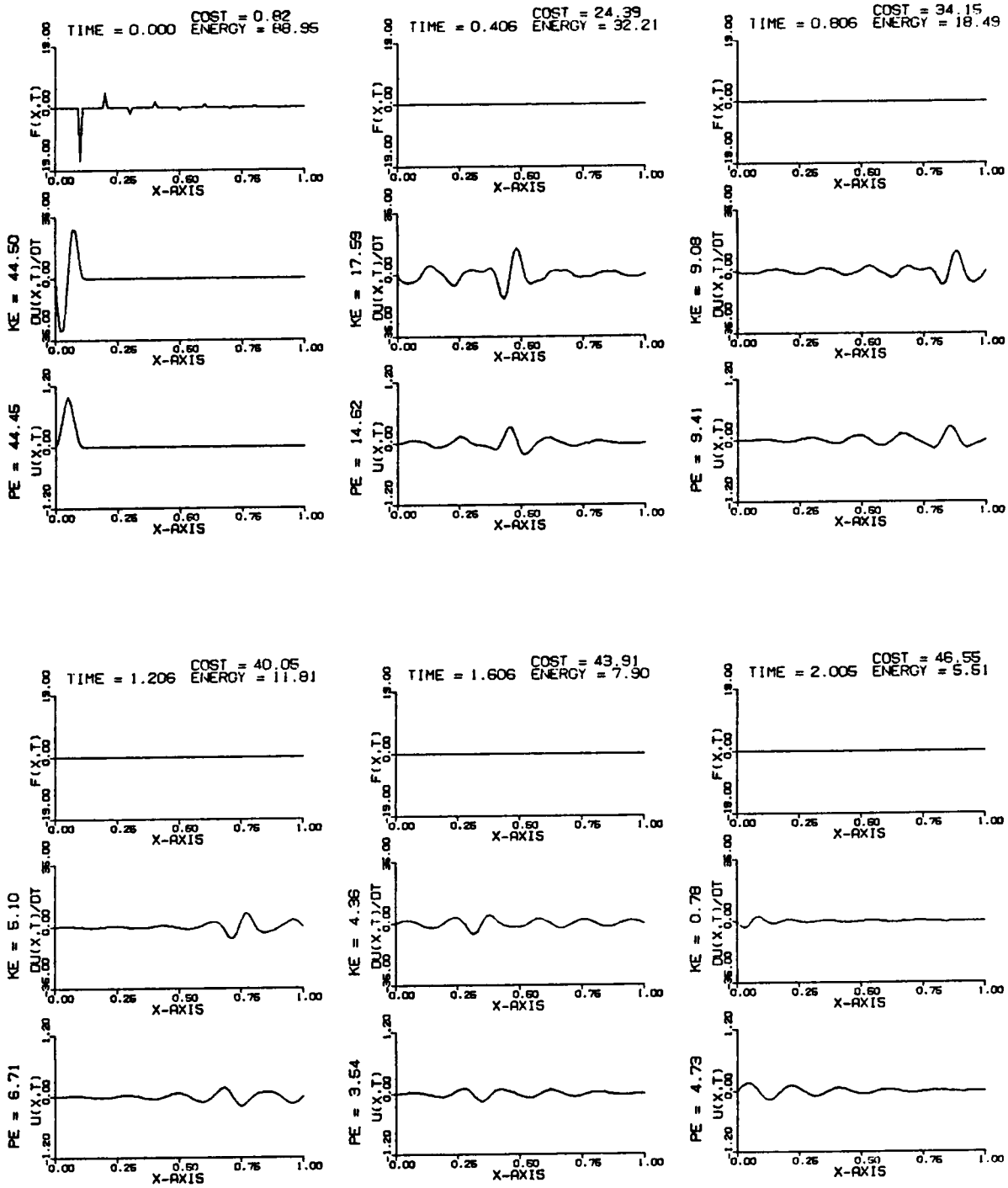

Figure 4.3. Modal control of a wave in a string, using discrete actuators.

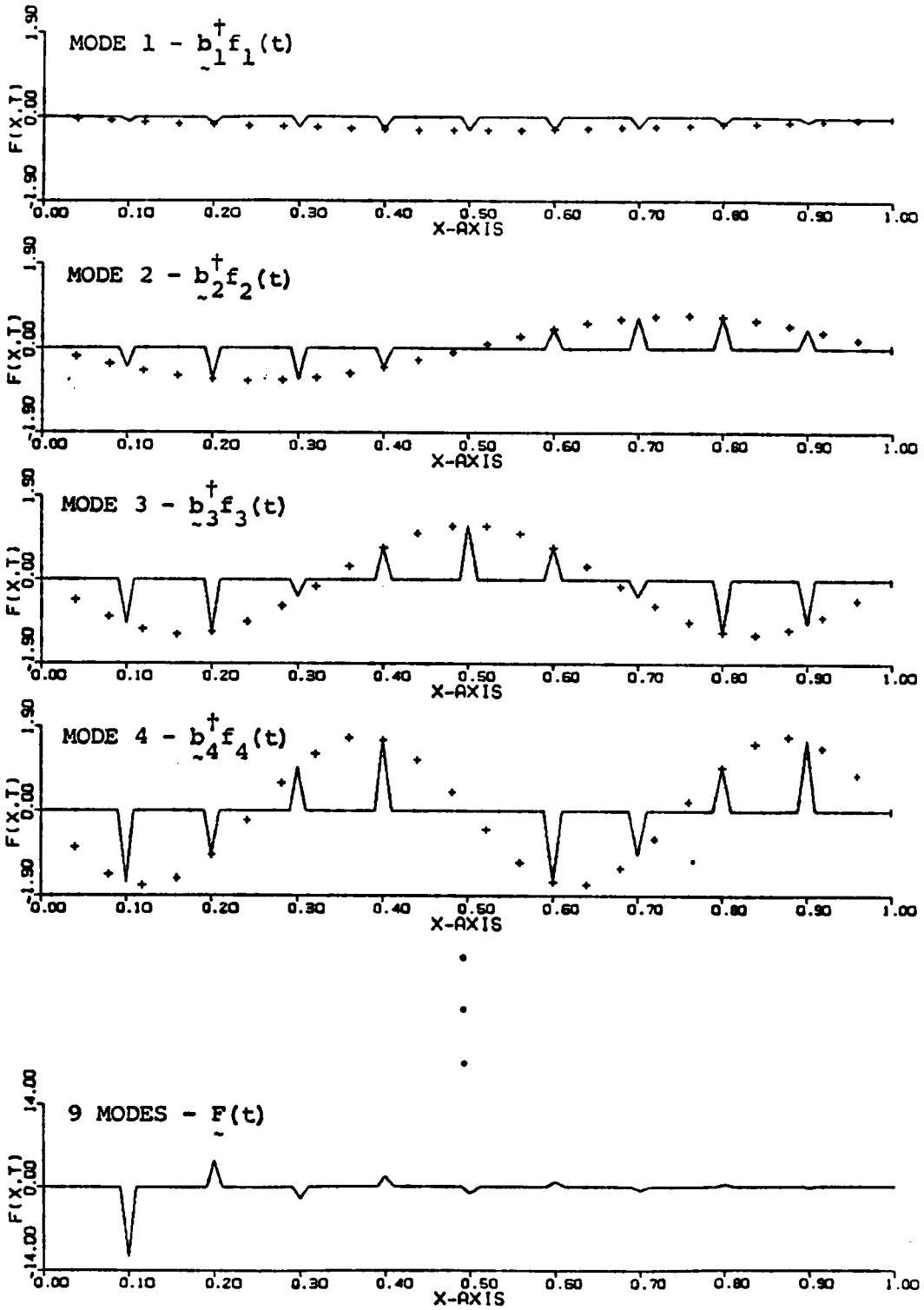

Figure 4.4. Modal contributions to the actuator forces and the resulting sum, the actual actuator forces, for the string in Fig. 4.3 at t = 0.

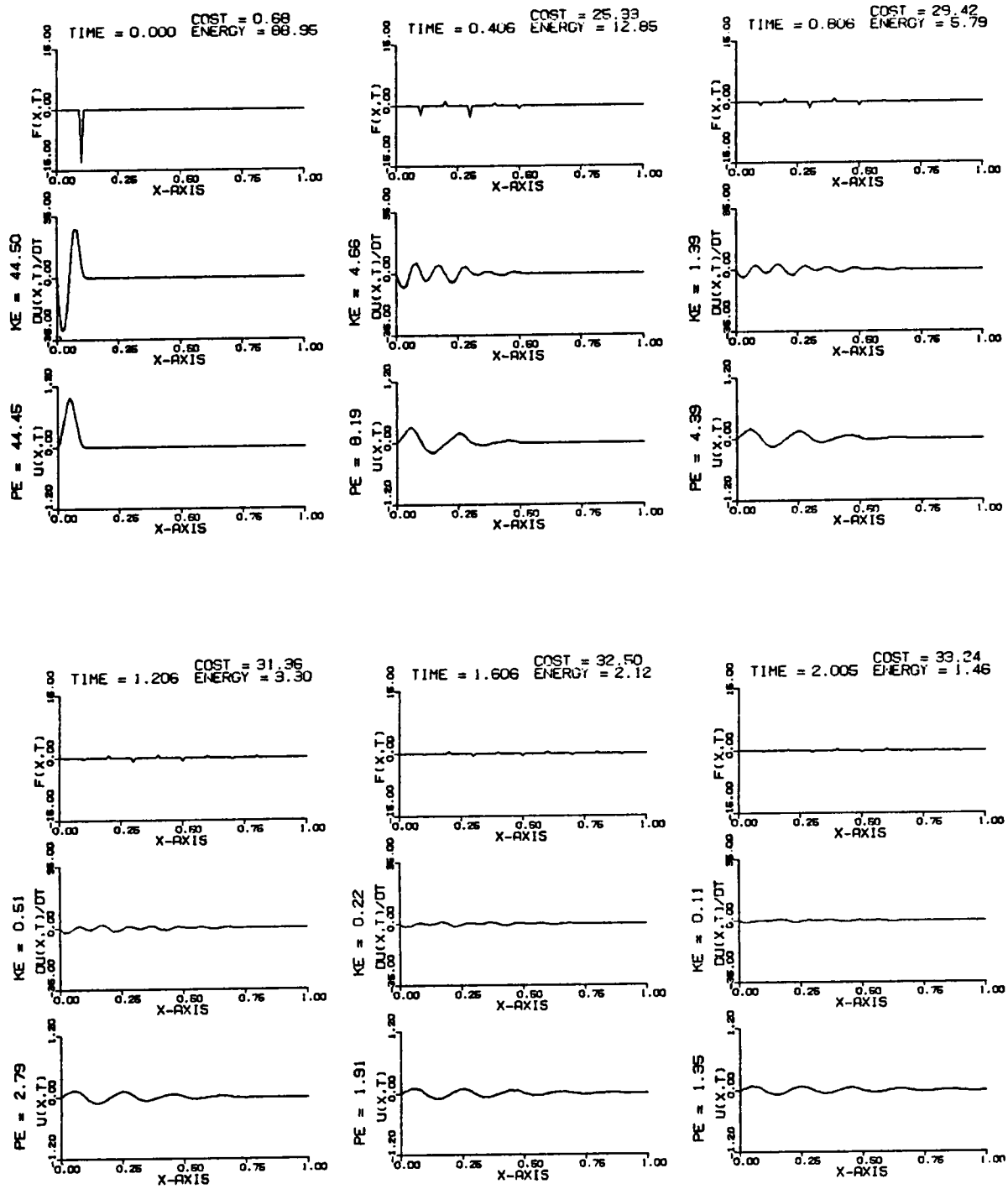

Figure 4.5. Direct feedback control of a wave in a string.

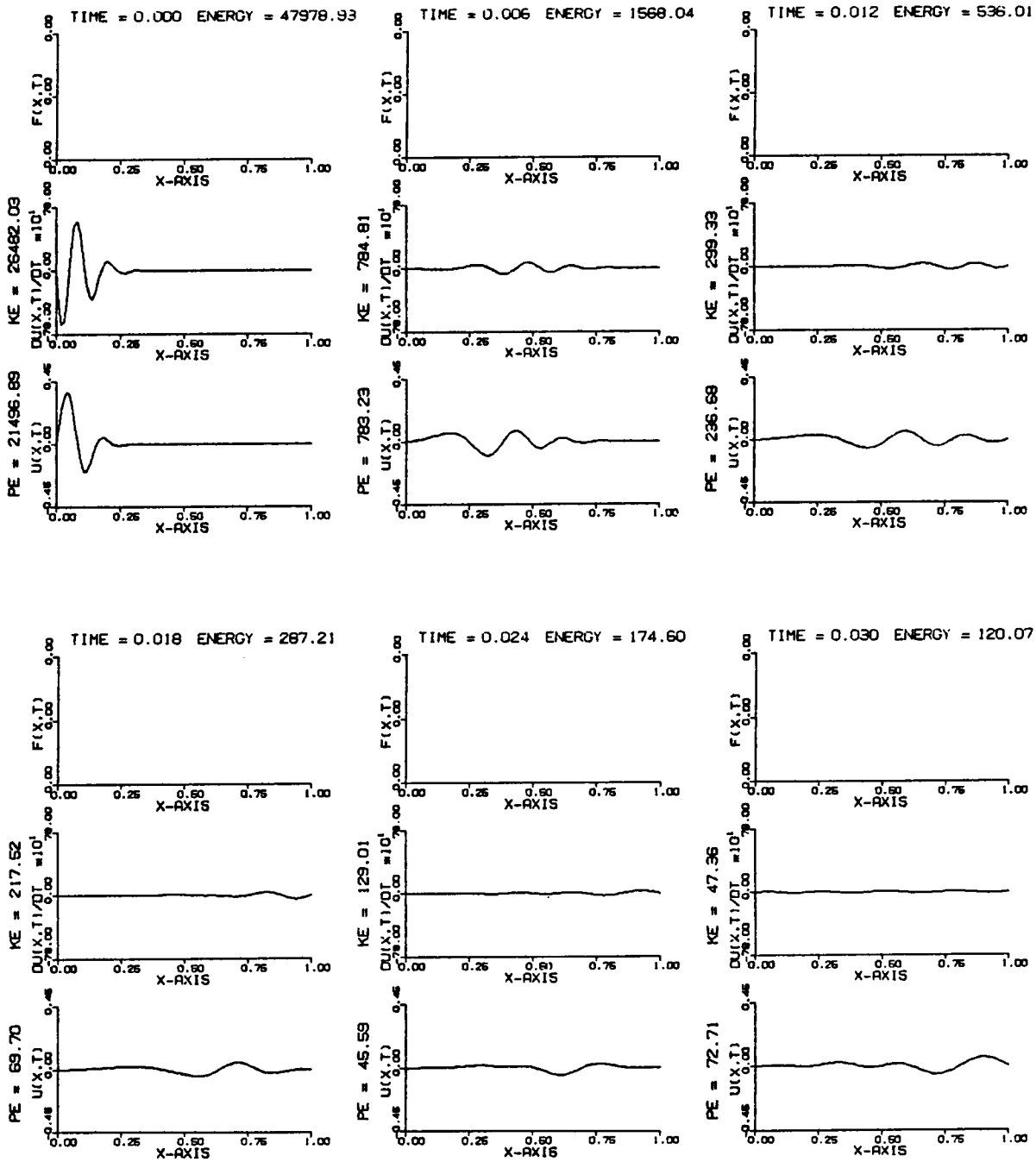

Figure 4.6. Uncontrolled damped wave motion in a beam.

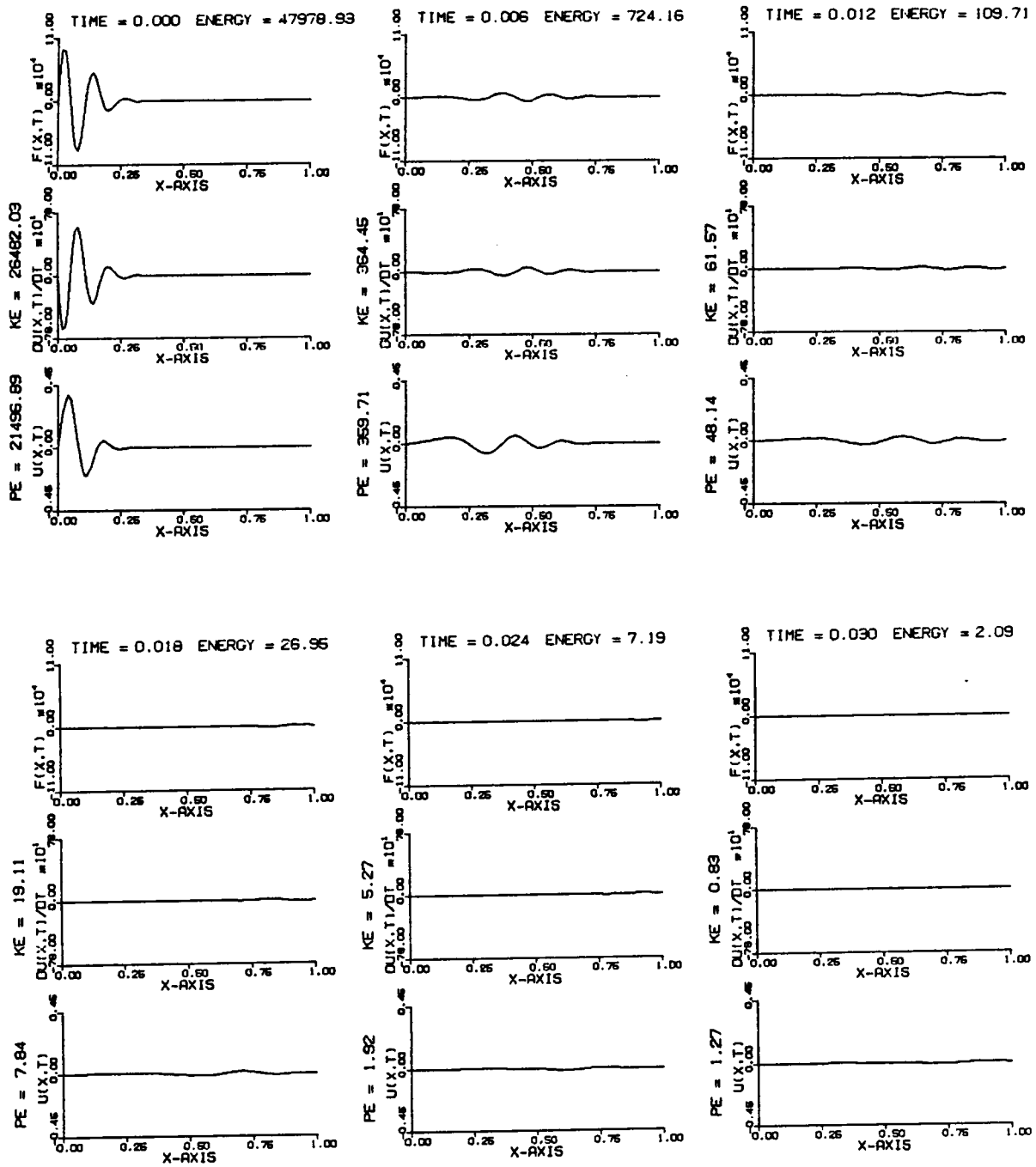

Figure 4.7. Globally optimal (distributed) control of wave motion in a beam.

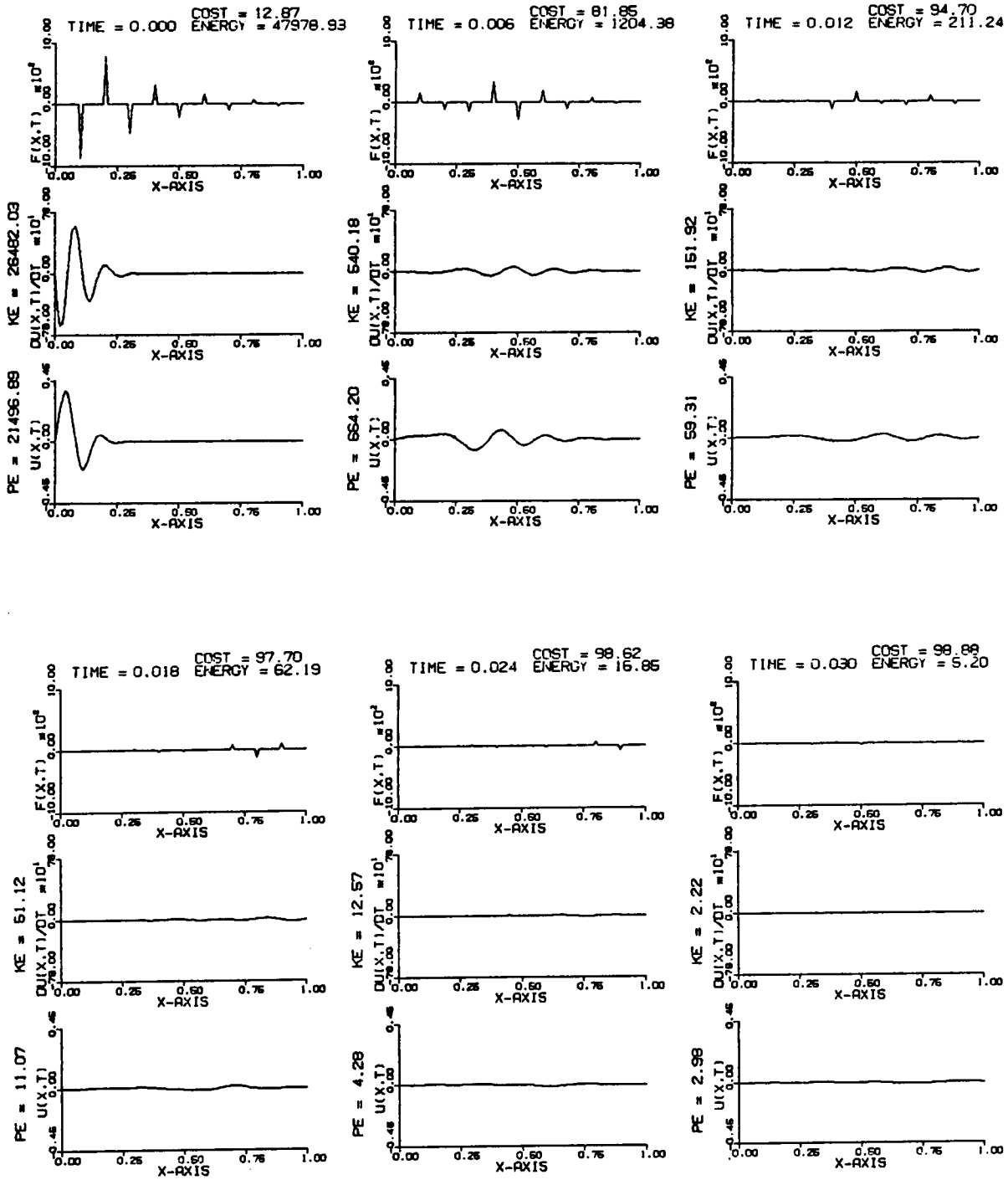

Figure 4.8. Modal control of a wave in a beam, using discrete actuators.

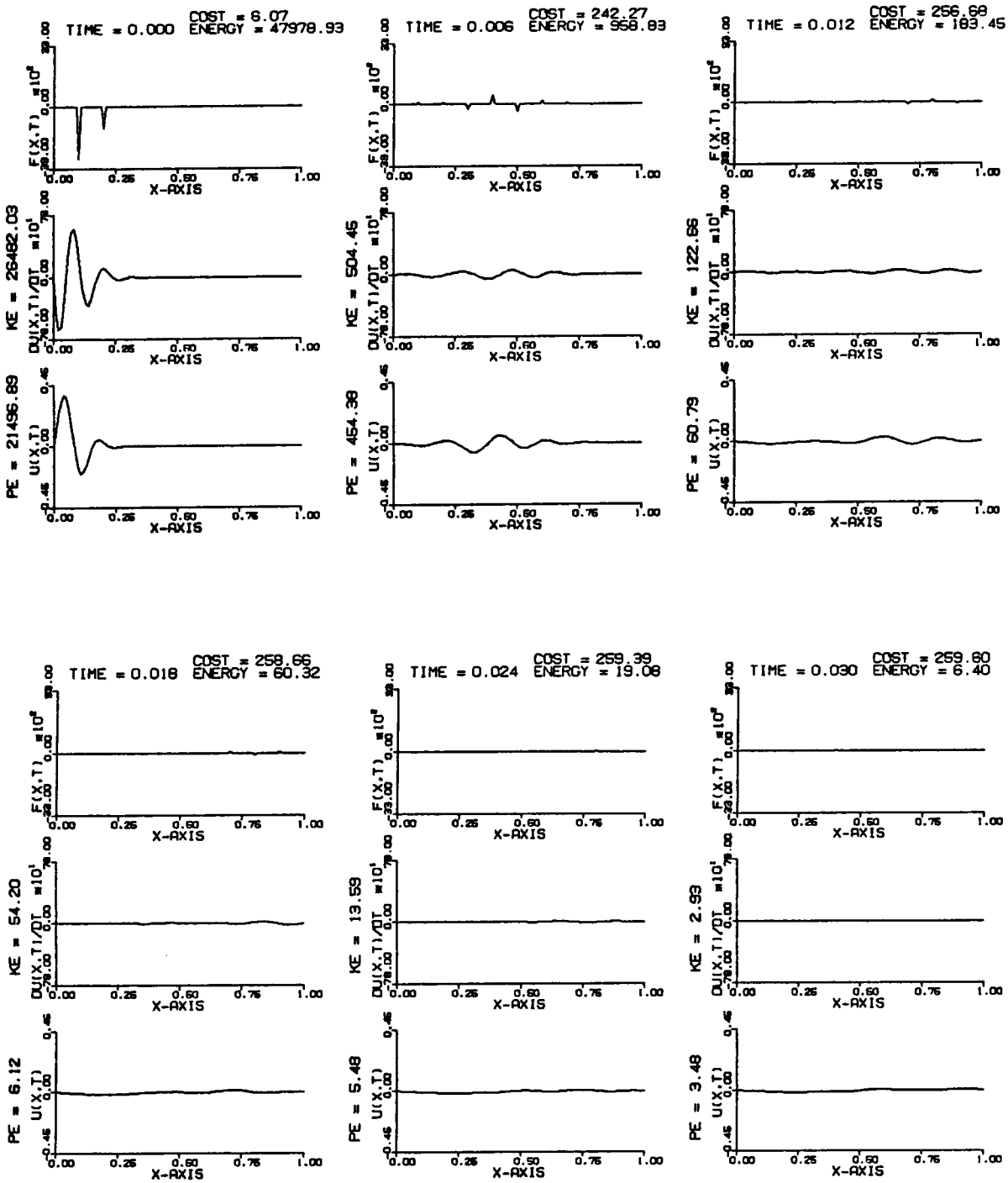

Figure 4.9. Direct feedback control of a wave in a beam.

Chapter 5

ACTIVE VIBRATION CONTROL OF A DISTRIBUTED SYSTEM WITH MOVING SUPPORT

5.1 INTRODUCTION

In this chapter, we are concerned with the active control of a flexible structure whose support is moving significantly. Quite often structures have distributed parameters, such as mass and stiffness, and their behavior is governed by partial differential equations. Yet, for the most part control theory is concerned with lumped-parameter systems described by ordinary differential equations.[24] A common approach has been to discretize the distributed system in space, thus permitting the use of theories developed for lumped systems. As mentioned in the previous chapter, a modal control permitting design of controls for distributed structures has been developed. The Independent Modal-Space Control method proposes to control the vibration of a structure by controlling the modes of the structure.[17] The method requires distributed controls, but can be implemented approximately by means of discrete actuators,[18] provided mode controllability is ensured. As in any modal control method, one must first derive the modal equations and then estimate the modal states for feedback. Modal state estimation requires mode observability. In theory, the entire infinity of modes is observable if the state can be measured at every point of the structure, which requires distributed sensors. If the modal state estimation is to be carried out by discrete sensors, then the question of mode observability does arise. Clearly, a mode is not observable if the sensors are placed at the nodes of the mode in question. For one-dimensional

structures, the nodal points for the lower modes, which are the most likely to be in need of control, are well spaced, so that the estimation of the associated modal states does not present any special problem. On the other hand, for two- and three-dimensional structures, in which the modes are characterized by nodal lines and nodal surfaces, respectively, the problem of mode observability can be critical. Of course, the problem can be obviated by good knowledge of the nodal pattern of the modes to be controlled. The problem of extracting the modal states from sensor measurements of actual states at given points in the structure remains. The process of extracting the modal states involves filtering of the sensor output. There are basically two types of filters, temporal and spatial. Temporal filters essentially resolve the sensor signal into a frequency spectrum. Here again, one-dimensional structures present no problem, as the frequencies tend to be well spaced. The situation is entirely different for two- and three-dimensional structures, for which frequencies can be closely spaced.[27] In fact, in the case of degenerate systems two modes belong to the same eigenvalue and a temporal filter cannot discriminate between the two modes. Spatial filters extract the modal states by making use of the orthogonality of modes, for which reason they are known as modal filters.[28] They require, however, displacement and velocity profiles, which implies distributed sensors. Modal filters can also be implemented by means of discrete sensors, but they tend to require a large number of sensors. In fact, the number of sensors required to estimate a given number of modal states is closely related to the number of elements required in a finite element approximation of the same

modes. In the case of two- and three-dimensional structures, this may mean a very large number of sensors.

The IMSC method is the only one capable of treating distributed structures in closed form. Any approximation enters only in the implementation of the closed-form solution. Yet, the large number of actuators and sensors required can be a drawback at times, so that the question arises whether distributed structures can be controlled by other techniques. As mentioned earlier, a common approach is to discretize the structure in space and treat it as if it were discrete. Such discretization can be carried out conveniently by means of the finite element method,[20] whereby the displacement is represented by a linear combination of admissible functions multiplied by generalized coordinates. The classical Rayleigh-Ritz and the Galerkin method use the same type of representation, but the admissible functions are global functions, whereas in the finite element method they are local functions. As a result, discrete models derived by the classical Rayleigh-Ritz or by the Galerkin method tend to have fewer degrees of freedom than models derived by the finite element method for comparable accuracy,[23] provided there are no pronounced nonuniformities in the mass and stiffness distributions. On the other hand, the advantage of the finite element method over the other methods is that the generalized coodinates represent actual displacements of the structure at given points. Hence, a modeling procedure combining the advantages of the classical Rayleigh-Ritz method and the finite element method is highly desirable. Such a modeling procedure was used in the previous chpater and is developed in a more general form in this chapter. The resulting

equations of motion resemble the equations for a lumped-parameter system in every respect, except that they are meant to represent a distributed system. Unfortunately, it is common practice to use the discrete model for the design of controls, without checking how these control forces work on the actual distributed system.

Early work on control of structures was dominated by the concept of single-input single-output (SISO) control, which implies a single sensor and a single actuator. The best stability characteristics are obtained for the case in which the sensor and actuator are collocated. Of course, SISO control is likely to encounter problems of controllability and observability. It is now commonly accepted that structures, which are characterized by a large number of degrees of freedom, require more than one sensor and one actuator, i.e., they require multi-input multi-output (MIMO) control.

An important problem in controls is the determination of the control gains, where the gains relate the system state to the control forces. In optimal control using a quadratic performance measure, the computation of the control gains requires the solution of a matrix Riccati equation. The control gains can be arranged in a gain matrix, which in general is rectangular. If control forces are applied at every point the state is measured, then the gain matrix consists of two square submatrices, one corresponding to the velocity vector and the other to the displacement vector. In general, the force at one point depends on the state at all the points, so that the gain matrices tend to be fully populated.

A method of control offering simplified implementation is direct feedback control,[19] whereby the control force at a given point depends only on the state at the same point. For this reason, direct feedback control is also known as decentralized control. In terms of the closed-loop equations of motion, direct feedback can be interpreted as providing decoupled inputs. By contrast, IMSC provides complete decoupling, as the modal equations of motion are decoupled by definition and each mode is controlled independently. However, in direct feedback the decoupling is in the actual space, whereas in IMSC the decoupling is in the more abstract modal space. In direct feedback, the gain matrix consists of two diagonal submatrices. The fact that the off-diagonal entries in the two submatrices are zero can be regarded as placing constraints on the controls, so that in general the control can be only suboptimal. Hence, one must weigh the ease of implementation of direct feedback against the desirability of optimal control. On occasions, the ideal situation occurs in which the gain matrix prescribed by optimal control is characterized by two diagonal or nearly diagonal submatrices. In the first case direct feedback is optimal, and in the second case not much is sacrificed by ignoring the off-diagonal elements and retaining the diagonal entries for direct feedback.

In this paper, we are concerned with the problem of controlling the motion of a two-dimensional distributed system with a support that is moving significantly. Because of practical considerations, the control is to be carried out by collocated sensors and actuators. The system is discretized by a Rayleigh-Ritz approach designed so as to retain some of the advantages of the finite element method, in the sense that the

generalized coordinates represent actual displacements. The control is separated into two parts, one designed to mitigate the effect of the moving support on the absolute motion of the plate and the other to minimize the absolute motion. An optimal control, whereby a balance is struck between the desire for a minimal control cost and the desire to keep the response close to zero, is developed. A numerical example illustrates the procedure for general MIMO control, which in this particular case is almost identical to direct feedback control. A check is also done to verify how the discrete control works on the actual distributed system.

5.2 PROBLEM FORMULATION

We consider the problem of suppressing the motion of a rectangular thin plate hinged to a supporting frame on all four edges (Fig. 5.1), where the frame displacement is a continuous function of time. Assuming that the plate is uniform, the equation of motion is[25]

$$m\ddot{w}(x,y,t) + D\nabla^4 w(x,y,t) = f(x,y,t) \qquad (5.1)$$

where m is the mass per unit area of the plate, $w(x,y,t)$ is the transverse deflection and D is the flexural rigidity of the plate, given by $D = Eh^3/12(1 - \nu^2)$, where E is Young's modulus, h is the plate thickness and ν is Poisson's ratio. Moreover, ∇^4 is the biharmonic operator and $f(x,y,t)$ is the control force per unit area of the plate. If $u(t)$ is the transverse displacement of the supporting frame, which is assumed to be rigid, then the plate satisfies the boundary conditions

$$w(0,y,t) = w(a,y,t) = w(x,0,t) = w(x,b,t) = u(t) \qquad (5.2a)$$

$$w_{xx}(0,y,t) = w_{xx}(a,y,t) = w_{yy}(x,0,t) = w_{yy}(x,b,t) = 0 \qquad (5.2b)$$

where a and b are the dimensions of the plate in the x and y directions, respectively. Note that the subscripts x and y denote derivatives with respect to these spatial variables.

It will prove convenient to express Eq. (5.1) in terms of the displacement v(x,y,t) of a point on the plate relative to the rigid frame. Hence, introducing

$$v(x,y,t) = w(x,y,t) - u(t) \tag{5.3}$$

into Eq. (5.1), we obtain

$$m\ddot{v}(x,y,t) + D\nabla^4 v(x,y,t) = f(x,y,t) - m\ddot{u}(t) \tag{5.4}$$

where we recognized that $\nabla^4 u = 0$. The relative displacement is subject to the boundary conditions

$$v(0,y,t) = v(a,y,t) = v(x,0,t) = v(x,b,t) = 0 \tag{5.5a}$$

$$v_{xx}(0,y,t) = v_{xx}(a,y,t) = v_{yy}(x,0,t) = v_{yy}(x,b,t) = 0 \tag{5.5b}$$

With these boundary conditions, we can express the relative displacement of the plate in terms of the eigenfunctions of a simply supported plate, or a set of admissible functions with zero displacement at the boundaries.

5.3 OPTIMAL CONTROL

The feedback control force f(x,y,t) depends on the transverse deflection and velocity of the plate. To establish a suitable relationship between the control force and the motion of the plate, we use an optimal control approach and attempt to minimize a performance measure of the form

$$J = \int_0^{t_f} \{\int_A [g(\dot{w}(x,y,t), w(x,y,t)) + rf^2(x,y,t)]dA\}dt \tag{5.6}$$

where A is the area of the plate, t_f is the final time, $g(\dot{w}(x,y,t),$

$w(x,y,t))$ is a function of the plate motion and $rf^2(x,y,t)$ represents the control effort. A distributed control problem does not ordinarily lend itself to closed-form solution, especially when the system is subjected to arbitrary motion of its support.

In view of the above, we propose to approximate the solution of the optimal control problem by constructing a discrete model of the plate by means of the Rayleigh-Ritz method. To this end, we assume that the relative displacement $v(x,y,t)$ can be represented by means of a series of n admissible functions $\psi_i(x,y)$ in the form

$$v(x,y,t) = \sum_{i=1}^{n} a_i(t)\psi_i(x,y) = \underset{\sim}{a}^T(t)\underset{\sim}{\psi}(x,y) \tag{5.7}$$

where $a_i(t)$ $(i = 1,2,\ldots,n)$ are generalized coordinates. We assume that the admissible functions are such that the components of the vector $\underset{\sim}{a}(t)$ represent the actual relative displacement of the plate at n discrete points, or

$$a_i(t) = v(x_i,y_i,t), \quad i = 1,2,\ldots,n \tag{5.8}$$

which implies that the admissible function $\psi_i(x,y)$ has unit amplitude at $x = x_i$ and $y = y_i$ $(i = 1,2,\ldots,n)$. We also assume that the distributed control force can be implemented by an n-dimensional control vector as follows:

$$f(x,y,t) = \sum_{i=1}^{n} F_i(t)\bar{f}_i(x,y) = \underset{\sim}{F}^T(t)\underset{\sim}{\bar{f}}(x,y) \tag{5.9}$$

where the components $F_i(t)$ of the control vector $\underset{\sim}{F}(t)$ play the role of amplitudes and the functions $\bar{f}_i(x,y)$ give the spatial distribution of the individual control forces.

Using Eqs. (5.3) and (5.7), the kinetic energy can be written in the form

$$T = \frac{1}{2}\int_A m\dot{w}^2(x,y,t)dA = \frac{1}{2}\int_A m[\dot{\underset{\sim}{a}}^T(t)\underset{\sim}{\psi}(x,y) + \dot{u}(t)]^2 dA$$

$$= \frac{1}{2}\dot{\underset{\sim}{a}}^T(\int_A m\underset{\sim}{\psi}\underset{\sim}{\psi}^T dA)\dot{\underset{\sim}{a}} + \dot{\underset{\sim}{a}}^T(\int_A m\underset{\sim}{\psi}\, dA)\dot{u} + \frac{1}{2}mA\dot{u}^2$$

$$= \frac{1}{2}\dot{\underset{\sim}{a}}^T M\dot{\underset{\sim}{a}} + \dot{\underset{\sim}{a}}^T\underset{\sim}{\rho}\dot{u} + \frac{1}{2}mA\dot{u}^2 \qquad (5.10)$$

where

$$M = \int_A m\underset{\sim}{\psi}\underset{\sim}{\psi}^T dA, \quad \underset{\sim}{\rho} = \int_A m\underset{\sim}{\psi}\, dA \qquad (5.11a,b)$$

in which M plays the role of a mass matrix. Similarly, the potential energy becomes

$$V = \frac{1}{2}\underset{\sim}{a}^T\{\int_A D[(\underset{\sim}{\psi}_{xx} + \underset{\sim}{\psi}_{yy})(\underset{\sim}{\psi}_{xx}^T + \underset{\sim}{\psi}_{yy}^T) - (1 - \nu)(\underset{\sim}{\psi}_{xx}\underset{\sim}{\psi}_{yy}^T$$

$$+ \underset{\sim}{\psi}_{yy}\underset{\sim}{\psi}_{xx}^T - 2\underset{\sim}{\psi}_{xy}\underset{\sim}{\psi}_{xy}^T)]dA\}\underset{\sim}{a} = \frac{1}{2}\underset{\sim}{a}^T K\underset{\sim}{a} \qquad (5.12)$$

where

$$K = \int_A D[(\underset{\sim}{\psi}_{xx} + \underset{\sim}{\psi}_{yy})(\underset{\sim}{\psi}_{xx}^T + \underset{\sim}{\psi}_{yy}^T) - (1 - \nu)(\underset{\sim}{\psi}_{xx}\underset{\sim}{\psi}_{yy}^T + \underset{\sim}{\psi}_{yy}\underset{\sim}{\psi}_{xx}^T$$
$$- 2\underset{\sim}{\psi}_{xy}\underset{\sim}{\psi}_{xy}^T)]dA \qquad (5.13)$$

plays the role of a stiffness matrix. The virtual work due to the actuators is

$$\delta W_{act} = \int_A f(x,y,t)\delta w(x,y,t)dA = \int_A \underset{\sim}{F}^T(t)\bar{\underset{\sim}{f}}(x,y)\underset{\sim}{\psi}^T(x,y)\delta\underset{\sim}{a}(t)dA$$

$$= \underset{\sim}{F}^T(t)(\int_A \bar{\underset{\sim}{f}}\underset{\sim}{\psi}^T dA)\delta\underset{\sim}{a}(t) = \underset{\sim}{F}^T Z^T\delta\underset{\sim}{a} \qquad (5.14)$$

where

$$Z^T = \int_A \bar{\underset{\sim}{f}}\underset{\sim}{\psi}^T dA \qquad (5.15)$$

The equations of motion for the discretized system can be obtained by inserting Eqs. (5.10), (5.12) and (5.14) into Lagrange's equations,[25] with the result

$$M\ddot{\underset{\sim}{a}} + K\underset{\sim}{a} = Z\underset{\sim}{F} - \underset{\sim}{\rho}\ddot{u} \qquad (5.16)$$

Remembering that $\underset{\sim}{a}$ contains actual relative displacements, we can construct a vector of actual absolute displacements by writing

$$\underset{\sim}{b}(t) = \underset{\sim}{a}(t) + \underset{\sim}{1}u(t) \tag{5.17}$$

where $\underset{\sim}{1}$ is a vector with every component having the value of unity. In terms of $\underset{\sim}{b}$, the equations of motion become

$$M\ddot{\underset{\sim}{b}} + K\underset{\sim}{b} = Z\underset{\sim}{F} + (M\underset{\sim}{1} - \underset{\sim}{\rho})\ddot{u} + K\underset{\sim}{1}u \tag{5.18}$$

The control task can be divided into two parts, one concerned with the reduction of the effect of the frame motion on the plate and another concerned with the actual reduction of the plate motion. To this end, we express the actuator force vector in the form

$$\underset{\sim}{F} = \underset{\sim}{F}_C + \underset{\sim}{F}_R \tag{5.19}$$

where

$$\underset{\sim}{F}_C = -Z^{-1}[M\underset{\sim}{1} - \underset{\sim}{\rho})\ddot{u} + K\underset{\sim}{1}u] \tag{5.20}$$

cancels the effect of the frame motion on the plate motion. Introducing Eqs. (5.19) and (5.20) into Eq. (5.18), we obtain

$$M\ddot{\underset{\sim}{b}} + K\underset{\sim}{b} = Z\underset{\sim}{F}_R \tag{5.21}$$

Equation (5.21) represents a simple regulator problem (in which the support motion has been eliminated) and the control gains can be obtained by standard optimal control theory. To this end, we introduce the state vector $\underset{\sim}{x} = [\underset{\sim}{b}^T \vdots \dot{\underset{\sim}{b}}^T]^T$, so that Eq. (5.21) can be expressed as

$$\dot{\underset{\sim}{x}} = A\underset{\sim}{x} + B\underset{\sim}{F}_R \tag{5.22}$$

where the coefficient matrices have the form

$$A = \begin{bmatrix} 0 & \vdots & I \\ \cdots & \vdots & \cdots \\ -M^{-1}K & \vdots & 0 \end{bmatrix}, \quad B = \begin{bmatrix} 0 \\ \cdots \\ M^{-1}Z \end{bmatrix} \tag{5.23}$$

Optimal control gains can be obtained by minimizing the performance measure

$$J = \int_0^{t_f} (\underset{\sim}{x}^T \underset{\sim}{x} + \underset{\sim}{F}_R^T R \underset{\sim}{F}_R) dt \tag{5.24}$$

which in turn implies solving the matrix Riccati equation[24]

$$\dot{P} = I - PBR^{-1}B^TP + A^TP + PA \tag{5.25}$$

for the Riccati matrix P. Then, the optimal control gain matrix can be computed from

$$G = R^{-1}B^TP \tag{5.26}$$

Finally, the actuator force vector can be written in the form

$$\underset{\sim}{F}_R = -G\underset{\sim}{x} = -G_d\underset{\sim}{b} - G_v\dot{\underset{\sim}{b}} \tag{5.27}$$

where G_d and G_v are control gain matrices associated with displacement and velocity feedback, respectively. The Riccati matrix obtained by solving Eq. (5.25) depends on time, and we prefer to work with constant gains. By letting t_f approach infinity, the Riccati matrix approaches a constant value. The constant Riccati matrix solves the steady-state Riccati matrix equation, an algebraic equation obtained by setting $\dot{P} = 0$ in Eq. (5.25).

Because $\underset{\sim}{F}_C$ was determined without regard to the cost of the control effort, it is likely that the cost associated with isolating the plate motion completely from the frame motion will be excessive. For this reason, we introduce a factor α representing a measure of how completely the control force cancels the effect of the moving support, so that the control force becomes

$$\underset{\sim}{F} = \alpha\underset{\sim}{F}_C + \underset{\sim}{F}_R \tag{5.28}$$

where $0 \leq \alpha \leq 1$. The implication is that if the effect of the moving frame is not cancelled completely by the first term in Eq. (5.28), the

response to the remainder of the excitation will be reduced further by the second term. We propose to determine a value for α so as to minimize the performance measure.

Although the frame motion u(t) is not likely to be known in advance, in many applications we have a reasonably good idea of its frequency spectrum. Because any function of time can be resolved into harmonic components by a Fourier transform, an attractive approach is to determine an optimal value of α for harmonic motion of the frame with an arbitrary frequency ω. This information, along with the expected power spectral density for u(t), will indicate what value of α is appropriate in a given case. To find an optimal value for α in Eq. (5.28), we find the steady-state response of the controlled plate to a harmonic motion of the frame using Eqs. (5.18), (5.20), (5.27) and (5.28) and minimize the resulting average value of the integrand in

$$J = \int_0^{t_f} (\dot{\underset{\sim}{b}}^T \dot{\underset{\sim}{b}} + \underset{\sim}{b}^T \underset{\sim}{b} + \underset{\sim}{F}^T R \underset{\sim}{F}) dt \tag{5.29}$$

with respect to α. Using Eqs. (5.20), (5.27) and (5.28), Eq. (5.18) becomes

$$M\ddot{\underset{\sim}{b}} + K\underset{\sim}{b} = -Z[G_v \dot{\underset{\sim}{b}} + G_d \underset{\sim}{b}] + (1 - \alpha)[(M\underset{\sim}{1} - \underset{\sim}{\rho})\ddot{u} + K\underset{\sim}{1}u] \tag{5.30}$$

Letting

$$u(t) = \cos \omega t = \mathrm{Re}(e^{i\omega t}) \tag{5.31}$$

and assuming the steady-state response in the form

$$\underset{\sim}{b}_{ss}(t) = \mathrm{Re}(\underset{\sim}{b}_0 e^{i\omega t}) \tag{5.32}$$

where $\underset{\sim}{b}_0$ can be complex, we obtain

$$[-\omega^2 M + i\omega Z G_v + K + Z G_d]\underset{\sim}{b}_0 = (1 - \alpha)[-\omega^2 (M\underset{\sim}{1} - \underset{\sim}{\rho}) + K\underset{\sim}{1}] \tag{5.33}$$

from which

$$\underset{\sim}{b}_0 = [-\omega^2 M + i\omega Z G_v + K + Z G_d]^{-1}[-\omega^2 (M\underset{\sim}{1} - \underset{\sim}{\rho}) + K\underset{\sim}{1}](1 - \alpha) \tag{5.34}$$

Letting

$$A = -\omega^2 M + K + ZG_d \ , \ B = \omega Z G_v \tag{5.35a,b}$$

and noting that

$$[A + iB]^{-1} = [B^{-1}A - iI][AB^{-1}A + B]^{-1} \tag{5.36}$$

we obtain the steady-state solution

$$\begin{aligned} \underset{\sim}{b}_{ss}(t) &= \mathrm{Re}\{[B^{-1}A - iI][AB^{-1}A + B]^{-1}[-\omega^2(M\underset{\sim}{1} - \underset{\sim}{\rho}) + K\underset{\sim}{1}](1 - \alpha)e^{i\omega t}\} \\ &= [B^{-1}A \cos \omega t + I \sin \omega t][AB^{-1}A + B]^{-1}[-\omega^2(M\underset{\sim}{1} - \underset{\sim}{\rho}) \\ &\quad + K\underset{\sim}{1}](1 - \alpha) \end{aligned} \tag{5.37}$$

and

$$\begin{aligned} \dot{\underset{\sim}{b}}_{ss}(t) &= [-B^{-1}A \sin \omega t + I \cos \omega t][AB^{-1}A + B]^{-1}[-\omega^2(M\underset{\sim}{1} - \underset{\sim}{\rho}) \\ &\quad + K\underset{\sim}{1}](1 - \alpha)\omega \end{aligned} \tag{5.38}$$

Then, the control force becomes

$$\underset{\sim}{F}_{ss} = -\alpha Z^{-1}[-\omega^2(M\underset{\sim}{1} - \underset{\sim}{\rho}) + K\underset{\sim}{1}] \cos \omega t - G_v \dot{\underset{\sim}{b}}_{ss} - G_d \underset{\sim}{b}_{ss} \tag{5.39}$$

Now, having Eqs. (5.37), (5.38) and (5.39), we can find the steady-state value of the integrand in Eq. (5.29). We refer to this steady-state value as $j_{ss}(\alpha,\omega,t)$ because it depends on the parameters α and ω and is periodic in time, having the same period as the frame motion. The next step is to average the integrand over one period in time, which yields

$$j_{ave}(\alpha,\omega) = p(\omega)\frac{(1 - \alpha)^2}{2} + q(\omega)\frac{\alpha^2}{2} + r(\omega)\alpha(1 - \alpha) \tag{5.40}$$

in which

$$\begin{aligned} p(\omega) &= [-\omega^2(M\underset{\sim}{1} - \underset{\sim}{\rho}) + K\underset{\sim}{1}]^T[AB^{-1}A + B]^{-T}\{(I + A^TB^{-T}B^{-1}A \\ &\quad + G_v^TRG_v + A^TB^{-T}G_v^TRG_vB^{-1}A)\omega^2 + (G_v^TRG_dB^{-1}A + A^TB^{-T}G_d^TRG_v \end{aligned}$$

$$- A^T B^{-T} G_v^T R G_d - G_d^T R G_v B^{-1} A)\omega + I + A^T B^{-T} B^{-1} A +$$

$$A^T B^{-T} G_d^T R G_d B^{-1} A + G_d^T R G_d\}[AB^{-1}A + B]^{-1}[-\omega^2(M\underset{\sim}{1} - \underset{\sim}{\rho}) + K\underset{\sim}{1}] \quad (5.41a)$$

$$q(\omega) = [-\omega^2(M\underset{\sim}{1} - \rho) + K\underset{\sim}{1}]^T Z^{-T} R Z^{-1}[-\omega^2(M\underset{\sim}{1} - \underset{\sim}{\rho}) + K\underset{\sim}{1}] \quad (5.41b)$$

$$r(\omega) = [-\omega^2(M\underset{\sim}{1} - \underset{\sim}{\rho}) + K\underset{\sim}{1}]^T Z^{-T} R[\omega G_v + G_d B^{-1} A][AB^{-1}A + B]^{-1}$$

$$\times[-\omega^2(M\underset{\sim}{1} - \underset{\sim}{\rho}) + K\underset{\sim}{1}] \quad (5.41c)$$

The final step in obtaining an optimal value for α is to set

$$\frac{\partial j_{ave}(\alpha,\omega)}{\partial \alpha} = 0 \quad (5.42)$$

and solve for α_{opt}, with the result

$$\alpha_{opt} = \alpha_{opt}(\omega) = \frac{p(\omega) - r(\omega)}{p(\omega) + q(\omega) - 2r(\omega)} \quad (5.43)$$

Now that the dependence of α_{opt} on the frequency has been determined, a suitable value of α can be chosen based on the expected frequency spectrum of the frame motion. This procedure is illustrated in the numerical example.

5.4 A NEW APPROACH TO SPATIAL DISCRETIZATION

In the Introduction, it was mentioned that the classical Rayleigh-Ritz method is a discretization procedure using space-dependent global admissible functions, with the time-dependent generalized coordinates being some abstract quantities. On the other hand, in the finite element method the admissible functions are local functions and the generalized coordinates are actual displacements of the system at given points. The advantage of the classical Rayleigh-Ritz method is that it tends to produce models of comparable accuracy to the finite element

method with far fewer degrees of freedom, provided the mass and stiffness distributions are relatively smooth.[23] On the other hand, the fact that in the finite element method the generalized coordinates are actual coordinates is a clear advantage in control, as the state estimation tends to be simpler. A modeling procedure combining the advantages of the classical Rayleigh-Ritz method and the finite element methods is highly desirable. We propose such a procedure in the following.

Let us consider a set of global admissible functions $\phi_1(x,y)$, $\phi_2(x,y)$,... for the system. The set of admissible functions is complete, so that the motion of the system can be represented to any desired degree of accuracy by a linear combinations of the functions in the set. Hence, let us represent the displacement at an arbitrary point by

$$v(x,y,t) = \sum_{j=1}^{n} \phi_j(x,y)q_j(t) = \underset{\sim}{\phi}^T(x,y)\underset{\sim}{q}(t) \tag{5.44}$$

where $\underset{\sim}{\phi}(x,y)$ is an n-vector of admissible functions and $\underset{\sim}{q}(t)$ is an n-vector of generalized coordinates. Next, we consider a given number of points in the structure and denote the displacement of these points by $a_i(t)$ $(i = 1,2,...,p)$, so that using Eq. (5.44) we can write

$$a_i(t) = v(x_i,y_i,t) = \sum_{j=1}^{n} \phi_j(x_i,y_i)q_j(t) = \underset{\sim}{\phi}^T(x_i,y_i)\underset{\sim}{q}(t), \quad i = 1,2,...,p \tag{5.45}$$

Equations (5.45) can be arranged in the matrix form

$$\underset{\sim}{a}(t) = \Phi\underset{\sim}{q}(t) \tag{5.46}$$

where

$$\Phi = [\Phi_{ij}] = [\phi_j(x_i,y_i)], \quad i = 1,2,...,p; \quad j = 2.3,...,n \tag{5.47}$$

The generalized coordinates can be expressed in terms of actual displacements by writing

$$\underset{\sim}{q}(t) = \Phi^{\dagger}\underset{\sim}{a}(t) \tag{5.48}$$

where $\Phi^{\dagger}$ is the pseudo-inverse of Φ. In the case of interest $p < n$, so that the pseudo-inverse represents a minimum-norm solution of Eq. (5.46) yielding

$$\Phi^{\dagger} = \Phi^{T}(\Phi\Phi^{T})^{-1} \tag{5.49}$$

Of course, when $p = n$ the pseudo-inverse of Φ reduces to the ordinary inverse Φ^{-1}.

Introducing Eq. (5.48) into Eq. (5.44), we obtain

$$v(x,y,t) = \underset{\sim}{\phi}^{T}(x,y)\Phi^{\dagger}\underset{\sim}{a}(t) = \underset{\sim}{\psi}^{T}(x,y)\underset{\sim}{a}(t) \tag{5.50}$$

where

$$\underset{\sim}{\psi}(x,y) = (\Phi^{\dagger})^{T}\underset{\sim}{\phi}(x,y) \tag{5.51}$$

is a vector of admissible functions with entries having the property

$$\psi_j(x_i,y_i) = \delta_{ij}, \quad i,j = 1,2,\ldots,p \tag{5.52}$$

To complete the discretization process, we wish to express the various coefficients in terms of the special admissible functions considered above. Inserting Eq. (5.51) into Eq. (5.11a), we obtain

$$M = \int_A m\underset{\sim}{\psi}\underset{\sim}{\psi}^{T}dA = (\Phi^{\dagger})^{T}(\int_A m\underset{\sim}{\phi}\underset{\sim}{\phi}^{T}dA)\Phi^{\dagger} = (\Phi^{\dagger})^{T}M^{*}\Phi^{\dagger} \tag{5.53}$$

where

$$M^{*} = \int_A m\underset{\sim}{\phi}\underset{\sim}{\phi}^{T}dA \tag{5.54}$$

is an $n\times n$ mass matrix corresponding to the set of admissible functions $\phi_1, \phi_2,\ldots,\phi_n$. Similarly, from Eq. (5.11b),

$$\underset{\sim}{\rho} = \int_A m\underset{\sim}{\psi}dD = (\Phi^{\dagger})^{T}\int_A m\underset{\sim}{\phi}dA = (\Phi^{\dagger})^{T}\underset{\sim}{\rho}^{*} \tag{5.55}$$

where

$$\underset{\sim}{\rho}^* = \int_A m\underset{\sim}{\phi}\, dA \tag{5.56}$$

is an n-vector. Finally, using Eq. (5.13), we obtain

$$K = (\Phi^\dagger)^T K^* \Phi^\dagger \tag{5.57}$$

where

$$K^* = \int_A D[(\underset{\sim}{\phi}_{xx} + \underset{\sim}{\phi}_{yy})(\underset{\sim}{\phi}^T_{xx} + \underset{\sim}{\phi}^T_{yy}) - (1 - \nu)(\underset{\sim}{\phi}_{xx}\underset{\sim}{\phi}^T_{yy} + \underset{\sim}{\phi}_{yy}\underset{\sim}{\phi}^T_{xx} - 2\underset{\sim}{\phi}_{xy}\underset{\sim}{\phi}^T_{xy})]dA \tag{5.58}$$

is an n×n stiffness matrix.

Quite often, discretization in controls is dictated by the fact that the actuators and sensors are discrete components, rather than by inability to obtain a closed-form solution to the distributed open-loop eigenvalue problem. If the distributed eigenvalue problem does admit a closed-form solution, then we can use the system eigenfunctions as admissible functions. If not, we can use the best available set of approximate eigenfunctions. These actual or approximate eigenfunctions are orthogonal and can be normalized so that $M^* = I$ and $K^* = \Lambda$, where I is the n×n identity matrix and Λ is the n×n diagonal matrix of eigenvalues. In this case, Eqs. (5.53) and (5.57) reduce to

$$M = (\Phi^\dagger)^T \Phi^\dagger \quad , \quad K = (\Phi^\dagger)^T \Lambda \Phi^\dagger \tag{5.59a,b}$$

Finally, in the special case in which there are as many eigenfunctions as discrete points, n = p, the pseudo-inverse of Φ reduces to the actual inverse of Φ, so that Eqs. (5.59) and (5.55) become

$$M = (\Phi^{-1})^T \Phi^{-1} \quad , \quad K = (\Phi^{-1})^T \Lambda \Phi^{-1} \quad , \quad \underset{\sim}{\rho} = (\Phi^{-1})^T \underset{\sim}{\rho}^* \tag{5.60a,b}$$

where $\underset{\sim}{\rho}^*$ is given by Eq. (5.56). This assumes that Φ is nonsingular, which cannot be guaranteed for two- and three-dimensional domains.

In addition to an increase in accuracy, the Rayleigh-Ritz approach proposed here offers another advantage over the finite element method in the case of fourth order problems. More specifically, for fourth-order problems, the finite element method requires the inclusion of rotational degrees of freedom, whereas the approach proposed here not only permits the displacement to be expressed in terms of translational degrees of freedom alone, but also these degrees of freedom represent actual displacements at the points of application of the actuator forces. We note that we could have added rotational degrees of freedom, if torque actuators were to be used. In general, this discretization approach facilitates the construction of a model equal in order to the number of actuators, with the displacements being consistent with the type of actuators inputs, in the sense that we can use translational displacements with force actuators and/or rotational displacements with torquers.

5.5 NUMERICAL EXAMPLE

As an illustration of the approach presented above, we consider the control of a steel plate with the dimensions a = 32 in, b = 24 in and h = 1/16 in, where h is the thickness. The plate is simply supported by a rigid moving frame, as shown in Fig. 5.1. The plate is controlled by means of 16 point actuators (Fig. 5.1), with displacement and velocity sensors at each actuator location. We assume that the relative motion can be represented in terms of sixteen of the lower modes, which are

$$\phi_i(x,y) = \frac{2}{\sqrt{mab}} \sin \frac{r_i \pi x}{a} \sin \frac{s_i \pi y}{b} \tag{5.61}$$

where r_i and s_i are integers corresponding to the ith mode. It turns out that, with our choice of actuator locations, the columns of Φ in Eq. (5.47) corresponding to the twelfth and fifteenth modes are linearly dependent on other columns of Φ. We replace them with rows corresponding to two higher modes, namely the seventeenth and twenty-first, so that Φ can be inverted. This still leaves us with a model that is likely to represent nearly all of the lower modes very well, from which we can obtain a near-optimal control system.

Because the actuators used in this example apply forces at points, the functions $\bar{f}_i(x,y)$ in Eq. (5.9) have the form

$$\bar{f}_i(x,y) = \delta(x - x_i, y - y_i) \tag{5.62}$$

where δ denotes a spatial Dirac delta function. As a result, the matrix Z in Eq. (5.15) becomes the identity matrix. The mass and stiffness matrices and the vector $\underset{\sim}{\rho}$ are obtained using Eqs. (5.60). We take the control effort weighting matrix R in Eq. (5.29) to be R = rI, where r is a scalar, so that the actuators are weighted equally.

Figure 5.2 shows the optimal value of α as a function of the frequency of the frame motion ω for several values of r. In the upper curves, r has a lower value, so that the control effort has a lower cost. As r increases, we note that in the lower curves $\alpha_{opt}(\omega)$ develops peaks in the neighborhood of natural frequencies for the symmetric modes, which are the only modes excited by the frame motion in this system. The reason is that isolation of the plate vibration from the frame excitation is more crucial near resonance. The frequencies for the lower symmetric modes are ω = 102, 398, 607 and 922 rad/s.

The question of how much difference the value of α makes to the performance of the system remains. In answer to this, Fig. 5.3 shows a plot of $j_{ave}(\alpha,\omega)$ versus α for several frequencies of the frame motion, with $r = 1.0\times10^{-3}$. The curves in Fig. 5.3 can perhaps be better understood by imagining a three-dimensional plot with ω as the third dimension. Then, the curves can be regarded as lines of constant ω on a surface having the form of a curving trough; each of these lines has a minimum corresponding to α_{opt}. As the frequency increases, α_{opt} increases to almost one, and then decreases again, as in the upper curve in Fig. 5.2. We note from Fig. 5.3 that choosing $\alpha = 0$ (strictly a regulator control) can cause an increase in the performance index of over 85%, and choosing $\alpha = 1$ (complete isolation from the frame motion) can increase the performance index by over 50%, for certain values of ω. The fact that the curves in Fig. 5.3 are relatively flat in the neighborhood of α_{opt} indicates that a deviation from α_{opt} alters the performance only slightly. Hence, if the frame motion is a relatively narrow-band random process rather than a simple harmonic function of time, we can still expect the control system to perform well.

In calculating the optimal gain matrices G_v and G_d, it was observed that the diagonal entries in G_v were several orders of magnitude greater than the off-diagonal entries, and that all of the entries in G_d were sufficiently small that their contribution to the control forces were negligible. This suggests that the off-diagonal entries in G_v and the entire G_d matrix can be ignored without degrading the optimal performance significantly. Use of a diagonal G_v matrix and zero G_d matrix simplifies implementation of the control system considerably, as each

actuator force has a regulator component that is simply proportional to the absolute velocity of the plate at that actuator location, and hence the control represents direct velocity feedback, and a vibration isolation component that is proportional to the frame displacement and acceleration, from Eq. (5.20). Such a system can be implemented with ease in continuous time, rather than in discrete time, because each of the actuator forces can be obtained by merely amplifying the corresponding sensor signals, instead of using all the sensor signals to compute each of these forces. The system response was computed both with fully populated gain matrices and with a diagonal G_V alone, and there was essentially no difference. Indeed, the controlled response of the plate was identical to within three significant digits in the two cases.

Figure 5.4 contains plots of the absolute plate motion at the fifth and sixth actuator locations, with the frame moving with a frequency of ω = 480 rad/s and an amplitude of 0.1 in. Optimal gains were based on a control effort weighting factor of r = 0.004. The actuators are inactive before t = 0, so that the plate is initially undergoing steady-state uncontrolled response to the frame motion. As time progresses, the system makes the transition to the steady-state controlled response. In the upper plot α = 0, so that the control is simply a regulator control. In the center plot $\alpha = \alpha_{opt} \approx 0.5$ and in the lower plot α = 1, so that in the latter case the plate is isolated from the frame motion. These time histories were obtained using a discrete-time approach, in which the actuator forces for each time step were determined from the plate and frame motion at the beginning of each time step. The plate

motion was assumed to be as predicted by the model described above. As expected, as α increases the plate motion decreases.

Figure 5.5 shows the integrand of the performance index in Eq. (5.29) for the three cases of Fig. 5.4. As expected, the curve corresponding to $\alpha = \alpha_{opt}$ has the lowest average cost.

The results obtained so far are based on the sixteen-degree-of-freedom model for the plate. We have assumed that this model is sufficiently accurate that the control system designed for the model will work well on the actual plate as well. To verify this assumption, a check was made to see how the control system designed for the Rayleigh-Ritz model works on the actual plate, which we modeled in terms of its lowest forty modes. Figure 5.6 contains plots similar to those in Fig. 5.4, except that for Fig. 5.6 forty modes of the plate were modeled.

The agreement between Figs. 5.4 and 5.6 attests to the quality of the model used to design the control system. Figure 5.7 again shows the integrand of the performance index versus time for the three values of α in Fig. 5.6 and again it agrees very well with Fig. 5.5. From Fig. 5.7 we can see that using $\alpha = 0$ results in an average performance index 39% greater than that obtained using $\alpha = \alpha_{opt}$ and using $\alpha = 1$ results in an increase in the performance index of 33%.

5.6 CONCLUSIONS

A method is presented for minimizing the motion of a plate attached to a moving rigid frame. Because the frame motion is not known in advance, optimal control cannot be obtained, even for a discrete model

of the plate. A suboptimal control consisting of two parts is developed, one part reducing the effect of the frame motion on the plate, and a regulator further reducing the plate motion. The reduction of the excitation due to the frame motion is optimized by minimizing a given performance index.

A modeling technique is developed which combines desirable features of both the classical Rayleigh-Ritz method and the finite element method. Global admissible functions are employed, so that greater accuracy can be obtained with fewer degrees of freedom, thus reducing the cost of computing optimal control gains. Also, the admissible functions have the property that the generalized coordinates are actual displacements of the plate at discrete points, as in the finite element method. This greatly simplifies the state estimation for feedback. The admissible functions obtained by this technique can be linear combinations of admissible functions from any given set, which can include actual or approximate open-loop system eigenfunctions.

A numerical example demonstrates both techniques described above. The admissible functions used to discretize the plate are linear combinations of the lower actual modes of the plate. The optimal gains for the regulator portion of the control result in actuator forces proportional to the local plate velocity, or direct velocity feedback. The control method presented here reduces the plate motion effectively, both for a sixteen-degree-of-freedom model used to calculate the control gains, and for the actual system, modeled in terms of its lowest forty modes. Although in the example the frame underwent simple harmonic motion, a look at the sensitivity of the system performance to devia-

tions from the optimal design indicates that the control method is still effective for a frame motion in the form of a relatively narrow-band random process. The agreement between the results for the model and for the actual system is excellent, indicating that the model duplicates the dynamic characteristics of the system very closely. Finally, the performance index is substantially lower when the reduction in the frame excitation is optimized than in either the case in which a simple regulator is used or the case in which excitation is cancelled entirely.

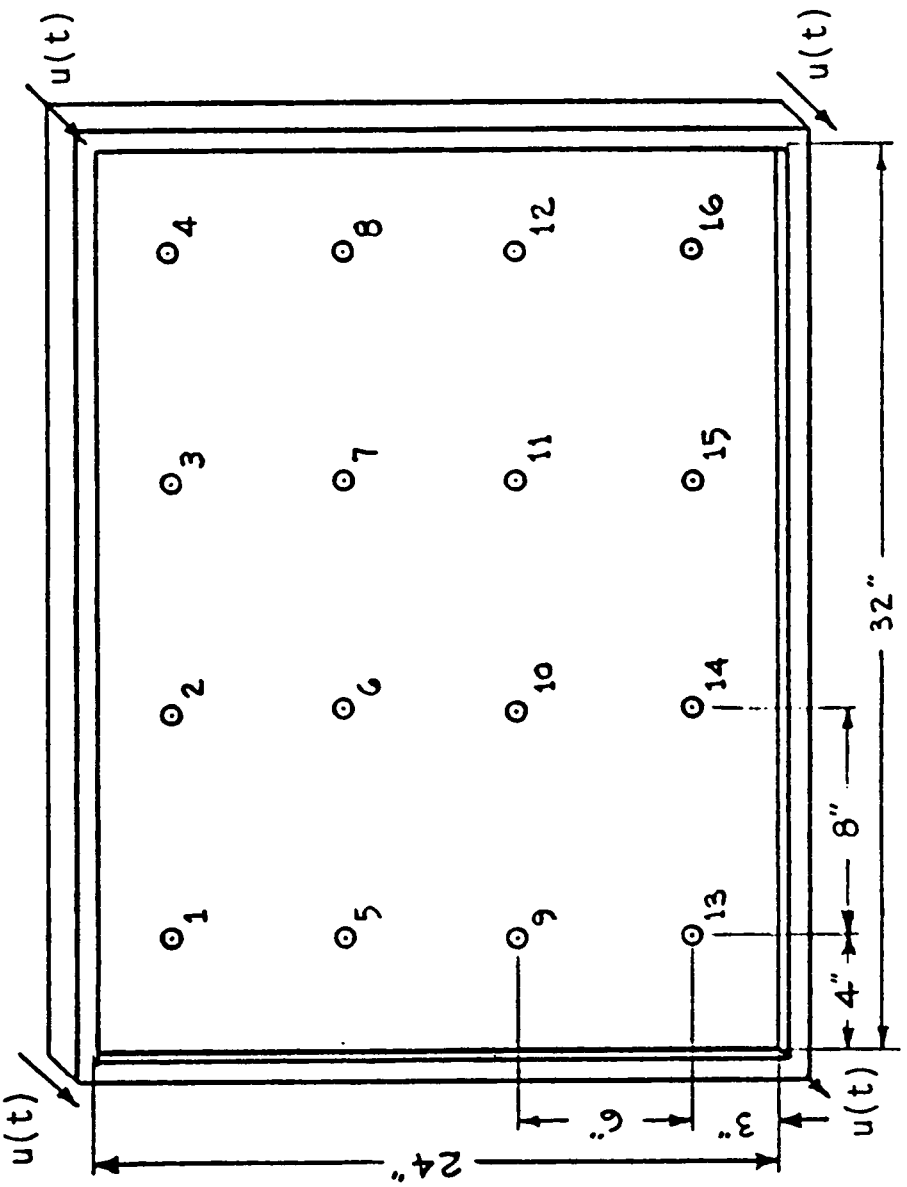

Figure 5.1 Thin plate simply supported on a rigid frame undergoing a displacement u(t). (Circles identify locations of the sixteen actuators.)

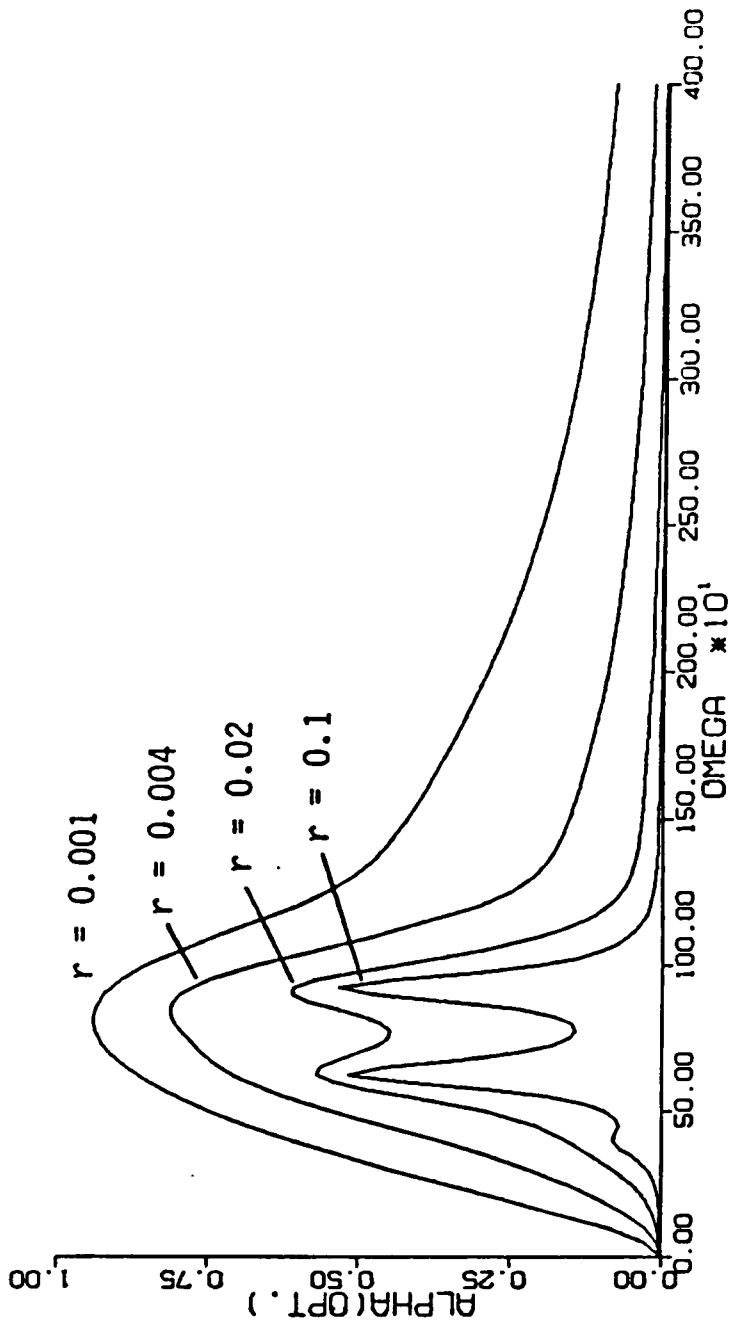

Figure 5.2. The optimal value of α as a function of the frequency of the frame motion ω, with r as a parameter.

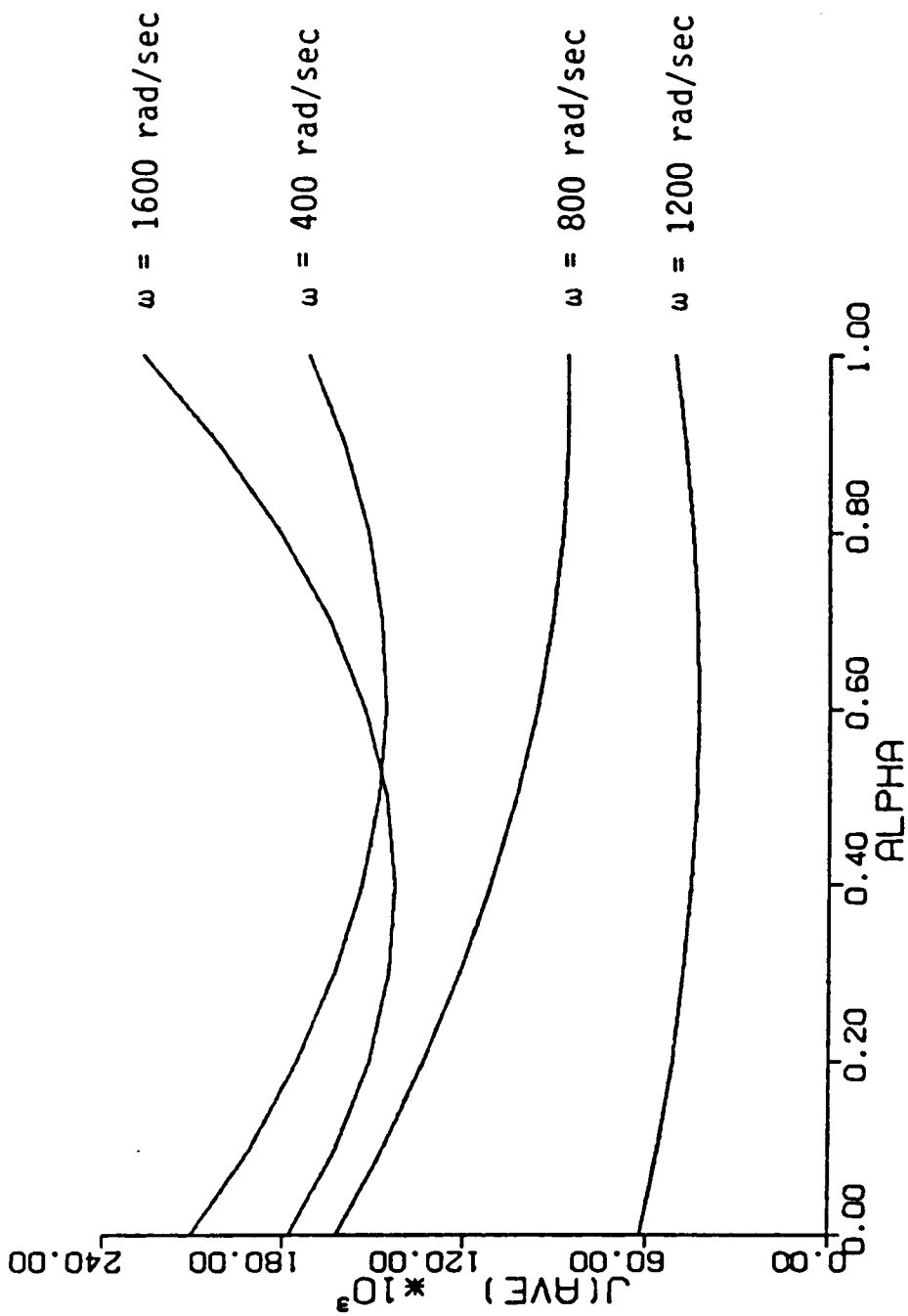

Figure 5.3. The average value of the integrand of the performance index as a function of α, with ω as a parameter.

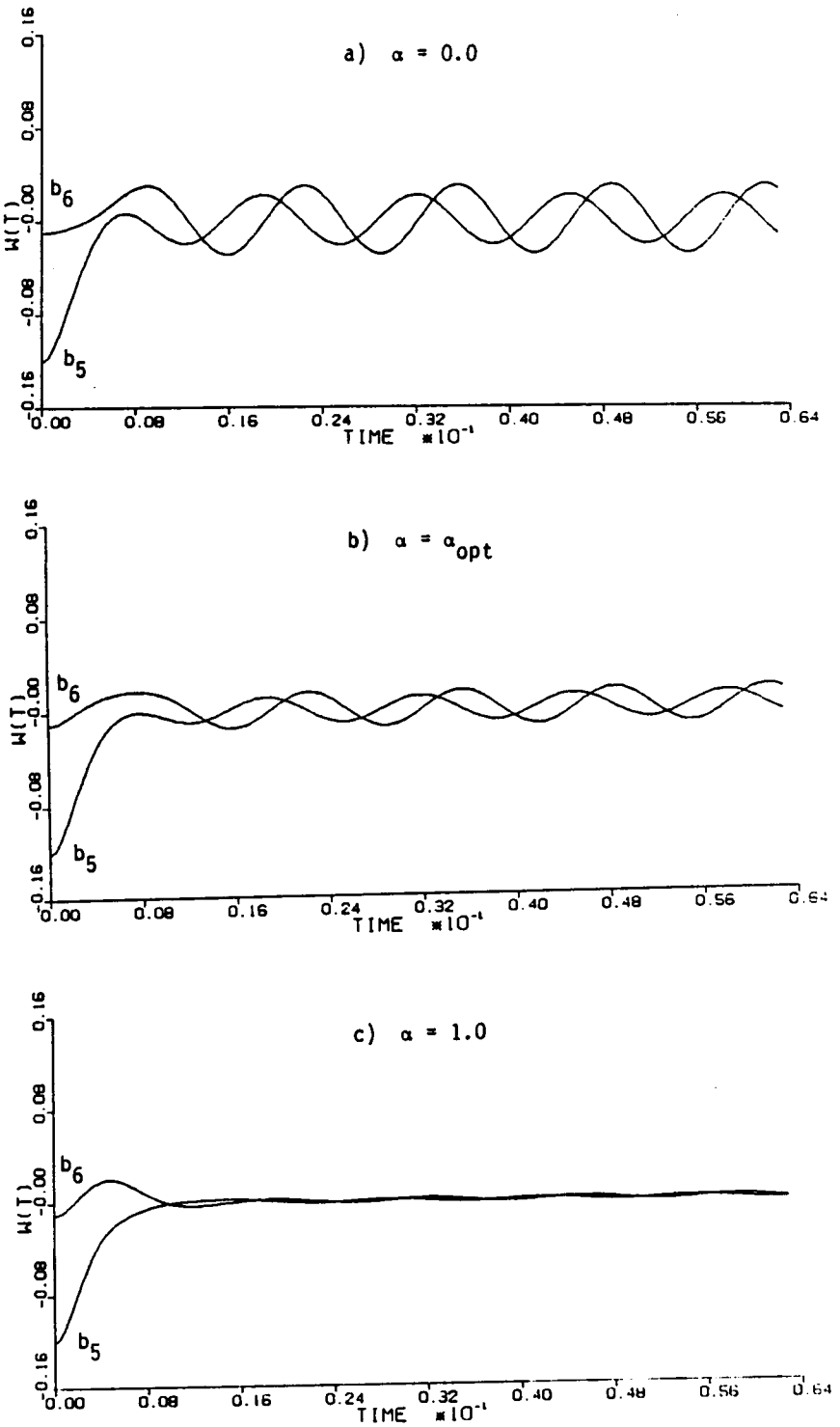

Figure 5.4. Displacement of the plate model at the fifth and sixth actuator locations for ω = 480 rad/s and a) α = 0, b) $\alpha = \alpha_{opt} \approx 0.5$ and c) α = 1.0

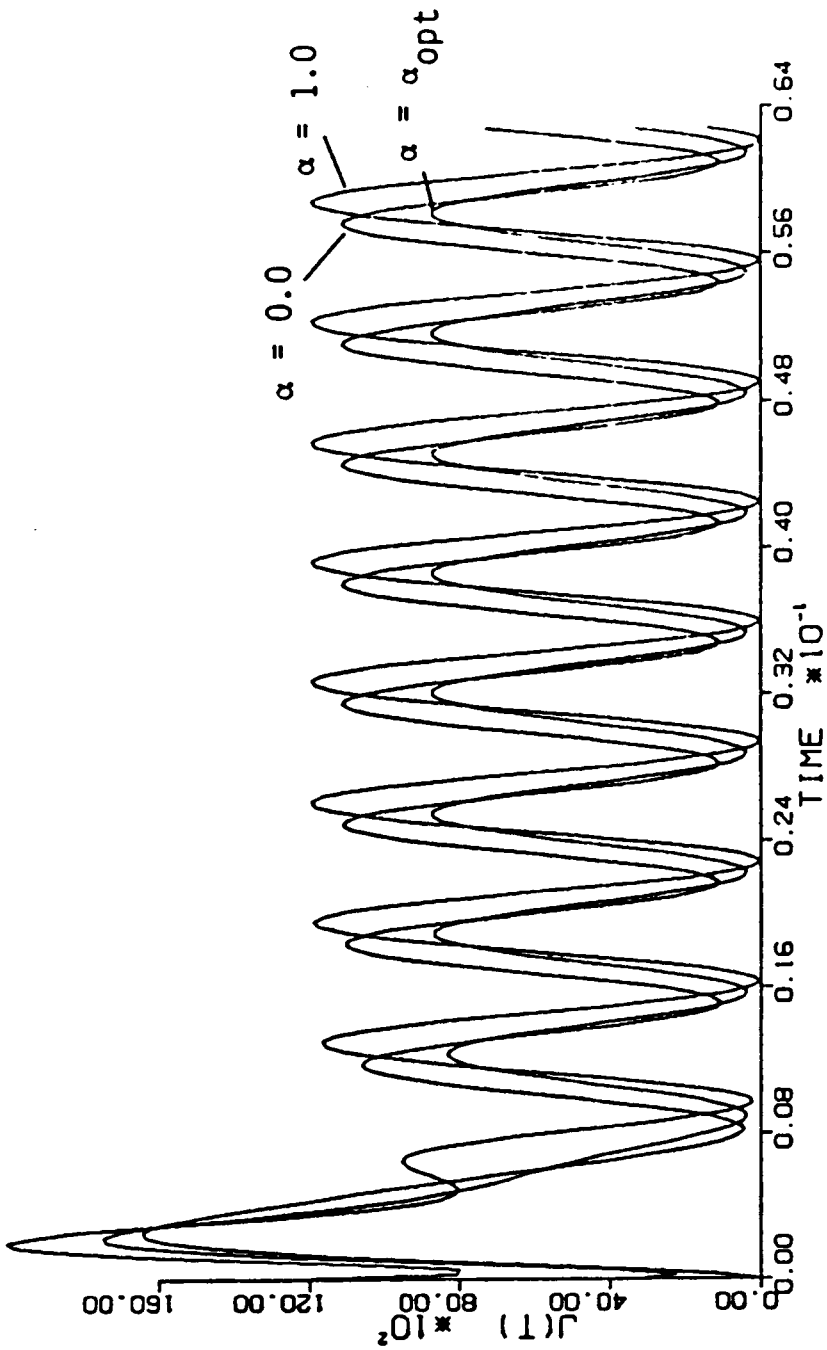

Figure 5.5. The integrand of the performance index as a function of time for the plate model for three values of α.

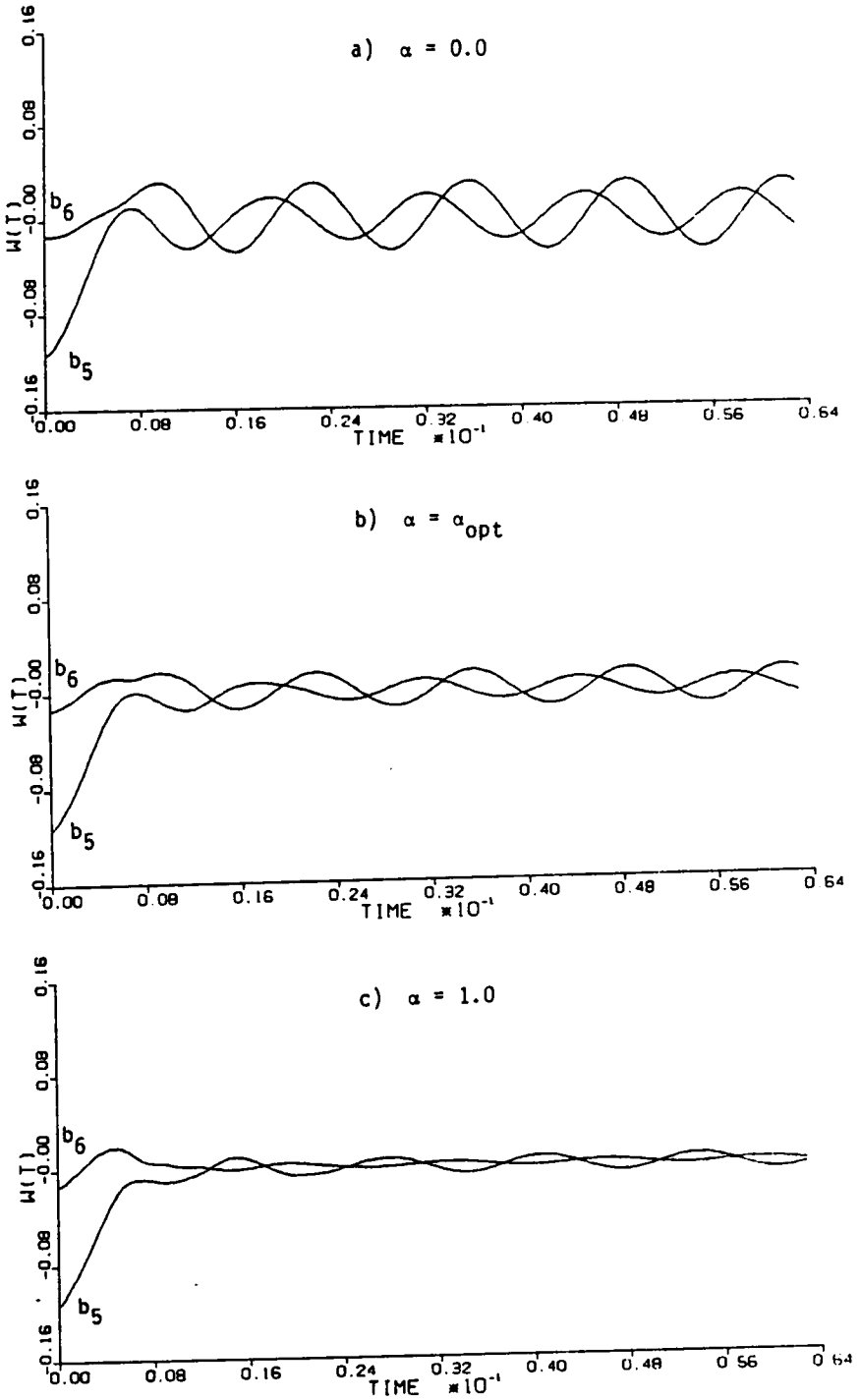

Figure 5.6. Displacement of the actual plate at the fifth and sixth actuator locations for ω = 480 rad/s and a) α = 0, b) $\alpha = \alpha_{opt} \approx 0.5$ and c) α = 1.0

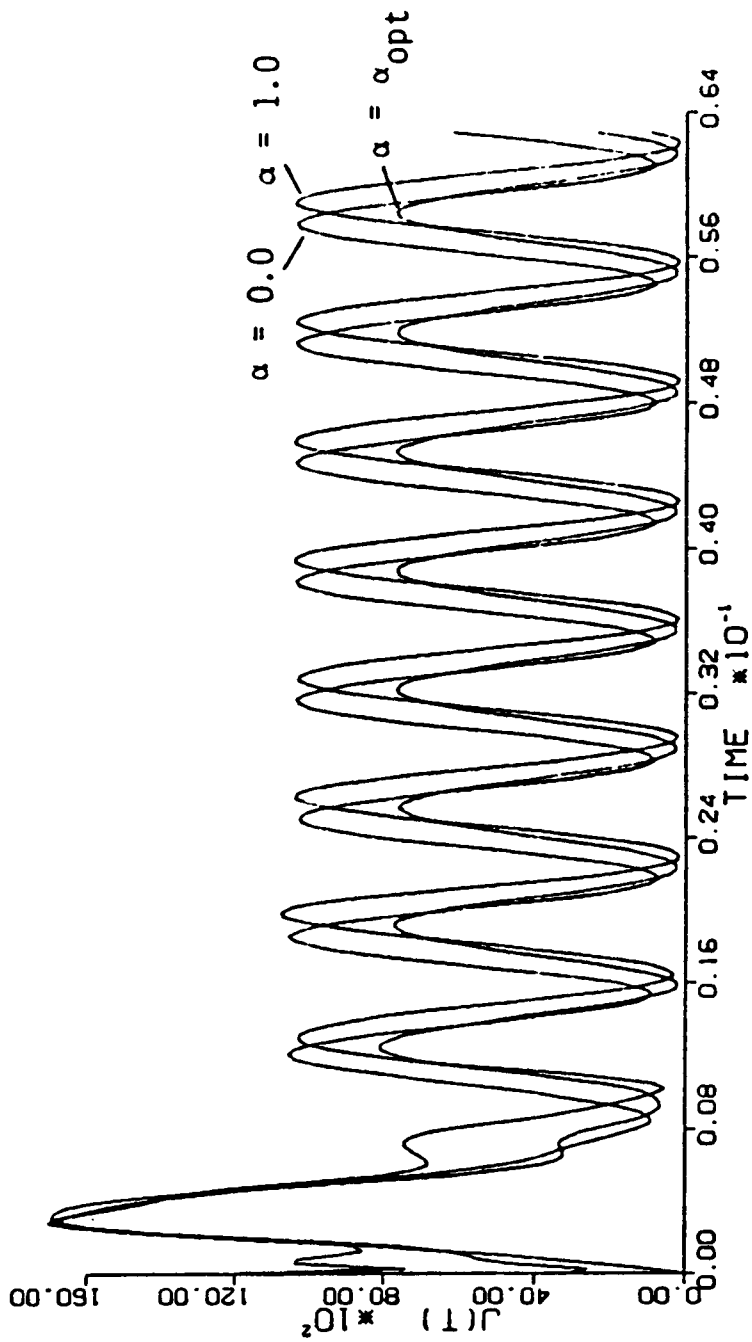

Figure 5.7. The integrand of the performance index as a function of time for the actual plate for three values of α.

REFERENCES

1. I. Babuska, B. A. Szabo, and I. N. Katz, "The p-Version of the Finite Element Method," SIAM J. Numer. Anal., Vol. 18, 1981, pp. 515-545.

2. I. Babuska and B. A. Szabo, "On the Rates of Convergence of the Finite Element Method," Int. J. Num. Meth. Engng., Vol. 18, 1982, pp. 323-341.

3. L. Meirovitch and H. Baruh, "On the Inclusion Principle for the Hierarchical Finite Element Method," Int. J. Num. Meth. Engng., Vol. 19, 1983, pp. 281-291.

4. L. Meirovitch and L. M. Silverberg, "Two Bracketing Theorems Characterizing the Eigensolution for the h-Version of the Finite Element Method," Int. J. Num. Meth. Engng., Vol. 19, 1983, pp. 1691-1704.

5. K. J. Bathe, "Solution Methods of Large Generalized Eigenvalue Problems in Structural Engineering," Report UC SESM 71-20, Civil Engineering Dept., University of California, Berkeley, 1971.

6. K. J. Bathe and S. Ramaswamy, "An Accelerated Subspace Iteration Method," J. Comp. Meth. Appl. Mech. & Engng., Vol. 23, 1980, pp. 313-331.

7. J. S. Arora and D. T. Nguyen, "Eigensolution for Large Structural Systems with Substructures," Int. J. Num. Meth. in Engnr., Vol. 15, No. 3, 1980, pp 333-341.

8. W. C. Hurty, "Vibration of Structural Systems by Component-Mode Synthesis," J. of the Eng. Mech. Div., ASCE, Vol. 86, Aug. 1960, pp. 51-60.

9. R. R. Craig, Jr. and M. C. C. Bampton, "Coupling of Substructures for Dynamic Analysis," AIAA J., Vol. 6, 1968, pp. 1313-1319.

10. W. A. Benfield and R. F. Hruda, "Vibration Analysis of Structures by Component Mode Substitution," AIAA J. Vol. 9, 1971, pp. 1255-1261.

11. A. Curnier, "On Three Modal Synthesis Variants," J. of Sound and Vibration, Vol. 90, Oct. 22, 1983, pp. 527-540.

12. R. R. Craig, Jr. and C-J. Chang, "On the Use of Attachment Modes in Substructure Coupling for Dynamic Analysis," Paper 77-405, AIAA/ASME 18th Struc., Struc. Dyn. and Materials Conf., San Diego, CA, 1977.

13. R. H. MacNeal, "A Hybrid Method of Component Mode Synthesis," Comp. and Struc., Vol. 1, 1971, pp. 581-601.

14. S. Rubin, "Improved Component-Mode Representation for Structural Dynamic Analysis," AIAA J., Vol. 13, 1975, pp. 995-1006.

15. L. Meirovitch and A. L. Hale, "A General Dynamic Synthesis for Structures with Discrete Substructures," J. of Sound and Vibration, Vol. 86, Dec. 22, 1982, pp. 445-457.

16. A. L. Hale and L. Meirovitch, "A General Procedure for Improving Substructure Representation in Dynamic Synthesis," J. of Sound and Vibration, Vol. 84, Sept. 22, 1982, pp. 269-287.

17. L. Meirovitch, and H. Baruh, "Control of Self-Adjoint Distributed-Parameter Systems," J. of Guidance, Control, and Dynamics, Vol. 5, No. 1, 1982, pp. 60-66.

18. L. Meirovitch, and L. M. Silverberg, "Globally Optimal Control of Self-Adjoint Distributed Systems," Optimal Control Appl. and Meth., Vol. 4, No. 4, 1983, pp. 365-386.

19. M. J. Balas, "Direct Velocity Feedback Control of Large Space Structures," J. of Guidance and Control, Vol. 2, No. 3, 1979, pp. 252-253.

20. L. Meirovitch, Computational Methods in Structural Dynamics, Sijthoff & Noordhoff, The Netherlands, 1980.

21. L. Meirovitch and J. K. Bennighof, "The h-Version and p-Version of the Finite Element Method and the Inclusion Principle," AIAA/ASME/ASCE/AHS 26th Struc., Struc. Dyn. and Materials Conf., April 1985, pp. 691-698.

22. K. J. Bathe, Finite Element Procedures in Engineering Analysis, Prentice-Hall, Englewood Cliffs, NJ, 1982.

23. J. K. Bennighof and L. Meirovitch, "Eigenvalue Convergence in the Finite Element Method," Int. J. Num. Meth. Engng. (to appear).

24. D. E. Kirk, Optimal Control Theory, Prentice-Hall, Englewood Cliffs, NJ, 1970.

25. L. Meirovitch, Analytical Methods in Vibrations, The Macmillan Co., New York, 1967.

26. R. W. Clough and J. Penzien, Dynamics of Structures, McGraw Hill, New York, 1975.

27. W. L. Hallauer, and G. R. Skidmore, "Active Vibration Damping Experiments at VPI&SU: Overview and Recent Results," Proc. Fifth VPI&SU/AIAA Symp. on Dynamics and Control of Large Structures, Blacksburg, VA, 1985, pp. 437-454.

28. L. Meirovitch, and H. Baruh, "On the Implementation of Modal Filters for Control of Structures," J. of Guidance, Control and Dynamics, Vol. 8, No. 6, 1985, pp. 707-716.

The vita has been removed from the scanned document